

# **Frequency- Adaptive Bilinear Reduced Order Modelling for Structures with Intermittent Contacts**

by

Adegbenga Odofin

A dissertation submitted in partial fulfillment  
of the requirements for the degree of  
Doctor of Philosophy  
(Mechanical Engineering)  
in the University of Michigan  
2020

Doctoral Committee:

Professor Bogdan Epureanu, Chair  
Professor Kenn Oldham  
Professor Armin Troesch  
Professor Nickolas Vlahopoulos

Adebenga O. Odofin  
doxydoxy@umich.edu  
ORCID iD: 0000-0003-4779-4576

© Adebenga O. Odofin 2020

## Table of Contents

List of Figures .....	iv
List of Tables .....	vii
List of Appendices .....	viii
Abstract .....	ix
Chapter	
1. Introduction .....	1
2. Frequency-Adaptive Bi-linear Reduced Order Model for Structures with Intermittent Contacts.....	9
2.1. Introduction .....	9
2.2. Methodology .....	13
2.2.1. Governing Equations .....	13
2.2.2. Application of the Harmonic Balance Method .....	14
2.2.3. Model Reduction.....	16
2.3. Results .....	25
2.3.1. Cracked Plate .....	27
2.3.2. Co-axial Cylinders .....	30
2.3.3. Jackup Platform .....	36
2.3.4. Computational Efficiency .....	39
2.4. Conclusions .....	40
3. Nonlinear Substructuring for Multiple Intermittent Contacts: FAR Approach.....	42
3.1. Introduction .....	42
3.2. Substructuring .....	46
3.3. Component Mode Synthesis.....	47

3.4.	Model Reduction .....	49
3.4.1.	Fixed Interface Bilinear Reduction .....	51
3.4.2.	Boundary Interface Reduction .....	54
3.5.	Global Assembly .....	59
3.6.	Results .....	62
3.6.1.	Test Case 1 .....	62
3.6.2.	Test Case 2 .....	64
3.7.	Conclusion.....	72
4.	Bi-linear modelling of legged micro-robot locomotion based on contact dynamics and vibration in multiple modes .....	74
4.1.	Introduction .....	74
4.2.	Robot Locomotion.....	76
4.3.	Robot Structural Modeling.....	78
4.4.	Nonlinear friction force .....	81
4.5.	Reduced order modeling .....	83
4.6.	Numerical Results .....	83
4.6.1.	Parameter Identification.....	84
4.6.2.	Model vs Experimental Results .....	87
4.7.	Conclusion.....	91
5.	Conclusions, Contributions and Future work .....	93
	Appendix A.....	97
	Appendix B .....	99
	References.....	102

## List of Figures

Figure 1. Contact model showing contact pairs in sliding, and contact pairs that are open .....	14
Figure 2. (a) Contact surface with three different types of contact pairs. (b) Contact conditions for the sliding linear system. (c) Contact conditions for the open linear system .....	18
Figure 3. The frequency-adaptive reduction (FAR) strategy (ALC represents arc-length continuation).....	26
Figure 4. Cracked plate: geometry and pre-stressed contact conditions.....	28
Figure 5. First four modes of the open linear system (cracked plate).....	28
Figure 6. First in-plane bending response of the cracked plate with pre-stress.....	30
Figure 7. Changes in the contact area over frequency for a cracked plate .....	31
Figure 8. Two co-axial cylinders (dimensions are in mm) .....	31
Figure 9. First bending response of the two coaxial cylinders without pre-stress (left) and with pre-stress (right).....	33
Figure 10. Changes in the contact area over frequency for the two coaxial cylinders with pre stress (‘o’ indicates sliding node pairs, and ‘*’ indicates switching node pairs).....	34
Figure 11. First four modes of the two co-axial cylinders (top), and the forced response obtained using FAR applied to multiple resonance excitation of the two co-axial cylinders with pre-stress (bottom) .....	36
Figure 12. Variation of ROM size over the multiple frequency locations A-G shown in Figure 11 .....	37
Figure 13. Jackup platform model with local intermittent contacts at then interface between the hull (triangular shape) and leg 3.....	38
Figure 14. The top 3 images show two modes of the jackup platform with fully open contact (left and center), and one mode with fully sliding contact; the bottom plot shows the	

amplitude of the nonlinear response of the jackup platform at point C obtained using two computational methods (FAR and CB-CMS) .....	39
Figure 15. An illustration of a partitioned rectangular plate with linear and nonlinear substructures .....	47
Figure 16. Schematic representation of the discretized model .....	50
Figure 17. Bilinear expansion of substructure 4 using fixed interface bilinear modes (FI-BLM) .....	52
Figure 18. Subassembly between substructures 3 & 4 with the bilinear combinations.....	56
Figure 19. A simple schematic to demonstrate the construction of boundary reduction matrices .....	58
Figure 20. Conceptual diagram showing the reduced order model process. ....	62
Figure 21. Geometry and pre-stressed contact condition of a Rectangular plate with double cracks.....	63
Figure 22. First in-plane bending response of double cracked plate excited at both ends with $F_{ex} = 0.01N$ (Left), and $F_{ex} = 0.1N$ (Right).....	65
Figure 23. First in-plane bending response of double cracked plate excited at one end with $F_{ex} = 0.1N$ . ....	65
Figure 24. Variation of the response amplitude curve with variation in excitation amplitude.....	66
Figure 25. Jackup platform model with two local intermittent contacts at then interface between the hull (triangular shape), leg 2 and leg 3. ....	67
Figure 26. FE model of the partitioned and exploded view of a Jackup platform with double intermittent contacts. ....	67
Figure 27. Mode shapes of the linearized fully open and fully closed contact BC of the jackup platform. ....	69
Figure 28. (a) Frequency response curve of platform measured at point A and B. (b) Frequency response curve of platform measured at point C and D. ....	69
Figure 29. Comparison of frequency response of platform from new approach to other standard methods. ....	71
Figure 30. ROM Size variation with variation in MPC cutoff parameter $\epsilon_2$ . ....	71
Figure 31. Parametrization effect of MPC cutoff value $\epsilon_2$ on the frequency response curve.....	72
Figure 32. FEM model of PZT actuated, centimeter scale hexapod microrobot.....	77
Figure 33. (a) Picture of a silicon micromachined millimeter-scale microwalking robot [84]. (b) Photo of a centimeter-scale walking robot prototype with the leg schematic [85].....	78

Figure 34. Rigid body motion considered in analysis of the microrobot.....	81
Figure 35. Schematic view of the contact model between the robot's foot and ground.....	82
Figure 36. Sensitivity analysis of model parameters from 1% to 10% perturbation .....	84
Figure 37. Frequency response of the forward and vertical displacement amplitude measured at the front and middle leg of the microrobot.....	86
Figure 38. Frequency response of the robot's forward velocity .....	87
Figure 39. Periodic motion of the dynamic, rigid body and combined motions of the microrobot. .....	88
Figure 40. Relationship between the average velocity frequency response of the experimental and simulation results of the microrobot with (a) wooden ground (b) steel ground. ...	89
Figure 41. Relationship between the excitation voltage and the average robot velocity of the experimental and simulation results with steel ground at (a) 110Hz (b) 120Hz (c) 130Hz (d) 140Hz. ....	90
Figure 42. Relationship between the excitation voltage and the average robot velocity of the experimental and simulation results with wooden ground at (a) 110Hz (b) 120Hz (c) 130Hz (d) 140Hz. ....	91
Figure B. 1. Excitation frequency vs robot speed at 30V with metal ground.....	99
Figure B. 2. Excitation frequency vs robot speed at 30V with wooden ground.....	100
Figure B. 3. Excitation voltage vs robot speed at 130Hz with metal ground .....	100
Figure B. 4. Excitation voltage vs robot speed at 130Hz with wooden ground .....	101

## List of Tables

Table 1. Parametric study on the MPC value $\epsilon_2$ for the two co-axial cylinders with pre-stress..	35
Table 2. A comparison of CPU times (seconds).....	40
Table 3. Robot model parameters obtained from optimization. ....	85
Table A. 1. Subassemblies of different combinations of substructures of the Jackup platform with bilinear BCs. ....	98



## **List of Appendices**

Appendix A. Subassemblies of Jackup Platform .....	97
Appendix B. Experimental Results of Microrobot .....	99

## **Abstract**

Computing the nonlinear forced response of structures with localized nonlinearity, such as intermittent contacts, is a time intensive task mainly because highly refined finite element models are necessary to properly model such structures. To alleviate this issue, temporal and spatial reduction methods have been proven to be beneficial in making nonlinear analyses faster. In this research, reduced order models for structures with intermittent contacts are presented. Models of systems with intermittent contacts such as jack-up platforms are reduced through the projection of the full system onto a basis of normal modes computed by enforcing special boundary conditions (full contact, partial contact, or fully open) at contact surfaces. The resulting low order models are used to predict the steady state forced response by the harmonic balance method coupled with a pseudo-arc length continuation algorithm. A frequency adaptive reduction (FAR) method is employed to accurately predict the behavior at the contact area during vibration and therefore establish special boundary conditions to be employed in generating the transformation matrix applied in the reduction process. The computation and strategic reduction of the set of basis vectors, at every frequency within the range of interest, provides an efficient optimization of the model size. Furthermore, the continuation approach is adjusted to handle models of varying size between solution frequencies. The proposed method is applied to multiple test cases to demonstrate its effectiveness and high numerical efficiency compared to classical reduction methods.

Despite the development of an optimal reduced order modelling tool such as the FAR, repetitive modeling of complex engineering structures in the design process can still be challenging because of the time needed to construct reduced order models. To address this challenge, substructuring can be employed. Analyzing a system's structural dynamics in such a component-wise fashion has proven to have important advantages over global methods. Such benefits include the ability to evaluate the dynamic behavior of structures that are too large or complex to be analyzed as a single entity. Also, by analyzing the subsystems, local dynamic behavior can be recognized more easily than when the entire system is analyzed. In cases when a single component's geometry or parameters are modified, only such subcomponent needs to be reanalyzed, therefore the total system can be analyzed at low additional cost. This advantage can be leveraged when dealing with local nonlinearities with intermittent contacts (e.g., cracks). If the length of a local crack within a large structure increases, only such local area needs to be remodeled without remodeling the entire structure completely. Despite their laudable advantages, most substructuring techniques are only capable of handling linear systems. Combining the FAR technique with conventional substructuring methods allow the handling of local nonlinear contact challenges. This idea is explored in detail in this research and the method is tested on a rectangular plate with two independent crack interfaces.

Finally, the novel reduction method developed herein is further challenged by its application on systems with friction and rigid body mode. Example of such system, analyzed in this work, is the prediction of the dynamic behavior of an untethered multi-legged microrobot. The proposed model is modified to incorporate rigid body dynamics and friction to predict the dynamics of such intricate system with complex motion. Simulation results are verified using experimental results from the microrobot prototype.

# CHAPTER I

## 1. Introduction

Predicting the deformation, vibration responses, stress distribution, and other structural characteristics to support the design process of structural components or systems require structural analysis mostly based on the finite element models (FEMs). These analysis are necessary in design chain to anticipate and forestall damages that could impact the original design function of the system. A special class of structural damages prevalent in structures operating under high fatigue stress is damages from localized intermittent contacts such as cracks and dents. Experimental analysis for reliability and testing of designs can be quite expensive compared to high capacity computing power available for simulations. Despite the recent development of high computing power, the structural complexities and size of modern designs continues to increase such that changes to an existing design can have a significant time delay in the design process. Thus, structural reduced order modelling (ROM) techniques are necessary to reduce computational time and cost. ROM has been an active research topic because of its relevance in modern structural analysis and because it provides a good understanding of the fundamental characteristics of a variety of dynamical systems. Many ROM techniques have been developed in the past for various systems especially as it relates to structural systems with localized piecewise nonlinearity. In general, ROM methods can be divided into two categories: linear transformation based methods and methods based on nonlinear normal modes (NNM).

Linear transformation based methods has been investigated by several researchers for model reduction of nonlinear systems with intermittent contacts. The system equivalent expansion process (SEREP) [1] and Irons-Guyan [2,3] reduction are example of linear transformation based reduction. These methods treats the degrees of freedom (DoFs) associated with the nonlinear nodes as master DoF and other DoFs as slave DoFs which can be removed from system depending on the selection the selection criteria. Another reduction method peculiar to systems with piecewise nonlinearity is named the local equivalent stiffness method researched by Butcher and Lu [4]. This is based on a linear approximation of the nonlinear intermittent contact using master-slave relationship. The transformation matrix of the ROM is such that it retains the degrees of the nonlinear nodes as master DoFs. The most important characteristics of this method is that it preserves the eigen-structure of the original system. One of the major alternative to direct, full order structural analysis and linear transformation based reduction method is the component mode synthesis (CMS). This techniques is particularly suitable for large systems with huge DoFs. Various CMS-based ROM methods have been proposed in the past [5] due to its flexibility to be integrated with other FEM-based techniques. In general, the concept is initiated by first dividing the structure into smaller components referred to as subcomponents or substructures. Next, each substructure is projected onto a small set of linearly independent Ritz vectors which spans the solution space of the vibration response. This projection significantly reduces the number of DoF needed to model each substructure compared to the number of DoFs in the initial problem. The resulting fewer DoFs of each substructure is finally assembled into a synthesized global reduced order model which can be solved using numerical solution techniques. Craig-Bampton component mode synthesis (CB-CMS) method is one of the widely used CMS techniques. In this technique, the Ritz vectors include the fixed interface modes of the substructures plus a set of static interface

constrain modes. This technique is well understood and frequently employed because of its simplicity, numerical stability and flexibility.

In numerous cases of nonlinear systems having a large numbers of DOFs, the actual nonlinear components are spatially localized. For example, an airplane model could be modelled with a relatively stiff fuselage (linear) and more flexible wings (nonlinear). Applications of local nonlinearities are also present in the uprising world of microelectromechanical systems (MEMS), where capacitors of accelerometers are mounted on springs that are able to handle large deflection. In the FE modelling of these cases, CMS can be used to isolate the nonlinear components for further analysis. Modelling structures with local intermittent contacts using FEM-based methods typically results in a very large system of models. Models in the neighborhood of the intermittent contacts are known to be nonlinear and have different structural characteristics from the other linear models. Note that the number of the nonlinear models can be significant despite its localization because elements in this neighborhood are usually discretized with a fine mesh to be able to capture the nonlinear response. The nonlinearity comes from the intermittent opening and closing of the contact surface. This piecewise linear motion was leveraged by Poudou and Pierre [6 7] when they proposed a method for predicting the resonant frequencies of a cracked structure using the direct solution of the nonlinear forced response of the system which is very complex and computationally intensive. They proposed a hybrid frequency-time domain technique called the bilinear frequency approximation to avoid the challenge just mentioned. Bilinear frequency approximation has also been used in predicting the resonant frequency of a single DoF [8] and also on multi-DoF vibration of cracked beams and plates [9,10] One slight draw back of the method is that it assumes all the nodes at the constant surface opens and closes instantaneously. Therefore the method doesn't capture gradual opening or closing of the contact interface though it is good

approximation for predicting the resonant frequency. This is one of the challenges addressed in this thesis.

For most of ROM techniques, the selection criteria for selecting an optimal set of modes that spans the solution space is usually a challenge. The selection of vectors included in the transformation matrix of a ROM obtained via Guyan reduction [3] problem is a very crucial factor in obtaining expected solution and minimizing challenges from numerical convergence. Henshell and Ong [11] presented a selection technique called an automatic master DoF selection algorithm. This algorithm is aimed at retaining set of nodes with lower vibration frequency (master DoFs) in a FEM analysis while removing nodes that contributed to higher vibration modes. Master nodes are nodes with high inertia and low stiffness and nodes with low inertia and high stiffness are the slave nodes. They are identified by calculating the natural frequency of the system when all nodes are fixed except the node under consideration. Higher natural frequencies are associated with slave nodes which are be iteratively removed using Guyan reduction from the system until a satisfactory number of node is left. Similar to this approach is another Algorithm proposed by Shah and Raymund [12] where a DoF is eliminated if its frequency is larger than a predefined cutoff frequency which is chosen as a multiple of the most significant frequency within the frequency range of interest. Matta [13] also presented a technique similar to the above but has the advantage that it can be applied to both Guyan reduction and CMS techniques. Another method that suffers similar rigorous and exhasutic serach criteria for selecting master DoFs is implemented by Grinenko and Mokeev [14]. Bouhaddi and Fillod [15] had a different approach to their selection technique. The concept involve fixing the DoF associated to an eigenmode such that the eigenvalue of both the fixed and unfixed cases remain the same. The rationale behind this technique is to maximize the minimum eigenvalue with all the master DoFs fixed. Another class of selection

different from the master DoFs based selection techniques in previous literatures, is the modal energy concept based selection. Kim and Choi [16] proposed a method that uses the energy distribution among the DoFs of each mode to select the primary DoFs by taking the partial sum over the rows of the energy distribution matrix. They further went on to use the energy estimation of discretized elements by using the Rayleigh quotient value of the elements. They went even further in ref. [17] to propose a two level selection process. First is the reduced order modelling by improved reduced system (IRS) which is based on the elemental energy estimation to select the primary DoFs, and followed by a sequential elimination method [18] with an iterative IRS. The main challenge with most of these method is that they are computationally intensive and sometime require the user's intuition to restrict the search algorithm to certain region of importance rather than searching through the entire system's DoFs. Later in this work, a new selection algorithm is presented named the FAR selection technique.

Chapter two of this work focuses on the development, implementation and application of the novel concept of the frequency adaptive reduction (FAR) as an improved approach of using the bi-linear ROM of structures with contact nonlinearity. As stated earlier, there is a continuous interest in developing faster and reliable methods for modelling finite element (FE) systems with intricate geometry and complex dynamic behavior. Example of such system include dynamic systems with localized piecewise-linear nonlinearity such as joints, cracks and interface between coupled parts. Different types of ROM has been developed to capture the spatial correlations in the vibration of these systems by reducing the number of model equations to be solved. In the study by Segalman [11], systems with local nonlinearities are reduced by means of a reduction basis which includes mode shapes of a reference linear system augmented by a set of additional modes with different boundary conditions at the contacts. Similar approach but with the concept



of bilinear modes (BLMs) was presented by Saito & Epureanu [19] and Epureanu & Zucca [20]. While the proposed BLM reduction techniques were good approximation of the nonlinear contact dynamics, they are not capable of predicting the gradual opening and closing of the contact surface. This is as result of the underlying assumption that all the contact nodes instantaneously transition between fully opened and fully closed.

The BLM reduction concept for structures with intermittent contacts, under harmonic excitation, as applied in this work assumes that the response of the nonlinear system is periodic and only contains a small number of invariant manifolds (Nonlinear normal modes) within the frequency range of solution. Therefore the response of the system can be approximated by a set of normal modes of the open or closed (sliding) linear system. Zucca and Epureanu [21] recently developed a ROM with similar BLM concept that captured the gradual opening and closing of the contact interface. However, made an underlying assumption that in the frequency range of interest the dynamics of the nonlinear system is dominated by one of the modes (that must be identified in advance) of either the open or the sliding system. This is a strong assumption which limits the applicability of the method as some systems with complex motion will flout this assumption. The FAR technique developed in chapter two addresses this challenge and presents a two-step mode selection technique to optimize the number of modes in the transformation matrix.

In chapter three the FAR method developed in chapter two is used to develop a methodology to solve large systems with multiple intermittent contacts using substructuring. In reality most systems do have more than one localized region with intermittent contacts which could be multiple of the same type of contact nonlinearity (e.g. multiple cracks or joints) or a hybrid (e.g. cracks and joints combination). In either case, solving the system using substructuring is advantageous because the system can be partitioned such that each intermittent contact and its

peculiarities can be handled within a smaller set of the system i.e. subcomponent. This approach handles localized modifications (either by design or failure) to the system very well in that only the subcomponent affected by the modification is required to be remodeled while other unaffected subcomponents remains the same. Majority of the previous literature use the CB-CMS as the substructuring tool for handling system with geometric nonlinear FE models [22,23]. Similar approach is employed in this work but with intermittent nonlinearities instead and reduction of the boundary interface DoFs. Reduction of the interface DoFs between subcomponents in substructuring techniques has been presented by several researchers. The use of a secondary modal analysis of the interface partitioned matrices to reduce the interface DoFs was proposed by Brahmī et al. [24]. This method is applied before the assembly of the subcomponents in CMS technique. The transformation matrix contains the combination of truncated modes obtained via singular value decomposition (SVD) and a selected few secondary interface modes. Cansister et al. [25] also proposed a similar method but the transformation matrix contains the truncated fixed interface modes combined with the constraint mode partition of the matrices produced by CMS. An inverse transformation of mode sets into the physical DoFs results in the characteristic constraint modes. The framework for generalizing the interface DoFs was introduced by Balmés [26]. He implemented the idea of considering a new basis set to represent the actual interface displacement also called the constraint modes. The work presented later herein, used the concept of bi-linearity to incorporate the effect of intermittent contacts during the boundary interface reduction. This new idea uses the FAR selection technique to create a transformation matrix containing fixed interface bilinear modes and bilinear constraint modes to reduce the linear, nonlinear and boundary DoFs.

In chapter four the FAR bilinear reduction was further challenged by introducing friction and rigid body motion into the dynamic modelling equation previously reduced by FAR. With these additional challenges, a new FAR based model is introduced and applied to predict the locomotion of a centimeter scale multi-legged micro-robot. The fundamental dynamics related to a small scaled movement of a robot has been studied in literatures. In ref. [27,28], studies on the locomotion of biological organisms like insects was investigated and extended to testing of robots intended to operate with similar locomotion process. Their prototypes, which are centimeter scaled, have legs that are modelled with lumped parameters and applied with a relatively simple ground interaction modelling. The interaction range from the foot contact with ground to foot motion in air. This concept exhibit the basic concept of the legged robot dynamics which always include the foot-ground interaction and sometimes the foot-body interaction. Factors that determine the dynamics of a microrobot include the scale of the robot, the number of legs and the amount of interaction allowed between component parts of the robot. Walking analysis based on different contact model in large systems has been investigated in several literatures. [29] used the coefficient of restitution based model, [30] adopted the continuous contact force model, and [31] applied a planar kinematic chain with a compliant ground model. These contact model unfortunately are not effective for microrobots because impact forces on the foot of the robot from the ground is only applied at single point of contact. The full FE based approach suggested in this work alleviates this issue by modelling the foot-ground interaction surfaces with multiple nodes which generates a distributed nonlinear forcing reaction from the ground to the foot.

## **Chapter II**

### **2. Frequency-Adaptive Bi-linear Reduced Order Model for Structures with Intermittent Contacts**

#### **2.1. Introduction**

Dynamic systems with localized nonlinearities (such as friction, cracks, or joints) continue to be of significant interest in the field of nonlinear structural dynamics. This is because of challenges associated with predicting the nonlinear dynamic responses of such systems especially when the nonlinearities are not smooth. Such calculations typically require high resolution finite element (FE) models with several million governing equations for the equally many DoFs.

Reduction methods for the linear portion of the governing equations have been intensely studied in the past. However, methods for nonlinear systems require further development to increase their efficiency and accuracy. Several techniques have been proposed to reduce the size of the nonlinear system to overcome the computational cost necessary to compute the nonlinear forced response. The rationale for these techniques is that spatial coherences exist over time in the displacements of the full order model. These coherences typically exist over a frequency range of interest and can be approximated by using projection on sets of (projection/basis) vectors specially computed and assembled into a reduction matrix. The displacements and the governing equations are projected onto this reduced order space.

One of the early methods for model reduction is Guyan's static reduction [3]. This technique requires the DoFs to be split into master and slave DoFs. Then, displacements are approximated as a linear combination of static modes, called constraint modes, obtained by applying a unitary displacement at each master DoF separately while forcing the others to be zero. As a result of this reduction process, the size of the reduced order model (ROM) equals the number of master DoFs. However, this technique disregards the inertial effects of the slave DoFs by assuming that they are connected to the master DoFs only statically. Thus, Guyan's method is less accurate for large models with distributed mass.

Another approach is component mode synthesis (CMS) [32]. In CMS, the full structure is split in several substructures. Each substructure is reduced, and then, provided that interface DoFs are selected as master DoFs of each substructure, the ROM of the full structure is assembled. One of the popular variants of this method is the one developed by Craig and Bampton [33]. In the Craig Bampton component mode synthesis (CB-CMS), the Guyan reduction matrix of each substructure is augmented with a set of modes, computed by assuming fixed boundary conditions (BCs) (i.e., null displacements) at the master DoFs. CB-CMS is commonly applied to structures with intermittent and friction contacts provided that contact DoFs are included in the set of master DoFs [34].

The main drawback of applying either the Guyan or the CB-CMS methods to structures with intermittent or friction contacts is that the size of the set of nonlinear governing equations to be solved equals or is larger than the number of contact nodes (if the contact kinematics is defined by means of absolute contact DoFs) or the number of contact pairs (if the contact kinematics is defined by means of relative contact DoFs) [35], [36]. Possible strategies to further reduce the size

of CMS-based ROMs and to lower the computational burden include node-downsampling when enforcing no-penetration BCs on the contact surfaces [11], [4], [37].

The application of proper orthogonal decomposition (POD) is another common technique that has been developed for order reduction of nonlinear systems. POD-based order reduction requires the construction of Proper orthogonal modes (POM) obtained from snapshots of the nonlinear solution of the system. These vectors form the reduction basis contained in the reduction matrix [38]. Al-Shudeifat and Butcher applied similar approach by augmenting the reduction matrix composed of the local equivalent linear stiffness method (LELSM) modes with new Ritz vectors [39]. In their method, the optimal basis vector of POMs is found via simulation. As is the case for POD-based reductions, the setback of these approaches is that, they require a priori simulation to determine the nonlinear solution of the system.

Other approaches are possible to reduce nonlinear systems by means of generalized coordinates, so that the size of the ROM does not depend on the mesh refinement of the contact area. One approach is based on the use of nonlinear normal modes (NNM), which extend the concept of linear normal modes to nonlinear systems. Peeters, Kerschen, and Golinval [40] have successfully used NNM as part of a numerical algorithm to compute the responses of aircraft structures. However, this method is computationally intensive and may require the full solution of the system before NNM can be calculated. Zuo and Curnier [41] studied the autonomous conewise linear multi-degree-of-freedom of gyroscopic systems (such as cracked beams) and non-gyroscopic systems (such as cracked rotating shafts) subject to unilateral contacts. Their approach combined analytical and numerical methods for investigating the fundamental dynamic characteristics of such systems, namely non-linear real and complex modes. That approach provides good fundamental insights. However, it is difficult to adopt for systems with large number

of nonlinear DoFs because of the large number of resulting equations of motion, which also require a large number of iterations to solve.

Another technique has been proposed by Saito and Epureanu [19], called bi-linear modal reduction. That method has been successfully applied to piece-wise linear oscillators. By exploiting the spatial coherences between two sets of normal modes of two dynamic systems with special BCs, referred to as bi-linear modes (BLMs), this technique is able to reduce the nonlinear model. The method has been extended to systems with pre-stressed intermittent contacts by Zucca and Epureanu [42] also. Despite the accuracy achieved by this technique, the size of the ROMs obtained is large and increases as the number of contact BCs increases. Consequently, the iterative solution of the nonlinear model with such frequency-invariant ROM size usually requires a significant computational time.

In this paper, the BLM formulation [19] is refined to enhance computational speed and accuracy through a frequency-adaptive reduction (FAR) technique. In the original approach, BLMs include modes of the linear system with sliding contacts along the entire contact area (referred to as the sliding linear system), and those of the linear system with open contacts along the entire contact area (referred to as the open linear system), where no penetration is allowed.

Distinct from previous work, in the current approach, the contact area is decomposed conceptually in three parts. The first part (a) contains all node pairs that are always in the sliding state during vibration. The second part (b) contains all nodes that are always in the open state. The third part (c) contains all nodes that switch from open to sliding states and vice-versa during each vibration cycle. Thus, the sliding linear system has all switching node pairs in the sliding state, and the open linear system has all switching node pairs in the open state. Both these linear systems have all node pairs in part (a) in the sliding state and all node pairs in part (b) in the open state.

Note that parts (a), (b) and (c) change when the excitation frequency (or amplitude) changes. The current approach adaptively estimates at every frequency the three parts (a), (b) and (c), and uses the estimates to predict the nonlinear time-periodic solution at nearby frequencies.

The modes of the two linear systems (open and sliding) with BCs based on the adaptively calculated contact areas are used to obtain BLMs for model reduction. In addition to the adaptive identification of the contact area, this paper also presents a modal selection criterion (MSC) to select the BLMs to be included in the reduction matrix, and a modal participation criterion (MPC) aimed at eliminating unnecessary BLMs from the reduction matrix. Thus, the novel approach does not only consider the adaptation of the contact area, but it also controls the size of the reduction matrix to contain only the BLMs with higher participation in the dynamics. Hence, unlike many previous approaches, the assumption that the response of the nonlinear structure is dominated by the same set of modes of either the sliding linear system or the open linear system in the frequency range of interest is not necessary.

The capabilities of proposed method are demonstrated by means of two example systems: a cracked plate and two cylinders with overlapped edges.

## **2.2. Methodology**

### **2.2.1. Governing Equations**

The forced response of a vibratory structure with intermittent contacts under pre-stress and harmonic excitation can be computed by solving the following set of dynamic differential equations of motion (EoMs) represented in the time domain as



$$\mathbf{M}\ddot{\mathbf{q}} + \mathbf{C}\dot{\mathbf{q}} + \mathbf{K}\mathbf{q} = \mathbf{F}_{ps} + \mathbf{F}_{ex} + \mathbf{F}_{nl}, \quad (1)$$

where  $(\dot{\phantom{x}})$  represents a time derivative.  $\mathbf{M}$ ,  $\mathbf{C}$  and  $\mathbf{K}$  are the mass, viscous damping and stiffness matrices associated with the linear model with no contact conditions enforced (i.e., with free BCs on the contacting surfaces),  $\mathbf{F}_{ps}$  is the vector of pre-stress forces,  $\mathbf{F}_{ex}$  is the excitation vector,  $\mathbf{F}_{nl}$  is the vector of nonlinear contact forces acting at the contact pairs (Figure 1), and  $\mathbf{q}$  is the vector of DoFs.

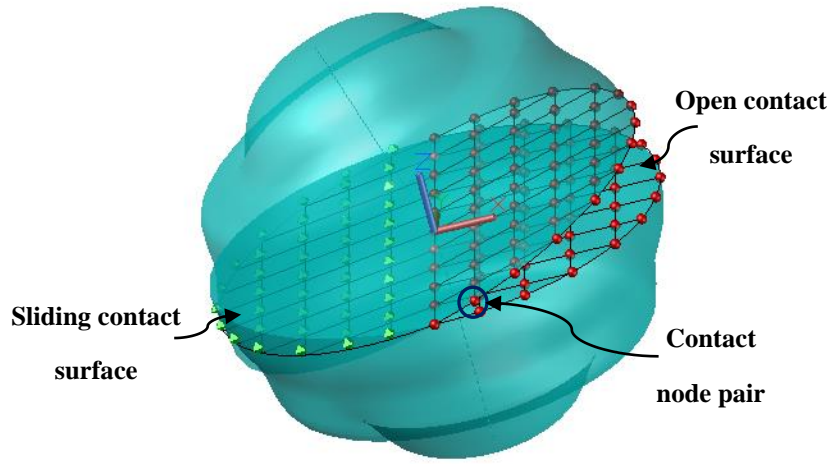


Figure 1. Contact model showing contact pairs in sliding, and contact pairs that are open

### 2.2.2. Application of the Harmonic Balance Method

The harmonic balance method (HBM) [43,44] is a well-known technique for computing periodic solutions for dynamic systems. This method allows for solving the EoMs in the frequency domain, rather than in the time domain. Given that the focus of this work is to study the periodic responses of a system under the influence of harmonic excitations, application of the HBM to the governing equations provides a fast computational solution.

In the HBM, all periodic quantities (excitation, steady-state displacements and nonlinear forces) are expressed as a sum of harmonic terms (i.e., a Fourier series) truncated at a desired

maximum  $H^{th}$  harmonic. Equating the coefficients of the linearly independent harmonic functions gives rise to a set of nonlinear complex algebraic equations written as

$$\begin{aligned} \mathbf{K}\mathbf{q}^0 &= \mathbf{F}_{ps} + \mathbf{F}_{ex}^0 + \mathbf{F}_{nl}^0, & h = 0, \\ [- (h\omega)^2 \mathbf{M} + jh\omega \mathbf{C} + \mathbf{K}] \mathbf{q}^h &= \mathbf{F}_{ex}^h + \mathbf{F}_{nl}^h, & h = 1, \dots, H, \end{aligned} \quad (2)$$

where superscript  $h$  denotes the  $h^{th}$  Fourier coefficient,  $\omega$  is the excitation frequency, and  $j = \sqrt{-1}$ .

The coupled set of equations in Eq. (2) above are usually solved iteratively for  $\mathbf{q}^h$  using nonlinear solvers such as the Newton-Raphson or arc-length continuation methods [45]. Both these iterative solvers employ the alternating frequency time (AFT) procedure [46] to compute the Fourier coefficients of the nonlinear contact force  $\mathbf{F}_{nl}^h$  at each iteration. The AFT utilizes the inverse fast Fourier transform (IFFT) of the normal relative displacements of all contact pairs  $\mathbf{q}_{nl}^h$  to expand the variables into periodic functions in the time domain. The temporal periodic normal force is computed via a contact model such as the one shown in Eq. (3), and then a fast Fourier transform (FFT) is used to calculate its Fourier coefficients assembled in  $\mathbf{F}_{nl}^h$ . In case of frictionless contacts, the compressive normal contact force  $N$  at each contact pair in Figure 1 can be expressed using a well-known approach as

$$N = \max(k_n q_n, 0), \quad (3)$$

where  $k_n$  is the normal contact stiffness [3], and  $q_n$  is the (small) penetration at the contact pairs in contact in the direction normal to the contacting surfaces (in the time domain). The value of  $k_n$  is chosen such that the eigenvalues of the system (in the frequency range of interest) after the application of  $k_n$  to the nodes of the contacting surfaces remain unchanged compared to the eigenvalues obtained when the nodes are rigidly coupled in the direction normal to the surfaces.

### 2.2.3. Model Reduction

Various approaches have been developed in the past to reduce the number of equations governing the dynamics of a structure with intermittent contacts. While most approaches have been successful in reducing the size of the nonlinear DoFs associated with the governing equations via the construction of nonlinear ROMs [42], a frequent drawback is that the size of the ROMs can be significantly large at certain frequencies of interest, and that large size impacts the computation time. In this section, a novel reduction technique is proposed to create frequency-adaptive nonlinear ROMs.

#### 2.2.3.1. Linear modal reduction (CB-CMS)

Linear model reduction techniques such as CB-CMS [33] have been proven to ameliorate the computational demands related to FE model formulations with large DoFs. In general, vector  $\mathbf{q}$  is partitioned into master and slave DoFs, i.e.  $\mathbf{q} = \begin{Bmatrix} \mathbf{q}_m \\ \mathbf{q}_s \end{Bmatrix}$ . Where  $\mathbf{q}_s$  contains the (slave) linear DoFs and  $\mathbf{q}_m$  contains the (master) nonlinear DoFs, i.e. DoFs related to the contact node pairs. The aim of this step is to reduce the sizes of the mass and stiffness matrices and the force vector corresponding to the slave DoFs in Eq. (1). According to the Craig-Bampton fixed-interface mode method, the Ritz coordinate reduction matrix is defined as

$$\begin{Bmatrix} \mathbf{q}_m \\ \mathbf{q}_s \end{Bmatrix} = \mathbf{T}_{CB} \begin{Bmatrix} \mathbf{q}_m \\ \boldsymbol{\alpha}_s \end{Bmatrix}, \text{ where } \mathbf{T}_{CB} = \begin{bmatrix} \mathbf{I} & \mathbf{0} \\ \boldsymbol{\Psi} & \boldsymbol{\Phi}_{CB} \end{bmatrix}, \quad (4)$$

with  $\mathbf{I}$  and  $\mathbf{0}$  being identity and zero matrix respectively.  $\boldsymbol{\Phi}_{CB}$  is referred to as the matrix of fixed interface modes, and contains a selected subset of modes of the model computed with fixed BCs at the master DoFs. The vector  $\boldsymbol{\alpha}_s$  contains the set of generalized coordinates reflecting the amplitudes of the modes in  $\boldsymbol{\Phi}_{CB}$ . Matrix  $\boldsymbol{\Psi}$  contains the interface constrain modes, i.e. the static nodal deflections of the structure due to a unitary displacement of each master DoFs (one at a time)

while constraining the remaining master DoFs to zero. Substituting Eq. (4) into the harmonic governing equation in Eq. (2) and pre-multiplying by  $\mathbf{T}_{CB}^T$  yields

$$[-(h\omega)^2 \mathbf{M}_{CB} + jh\omega \mathbf{C}_{CB} + \mathbf{K}_{CB}] \begin{Bmatrix} \mathbf{q}_m^h \\ \boldsymbol{\alpha}_s^h \end{Bmatrix} = \mathbf{F}_{ps,CB} + \mathbf{F}_{ex,CB}^h + \mathbf{F}_{nl,CB}^h, \quad (5)$$

$$h = 0, 1, \dots, H,$$

where

$$\mathbf{M}_{CB} = \mathbf{T}_{CB}^T \mathbf{M} \mathbf{T}_{CB}, \quad \mathbf{C}_{CB} = \mathbf{T}_{CB}^T \mathbf{C} \mathbf{T}_{CB}, \quad \mathbf{K}_{CB} = \mathbf{T}_{CB}^T \mathbf{K} \mathbf{T}_{CB}, \quad \mathbf{F}_{ps,CB} = \mathbf{T}_{CB}^T \mathbf{F}_{ps}, \quad (6)$$

$$\mathbf{F}_{nl,CB}^h = \mathbf{T}_{CB}^T \mathbf{F}_{nl}^h, \quad \text{and} \quad \mathbf{F}_{ex,CB}^h = \mathbf{T}_{CB}^T \mathbf{F}_{ex}^h.$$

Note that only a selected few modes out of the total fixed interface modes are contained in  $\boldsymbol{\Phi}_{CB}$ . Therefore, the size of  $\boldsymbol{\alpha}_s$  is much smaller than the size of  $\mathbf{q}_s$ , while the size of  $\mathbf{q}_m$  remains unchanged after the transformation.

### 2.2.3.2. Bi-linear modes

Despite the significant level of reduction that could be achieved through the application of methods such as the CB-CMS [33], a typical vibrating system with intermittent contacts can still pose substantial computational challenges arising from the number of nonlinear DoFs present in the EoM. The bi-linear modal reduction offers a convenient solution to this challenge by approximating the nonlinear characteristics (intermittent contacts) of the system through the construction and application of a set of suitable Ritz vectors chosen to approximate the space correlations in the system during its forced response. These vectors are a combination of selected sets of modes of the sliding linear system (referred to as sliding linear modes) and modes of the open linear system (referred to as open linear modes).

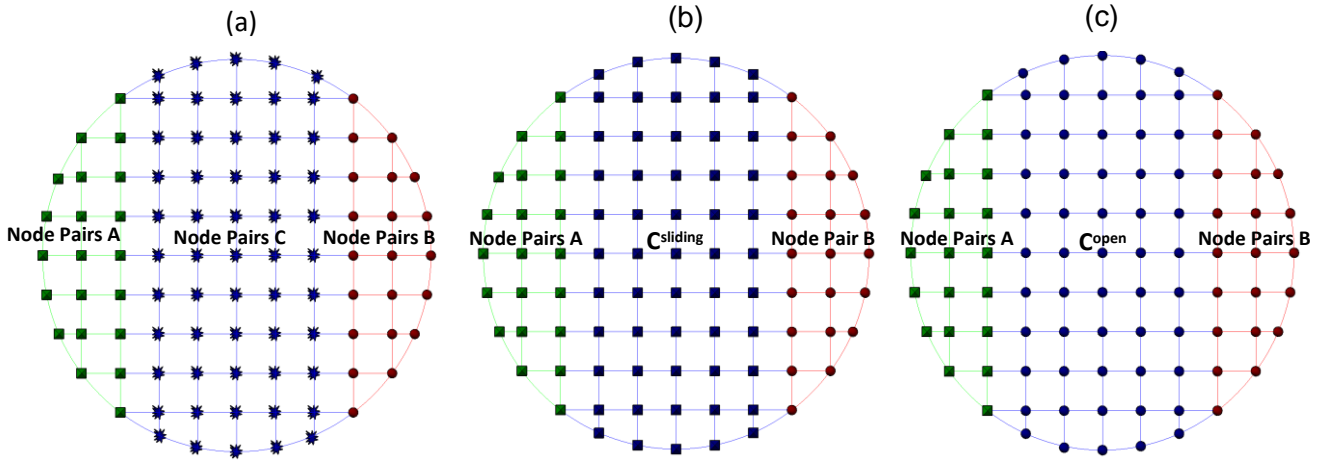


Figure 2. (a) Contact surface with three different types of contact pairs. (b) Contact conditions for the sliding linear system. (c) Contact conditions for the open linear system

Consider the contact conditions at three different contact node pairs in a vibrating system with intermittent contacts shown in Figure 2. Node pair A is representative of part (a) of the contact, i.e. the contact node pairs that are always sliding during vibration, and are shown by symbols ‘■’. Node pair B is representative of part (b) of the contact, i.e. the contact node pairs that are always open during vibration, and are shown by symbols ‘●’. Node pair C is representative of part (c) of the contact, i.e. the contact node pairs that are sometimes sliding and other times open during vibration, and are referred to as switching node pairs. The switching node pairs are shown by symbols ‘★’. The nonlinear contact conditions in Figure 2a can be approximated by using the characteristics of the two linear systems with special BCs shown in Figure 2b and Figure 2c. Specifically, Figure 2b shows the contact condition with all switching node pairs in the sliding state. Figure 2c shows the contact condition with all switching node pairs in the open state.

Once the sliding linear system and the open linear system are defined, BLMs are computed by solving their corresponding eigen-problems expressed as

$$\mathbf{K}_s \mathbf{V}_s = \lambda_s \mathbf{M}_s \mathbf{V}_s \quad \text{and} \quad \mathbf{K}_o \mathbf{V}_o = \lambda_o \mathbf{M}_o \mathbf{V}_o, \quad (7)$$

where  $\mathbf{M}_s$ ,  $\mathbf{M}_o$ ,  $\mathbf{K}_s$  and  $\mathbf{K}_o$  are the mass matrices and stiffness matrices of the sliding and open linear systems respectively,  $\lambda_s$  and  $\lambda_o$  are the eigenvalues of the sliding and open linear systems respectively, and  $\mathbf{V}_s$  and  $\mathbf{V}_o$  are the BLMs. Note that the mass matrices  $\mathbf{M}_s$  and  $\mathbf{M}_o$  are most often equal. The stiffness matrix  $\mathbf{K}_s$  of the sliding linear system is achieved by appropriately augmenting the values of the stiffness matrix  $\mathbf{K}_o$  of the linear open system such that the nodes of each switching contact node pair are coupled via the penalty a large stiffness  $k_n$  in Eq. (1) (for example by using local coordinates  $q_n$  rotated such that they are normal to the contact surface).

### 2.2.3.3. BLM selection algorithm

Building on previous work where BLMs have been used to reduce the size of nonlinear dynamic systems [19,42, 47], a new selection process adopted in this paper, as described next.

First, a frequency-based approach based on the bi-linear frequency (BLF) [8] (for the sliding and open linear systems) is used to select a first set of BLMs. This is done because all BLMs whose natural frequency is close to the frequency of interest  $f_{NLR}$  (i.e., the frequency at which we seek a solution) might contribute to the dynamics of the nonlinear system, and they must be included in the reduction matrix.

Next, the BLMs in  $\mathbf{V}_s$  and  $\mathbf{V}_o$  (see Eq. (7)) are ordered in ascending order of their associated eigenvalues. Then, BLM pairs are created, with one mode from the sliding linear system and the other corresponding mode from the open linear system. The  $n^{th}$  BLM pair includes the  $n^{th}$  mode in  $\mathbf{V}_s$  and the  $n^{th}$  mode in  $\mathbf{V}_o$ . For each BLM pair, a bi-linear frequency range  $\Delta f_n$  is defined as

$$\Delta f_n = [\min(f_{s,n}, f_{o,n}) \quad \max(f_{s,n}, f_{o,n})], \quad (8)$$

where  $f_{s,n}$  and  $f_{o,n}$  are the natural frequencies associated with  $n^{th}$  mode of  $\mathbf{V}_s$  and  $\mathbf{V}_o$ .

Next, a frequency range of interest  $\chi_h$  is defined for each harmonic  $h$  included in the nonlinear forced response process, as

$$(f_{NLR} - \Delta f)h \leq \chi_h \leq (f_{NLR} + \Delta f)h, \quad h = 1, 2, \dots, H, \quad (9)$$

where  $\Delta f$  is a user defined input, which defines the size of the frequency range around  $f_{NLR}$ .

Finally, each bi-linear frequency range  $\Delta f_n$  is compared to each frequency range of interest  $\chi_h$ . If  $\Delta f_n$  has an overlap with any of  $\chi_h$  (for all  $h = 1, 2, \dots, H$ ), then the  $n^{th}$  BLM pair is selected and included in the matrix  $\mathbf{T}$  which contains candidate BLMs, namely

$$\mathbf{T} = [ \mathbf{V}_{s,1}, \mathbf{V}_{s,2}, \dots, \mathbf{V}_{s,n_{max}}, \mathbf{V}_{o,1}, \mathbf{V}_{o,2}, \dots, \mathbf{V}_{o,n_{max}} ], \quad (10)$$

where  $n_{max}$  is the largest index of BLM pairs included in  $\mathbf{V}_s$  and  $\mathbf{V}_o$ .

Once all pairs of BLMs that fit the frequency criteria are included in  $\mathbf{T}$ , the algorithm proceeds to the next stage of selection described in the next section. Note that the size of the candidate BLMs in  $\mathbf{T}$  might vary depending on the magnitude of  $\Delta f$  in Eq. (9). The potential effects (notably the possibility of including excessively many modes in  $\mathbf{T}$ ) are addressed in the next section.

#### **2.2.3.4. Frequency-adaptive reduction (FAR)**

Previous approaches adopted in predicting the dynamics of systems with intermittent contacts over a certain frequency range of interest use the idea that the nonlinear response is dominated by a set of bi-linear modes in that frequency range. Hence, it is assumed that the two sets of contact BCs for generating the reduction matrix applied during a frequency sweep are the same at all frequencies. However, it is often the case that the contact BCs change with frequency. Thus, not only do the contact conditions of structures with intermittent contact vary with time, but they vary

with frequency also. In addition, being able to accurately represent the three parts (sliding, open and switching) of the contact area at each frequency can significantly improve the convergence and accuracy of the forced response analysis.

Next, we propose a frequency-adaptive technique. The main idea is to construct a reduction matrix that can be updated easily at every frequency and readjusted to be applied at the next frequency. The first step is to initialize the reduction matrix  $\Phi$  with BLMs computed by assuming a completely sliding contact surface (at the first frequency in the analysis) as described in Eq. (11). This initialization is based on the observation that most analyses start at a frequency away from the resonant frequency so that the response amplitude of the system is low at the first frequency in the analysis, therefore keeping the switching contact conditions at that frequency in the sliding state. Hence, at the initialization

$$\Phi = [ \mathbf{V}_{s,1}, \mathbf{V}_{s,2}, \dots, \mathbf{V}_{s,n_{max}} ]. \quad (11)$$

At subsequent frequencies in the frequency sweep, the reduction matrix is updated using BLMs calculated from the contact conditions of the previous frequency. Herein, this procedure is referred to as the modal selection criterion (MSC). The MSC algorithm for updating the reduction matrix  $\Phi$  allows the addition of modes which are linearly independent of the modes already contained in  $\Phi$  by projecting each candidate column  $\mathbf{T}_i$  (all columns, considering one column at a time, starting with  $i = 1$ ) from the candidate BLMs in matrix  $\mathbf{T}$  defined in Eq. (10) onto the current reduction matrix. This projection is performed by (least squares) solving the following linear equation for  $\mathbf{k}_i$

$$\Phi \mathbf{k}_i = \mathbf{T}_i. \quad (12)$$

The relative residual  $r_i$  of Eq. (12) is computed as



$$r_i = \frac{\|\mathbf{T}_i - \Phi \mathbf{k}_i\|}{\|\mathbf{T}_i\|}, \quad (13)$$

where  $\|\cdot\|$  is the  $L_2$  norm operator. The residual  $r_i$  is compared to a user-defined threshold  $\varepsilon_1$ , a positive value less than 1 ( $\varepsilon_1 < 1$ ). If  $r_i > \varepsilon_1$ , the candidate BLM being projected is added to the reduction matrix  $\Phi$  before proceeding to the next BLM candidate. Otherwise,  $\Phi$  remains the same. This procedure guarantees the full rank of the reduction matrix by avoiding the inclusion of linearly dependent BLMs.

Equation (2) includes not only harmonic terms, but also a static term ( $0^{th}$  harmonic), which deserves special attention. In many applications, pre-stress exists in structures before vibrations occur. Pre-stress can be due to the assembly process, static forces, thermal gradients, etc. In such cases, the static deflection of the structure can be spatially uncorrelated to its dynamic response. As a consequence, BLMs in  $\Phi$  are likely not representing well the static deflection of the structure, and that can have negative consequences on the accuracy of the ROM [19]. To improve the ROM accuracy, the reduction basis of the  $0^{th}$  harmonic term is augmented by including the static deflection of the structure  $\mathbf{q}_{ps}$  due to pre-stress.  $\mathbf{q}_{ps}$  is obtained by solving

$$\mathbf{K}\mathbf{q}_{ps} = \mathbf{F}_{ps} + \mathbf{F}_{nl}. \quad (14)$$

The reduction matrix becomes

$$\Phi_o = [\Phi \ \mathbf{q}_{ps}]. \quad (15)$$

The governing EoMs of the ROM in the frequency domain can be expressed as

$$\mathbf{k}_o \mathbf{p}^0 = \mathbf{f}_{ps} + \mathbf{f}_{ex}^0 + \mathbf{f}_{nl}^0, \quad (16)$$

$$[-(h\omega)^2 \mathbf{m} + jh\omega \mathbf{c} + \mathbf{k}] \mathbf{p}^h = \mathbf{f}_{ex}^h + \mathbf{f}_{nl}^h, \quad h = 1 \dots, H,$$

where

$$\begin{aligned}
\mathbf{k}_o &= \Phi_o^T \hat{\mathbf{K}} \Phi_o, \quad \mathbf{p}^0 = \Phi_o^T \hat{\mathbf{q}}^0, \quad \mathbf{f}_{ps} = \Phi_o^T \hat{\mathbf{F}}_{ps}, \quad \mathbf{f}_{ex}^0 = \Phi_o^T \hat{\mathbf{F}}_{ex}^0, \quad \mathbf{f}_{nl}^0 = \Phi_o^T \mathbf{F}_{nl}^0, \\
\mathbf{m} &= \Phi^T \hat{\mathbf{M}} \Phi, \quad \mathbf{c} = \Phi^T \hat{\mathbf{C}} \Phi, \quad \mathbf{k} = \Phi^T \hat{\mathbf{K}} \Phi, \quad \mathbf{p}^h = \Phi^T \hat{\mathbf{q}}^h, \quad \mathbf{f}_{ex}^h = \Phi^T \mathbf{F}_{ex}^h, \\
\mathbf{f}_{nl}^h &= \Phi^T \mathbf{F}_{nl}^h,
\end{aligned} \tag{17}$$

with

$$\hat{\mathbf{M}} = \mathbf{M}, \quad \hat{\mathbf{C}} = \mathbf{C}, \quad \hat{\mathbf{K}} = \mathbf{K}, \quad \hat{\mathbf{q}} = \mathbf{q}, \quad \hat{\mathbf{F}}_{ps} = \mathbf{F}_{ps}, \quad \hat{\mathbf{F}}_{ex} = \mathbf{F}_{ex}, \tag{18}$$

if the full FE model is used for the BLMs calculation, and

$$\hat{\mathbf{M}} = \mathbf{M}_{CB}, \quad \hat{\mathbf{C}} = \mathbf{C}_{CB}, \quad \hat{\mathbf{K}} = \mathbf{K}_{CB}, \quad \hat{\mathbf{q}} = \mathbf{q}_{CB}, \quad \hat{\mathbf{F}}_{ps} = \mathbf{F}_{ps,CB}, \quad \hat{\mathbf{F}}_{ex} = \mathbf{F}_{ex,CB}, \tag{19}$$

if a CB-CMS reduced model is used instead (Appendix A provides details about CB-CMS).  $\mathbf{M}_{CB}$ ,  $\mathbf{C}_{CB}$ , and  $\mathbf{K}_{CB}$  are the mass, viscous damping and stiffness matrices and  $\mathbf{F}_{ps,CB}$ , and  $\mathbf{F}_{ex,CB}$  are the pre-stress and excitation force vectors in the CB-CMS coordinates.

Evidently, repeating the MSC procedure at every frequency within the frequency range of interest will gradually increase the size of matrix  $\Phi$  such that the ROM size at later frequencies will become large. Thus, a modal participation criterion (MPC) is established to address this challenge. The proposed MPC algorithm is designed such that BLMs with relatively low contribution in the forced response of the system at a certain frequency are eliminated from the reduction matrix  $\Phi$  before its application in the MSC procedure at the following frequency. The condition to eliminate a projection vector  $i$  (namely column  $i$  of the projection matrix  $\Phi$ ) used in MPC is expressed as

$$\frac{|p_i^h|}{\|\mathbf{p}^h\|_\infty} < \varepsilon_2, \quad \forall h = 0, 1, \dots, H, \tag{20}$$

where  $p_i^h$  is the  $h^{th}$  harmonic modal amplitude of projection vector  $i$  in the reduction matrix  $\Phi$ .  $\mathbf{p}^h$  is the  $h^{th}$  harmonic modal amplitude vector.  $| \cdot |$  denotes the absolute value, and  $\| \cdot \|_\infty$  represents

the infinity norm. Using Eq. (20), projection vectors which correspond to subspaces where the response of the system is very low are discarded, which can lower the size of the ROM at subsequent frequencies.

The combination of MSC and MPC allows the adaptation of the ROM to contain only modes that are more likely to contribute to the prediction of the system's dynamics. Also, the possible effect of a large  $\Delta f$  to increase the size of the ROM is controlled via the MPC algorithm. Figure 3 shows the outline of the reduction method highlighting the MSC and MPC algorithms.

As a consequence of the variation of the reduction matrix  $\Phi$  from frequency to frequency, the modal amplitude vector  $\mathbf{p}$  also changes meaning. This poses a slight challenge for the arc-length continuation solver, which uses the solution at the previous frequency as an initial guess to seek the solution at the current frequency. To address this issue, denote by subscript  $(k)$  quantities computed at frequency step  $k$ . For each harmonic, an initial guess  $\tilde{\mathbf{p}}_{(k)}^h$  is created at frequency step  $k$  by using the solution  $\mathbf{p}_{(k-1)}^h$  at frequency step  $k - 1$ . The initial guess  $\tilde{\mathbf{p}}_{(k)}^h$  is obtained by first calculating an initial guess  $\tilde{\mathbf{q}}_{(k)}^h$  in the physical coordinates in the frequency domain. Specifically,  $\tilde{\mathbf{q}}_{(k)}^h$  is chosen to be equal to the computed response in physical coordinates at frequency step  $k - 1$ . Thus,  $\tilde{\mathbf{q}}_{(k)}^h = \mathbf{q}_{(k-1)}^h$ . Since  $\tilde{\mathbf{q}}_{(k)}^h = \Phi_{(k)} \tilde{\mathbf{p}}_{(k)}^h$  and  $\mathbf{q}_{(k-1)}^h = \Phi_{(k-1)} \mathbf{p}_{(k-1)}^h$ , one obtains

$$\tilde{\mathbf{p}}_{(k)}^h = \Phi_{(k)}^{-1} \Phi_{(k-1)} \mathbf{p}_{(k-1)}^h, \quad h = 0, 1, \dots, H, \quad (21)$$

where  $\Phi_{(k)}^{-1}$  is the pseudo-inverse of the reduction matrix at current frequency step. Unlike previous reduction methods, FAR is suitable for predicting the forced response of a system with multiple nonlinear resonances existing within the frequency range of interest.

### 2.3. Results

In this section, we explore the efficacy of the proposed method in predicting the dynamics of a rectangular plate with a breathing crack, the dynamics of two co-axial cylinders where one is partially inserted into the other and the nonlinear behavior of a 3-legged jackup platform. The validity and the computational efficiency of the results obtained from the approach in comparison with a standard reduction approach is discussed. A CB-CMS model with nonlinear active DoFs at all interface contact points and without any further reduction is used as the benchmark to validate the proposed approach.

The first results presented are for systems without pre-stress, where the proposed ROMs are compared with the full order analysis. Given that the primary objective of this study is to devise a method for the reduction of the nonlinear DoFs in the governing EoMs, CB-CMS is used as an initial reduction method in subsequent analyses. Observe that the switch from the full model to the CB-CMS reduced model is only to alleviate the unnecessary computational demand associated with the application of the full order model, and therefore has no impact on the quality of the results obtained with FAR and BLMs.

CB-CMS is used to reduce the DoFs which are not on the contact surfaces while retaining as master DoFs all the other DoFs. For this study, CB-CMS is applied in ANSYS, and the resulting mass and stiffness matrices are exported to MATLAB for the nonlinear analysis. With the possibility of having multiple solutions within a frequency range, as is common in nonlinear solutions, the arc-length continuation solution method is used to solve the nonlinear governing equations in all cases.

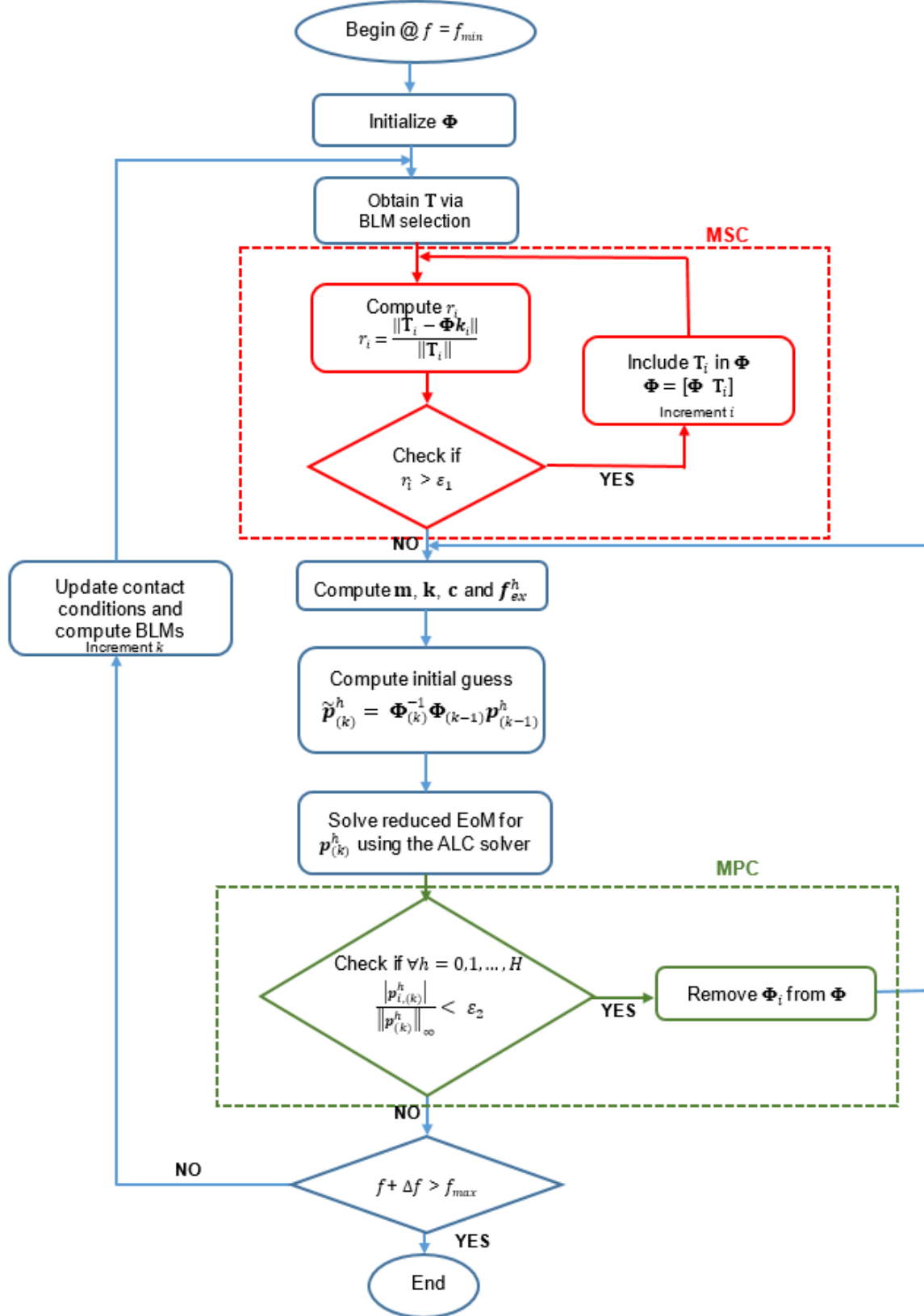


Figure 3. The frequency-adaptive reduction (FAR) strategy (ALC represents arc-length continuation)

### 2.3.1. Cracked Plate

The first case to apply the FAR and BLM reduction described in the previous sections is a rectangular cracked plate. Figure 4 shows the geometric configuration of the plate with a lateral crack, highlighted by the thick line in the mid-height of the plate. The material properties of the plate include the Young's modulus  $E = 2.0 \times 10^5$  MPa, Poisson's coefficient  $\nu = 0.3$ , and density  $\rho = 7,800$  kg/m<sup>3</sup>. The plate is modelled in ANSYS using linear solid elements with 8,230 DoFs. For this application case, the nodal normal contact stiffness used is  $k_n = 2.25 \times 10^7$  N/m. Note that tangential forces in this case do not affect the response of the plate significantly within our frequency range of interest because the modes in this range primarily involve the normal separation of the crack rather than its transverse/slip motion.

The crack is modeled with 40 contact pairs whose nodes together with the pre-stress, forcing and response nodes form the master DoFs, and the remaining nodes constitute the slave DoFs. The total number of DoFs involved in the nonlinear solution is 417. For this this model, our attention is focused on the in-plane bending mode of the plate (4<sup>th</sup> mode). The system is excited as shown in Figure 4. Note that the slip motion between contact node pairs is negligible. Also, a distributed compressive static force, acting as a pre-stress load, is applied at the top of the plate, and the contact condition of the plate at rest is such that all the contact node pairs are in the sliding state (Figure 4). Figure 5 shows the first four frequencies and the corresponding linear modes of the plate with open contact conditions.

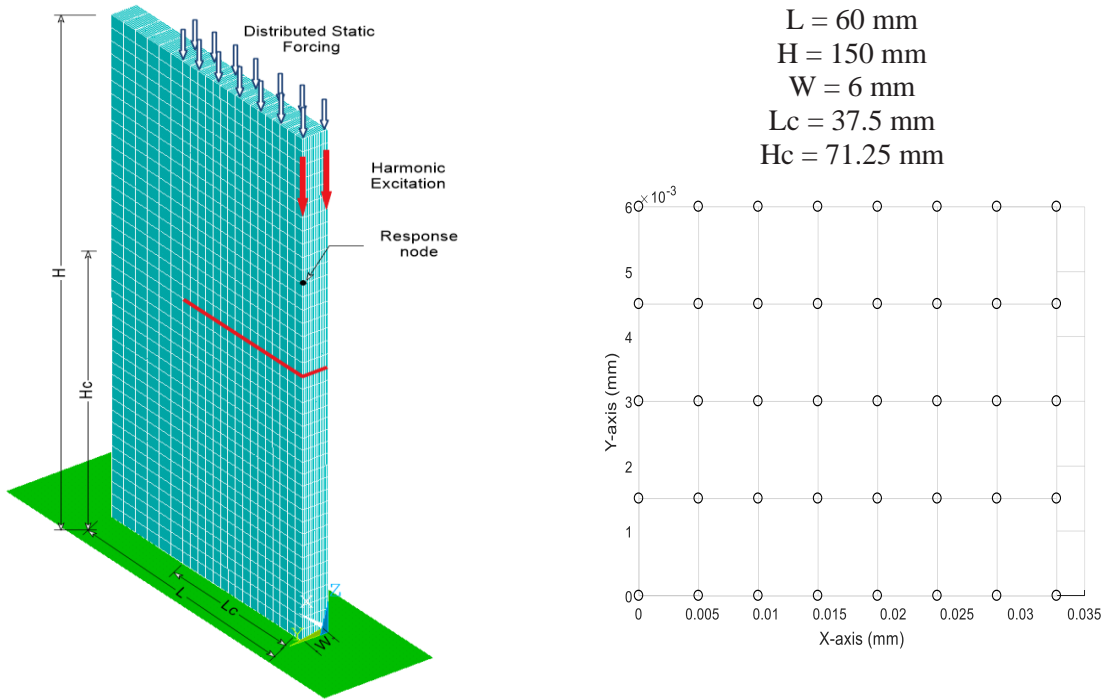


Figure 4. Cracked plate: geometry and pre-stressed contact conditions

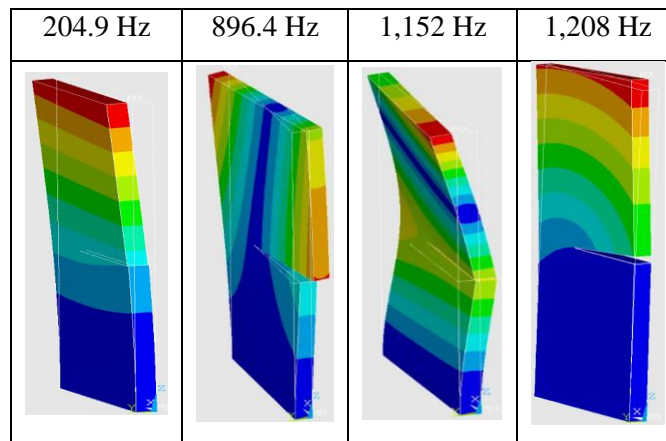


Figure 5. First four modes of the open linear system (cracked plate)

The mode selection for the ROM is applied at every frequency with the frequency approach based on the BLF selection and the MSC. The MSC value  $\epsilon_1$  used for this analysis is  $5 \times 10^{-4}$ . This value is high enough to remove linearly dependent BLMs. Note that this step is an efficient step that substitutes SVD for ROM conditioning. Unlike conditioning via SVD, the MSC conditions the ROM while keeping the original BLMs in the reduction matrix used to construct the ROM.

Hence, an addition/removal of columns in the reduction matrix is simply an addition/removal of rows and columns in the ROM matrices.

The MPC algorithm is applied also at each frequency step. The MPC value  $\varepsilon_2$  used for this analysis is  $1 \times 10^{-3}$ . This value adjusts the size of the ROM by removing modes from  $\Phi$  with negligible response magnitude. The value chosen for  $\varepsilon_2$  is sufficiently small to eliminate less participating BLMs from the ROM. Thus, the number of nonlinear equations to be solved at any given frequency step can be reduced. Such a reduction occurs especially at frequency steps after a resonance. Both  $\varepsilon_1$  and  $\varepsilon_2$  were selected after a quick convergence analysis on the system with low amplitude forcing and zero pre-stress.

The nonlinear forced response within the frequency range of the first in-plane bending mode is shown in Figure 6. Circles indicate results obtained with CB-CMS, which are the reference results. The SVD acronym refers to results obtained using the singular value decomposition to condition the ROM. In that approach, SVD is applied to reduce the size of the reduction matrix used to construct the ROM. FAR refers to results obtained using the proposed FAR approach (combining MSC and MPC).

At frequencies far from resonance, the solution accurately predicts the contact surface to be in the completely sliding state. At these frequencies, only two BLMs are required to reduce the dynamic equations. As the system approaches the resonant frequency, the number of switching contact node pairs that alternate between liftoff/sliding states during each vibration cycle increases as shown in Figure 7. At resonance, all contact node pairs are switching (for the magnitude of forcing considered), and the maximum ROM size (which consists of 18 BLMs) is used to transform the dynamic equations at this frequencies near resonance. At even higher frequencies, the size of the ROM gradually decreases as the response amplitude decreases, to a minimum size of 6 BLMs



at frequencies when all the contact nodes return to the sliding state.

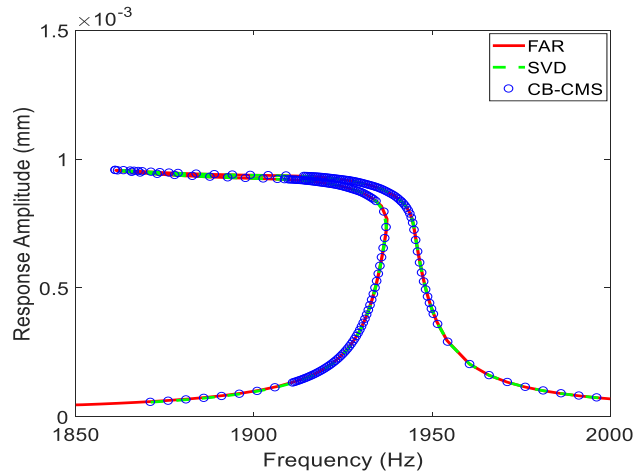


Figure 6. First in-plane bending response of the cracked plate with pre-stress

As expected in intermittent nonlinear contact systems under pre-stress, the forced response curve exhibits a softening behavior. The softening is very significant in this model because of the complete liftoff of all the contact node pairs at frequencies around the resonant frequency. Multiple solutions are also apparent at frequencies between 1,860 Hz and 1,925 Hz.

### 2.3.2. Co-axial Cylinders

A second application of the proposed approach considers two coaxial cylinders slightly overlapped at one of their ends. Both cylinders are fixed at their other ends and at two nodes each along the length of the cylinders, as shown in Figure 8. This type of setup is similar to some section in the hull-leg assembly of some offshore structures.

As a first analysis, a harmonic transverse force is applied to the node labelled F1 on cylinder 2, and the forced response is computed at the node labelled R1 on cylinder 1. First, we consider the case where there is zero pre-stress on the overlapping surfaces. This analysis is useful to study the system response around its first resonance to identify possible ranges of values for  $\varepsilon_1$  and  $\varepsilon_2$  required for the MSC and the MPC algorithms as well as to determine the sufficient number of

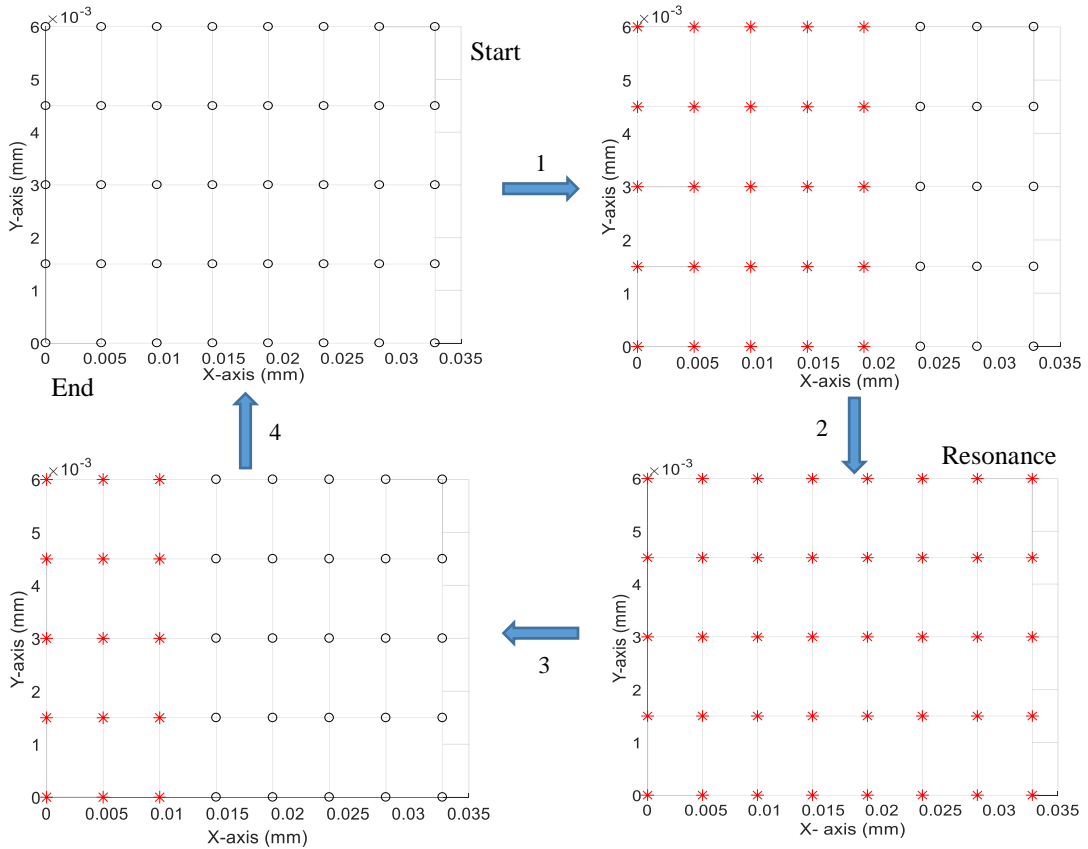


Figure 7. Changes in the contact area over frequency for a cracked plate ('o' indicates sliding node pairs, and '\*' indicates switching node pairs)

harmonics needed for convergence. Five harmonics were deemed sufficient and retained in the HMB. The values of  $\epsilon_1$  and  $\epsilon_2$  used for this analysis are  $5 \times 10^{-5}$  and  $1 \times 10^{-3}$  respectively.

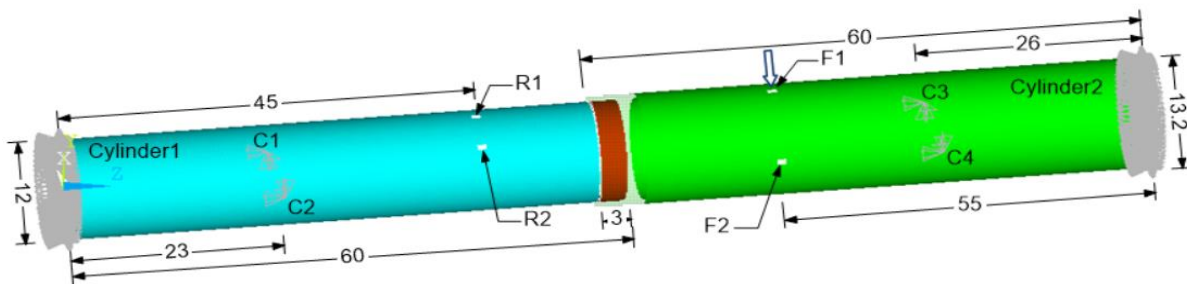


Figure 8. Two co-axial cylinders (dimensions are in mm)

Note that even though  $\epsilon_1$  and  $\epsilon_2$  are not necessarily limited to specific values,  $\epsilon_1$  must be large enough to avoid singularity of the reduction matrix, and  $\epsilon_2$  must be small enough to retain only relevant modes in the ROM.

To begin the mode selection process, the BLF modal selection procedure was used as a preliminary process to identify potential candidates from the modes obtained from the linear systems with sliding and open BCs at the contact. The modes resulting from this process are then considered and re-selected in the MSC algorithm.

The MSC procedure described in the previous section is used to select candidate modes to be included in the ROM at every frequency. For the zero pre-stress case, the first four modes of the linear system with complete sliding BCs were used to initialize the selection process. The purpose of choosing so many modes rather than just one or two is to probe the effectiveness of the  $\varepsilon_2$  value used in the MPC algorithm, and to ascertain the elimination of unresponsive modes. It is important to note that the frequency range from which the preliminary candidate modes are selected in our approach via the BLF selection procedure does not necessarily need to be very narrow.

As shown in Figure 9 (left), the nonlinear forced response of the assembly via the FAR method accurately describes the vibration of the system with less than 0.05% error in amplitude, and less than 0.02% error in frequency at resonance.

To further challenge the proposed approach, a second analysis involving an initial pre-stress of the contact surface is carried out. For this analysis, static forces are applied on the contact nodes of cylinder 1 in the outward radial direction. This action induces a stress on the contact surface, therefore keeping all the contact node pairs in the complete sliding state before vibration. The forced response of the assembly was obtained by a procedure similar to the case of zero pre-stress, and is shown in Figure 9 (right). The number of contact node pairs converting from the sliding state to the switching state gradually increases as the frequency increases and the expected

softening effect is manifest around the resonant frequency where about 65% of the contact node pairs are in the switching state.

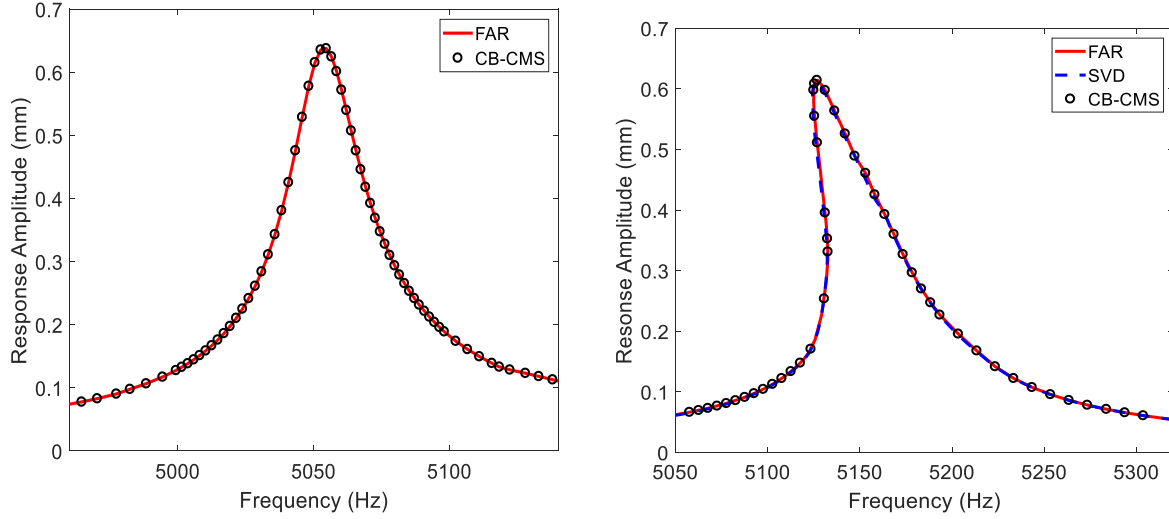


Figure 9. First bending response of the two coaxial cylinders without pre-stress (left) and with pre-stress (right)

As shown in Figure 10, at the beginning of the analysis when the frequency is low, all 256 contact pairs are in sliding during the entire vibration, and hence only 4 modes are sufficient to predict the response at these frequencies. As more contact node pairs start to switch, the size of the ROM grows up to 55 modes at the resonant frequency. Beyond the resonant frequency, the ROM gradually decreases in size as switching node pairs return to the sliding state. The ROM has 18 modes when all the contact nodes are back to the sliding state. Note that there are more modes at the end of the analysis than at the beginning of the analysis although the contact conditions are similar in both situations. The reason is that higher frequency modes start to be involved in the vibration of the system as the frequency increases. The higher frequency modes are not included at the beginning of the analysis where they are not involved.

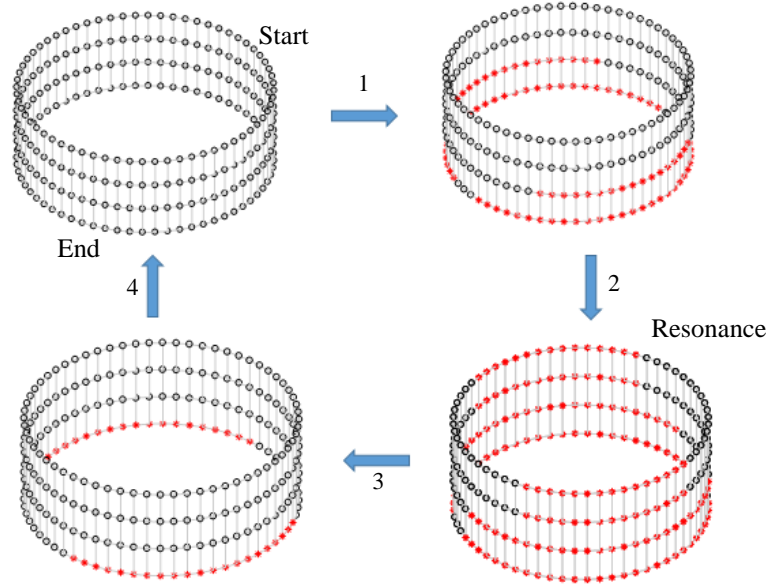


Figure 10. Changes in the contact area over frequency for the two coaxial cylinders with pre stress ('o' indicates sliding node pairs, and '\*' indicates switching node pairs)

A parametric study of the novel approach is carried out by varying  $\varepsilon_2$ , which regulates the size of the ROM at every frequency step. Relatively high  $\varepsilon_2$  values result in smaller ROM sizes both at and beyond the resonant frequency, which correspond to shorter computational time. However, results show that the errors accrued are significant. An optimal value of  $1 \times 10^{-3}$  was used for  $\varepsilon_2$  in this analysis which gives a solution with good balance between the ROM size (55 modes at resonance, and 18 modes on completion) and the predicted error (0.02% error in frequency, and 0.04% error in amplitude).

A second analysis is carried out to further explore the effectiveness of the proposed approach. In this case, the analysis is done over a wide range of frequency with the system excited to propagate multiple resonances. To excite the first few resonant frequencies, the axial symmetry

Table 1. Parametric study on the MPC value  $\varepsilon_2$  for the two co-axial cylinders with pre-stress

MPC value $\varepsilon_2$	ROM Size			% Error at Resonance	
	Start	Resonance	End	Amplitude	Frequency
$1 \times 10^{-4}$	4	88	32	0.04	0.02
$1 \times 10^{-3}$	4	55	18	0.04	0.02
$1 \times 10^{-2}$	4	39	16	1.20	1.00
$5 \times 10^{-2}$	4	30	15	5.40	4.80

of the system is broken by adding the constraints labeled C1 through C4 shown in Figure 8. The first four modes of the system are shown in Figure 11 (top) together with their natural frequencies. The system is excited at nodes F1 and F2 shown in Figure 8 with similar forcing magnitude, but with  $90^\circ$  phase difference. The forced response is tracked at nodes R1 and R2, and the multiple excited resonant frequencies are shown in Figure 11 (bottom). From a computational point of view, it is better to begin the simulation from the upper limit of the frequency range to ensure that the size of the ROM applied at frequencies between distant resonances (5,230 Hz to 11,959 Hz in this case) is minimal. The size of the ROM is sampled at 7 frequencies labelled A through G. Figure 13 shows the ROM sizes at these 7 frequency locations. The results in Figure 12 show the variation of the ROM size over frequency, which demonstrates the adaptability of the ROM to contain only the modes needed at each frequency.

### 2.3.3. Jackup Platform

The coaxial cylinders analyzed in the previous section up can be found in the hull-leg assembly of fixed offshore structures like such as jackup platforms [48,49]. To further demonstrate the applicability of the FAR approach for structures with higher geometric complexity, a 3-legged

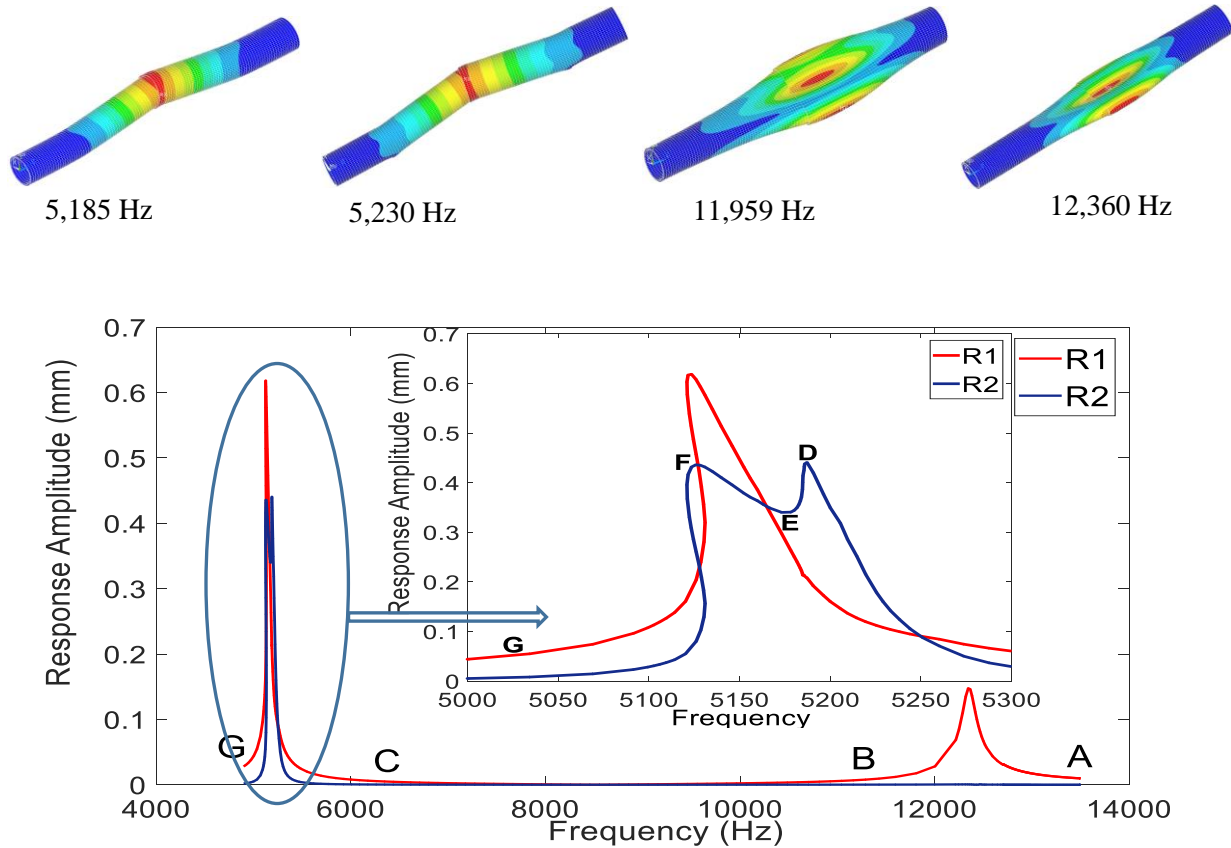


Figure 11. First four modes of the two co-axial cylinders (top), and the forced response obtained using FAR applied to multiple resonance excitation of the two co-axial cylinders with pre-stress (bottom)

jackup platform (shown in Figure 13) is investigated. The bottom ends of the legs are connected to the seabed and thus we model them as fixed to the ground. The triangular hull is attached to the 3 legs which can be moved axially with respect to the hull (allowing for raising or lowering the legs).

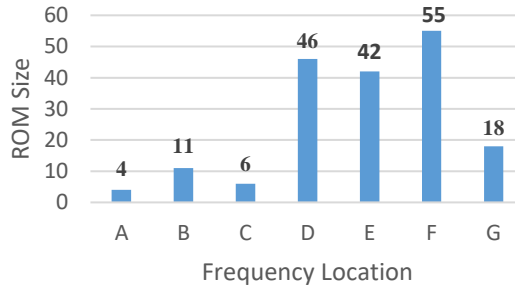


Figure 12. Variation of ROM size over the multiple frequency locations A-G shown in Figure 11

In this analysis we consider that the connection between the hull and one of the legs exhibits intermittent contacts. Specifically, we consider that separation and sliding (i.e., intermittent contact) may occur at the interface between the hull and the third leg. We further consider that the leg is assembled to the hull with radial prestress. Thus, intermittent contact node pairs exist at the contact interface on leg 3. To simulate hydrodynamic loads, the system is harmonically excited at points A and B. Figure 14 (top) also shows three modes of the platform dominated by leg bending. The first two modes (left and center) are for the fully open contact node pairs, and the third mode (right) is for the fully sliding contact node pairs. Figure 12 (bottom) shows the resulting nonlinear response at point C (shown in Figure 11) obtained using the FAR method and the conventional CB-CMS.

Similar to the cases of the cracked plate and co-axial cylinders discussed in sections 3.1 and 3.2, the platform vibrates with low amplitude and closed contacts at low non-resonant frequencies. As the frequency increases, the number of contact node pairs that switch (from sliding to open) during each vibration cycle increases until the resonance is reached. This explains the softening behavior observed in the forced response curve shown in Figure 14 (bottom). At frequencies higher than the



resonant frequency, the system continues to harden as the number of switching node pairs decreases until all contact node pairs return to being closed during the entire vibration cycle.

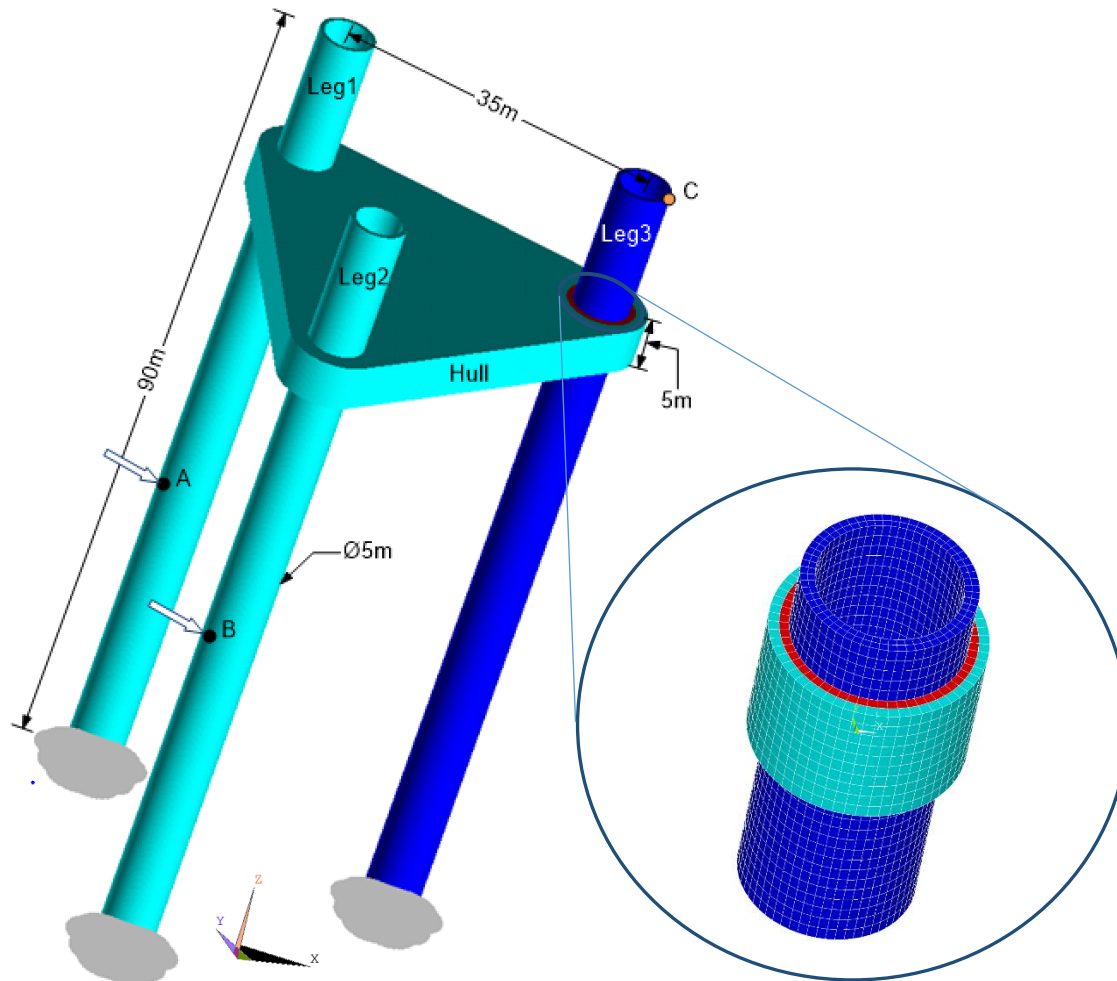


Figure 13. Jackup platform model with local intermittent contacts at then interface between the hull (triangular shape) and leg 3.

The platform is modelled with over 700,000 DoFs. That model was reduced to 6,078 DoFs by the CB-CMS reduction (applied only to the DoFs not involved in the contact) and without any BLM reduction. Application of the FAR approach with similar MSC and MPC values as in the case of the coaxial cylinders, resulted in a ROM size of 2 at states when the contact node pairs are fully sliding and a maximum ROM size of 61 at resonance.

### 2.3.4. Computational Efficiency

Since ROMs require calculation time for their generation, the use of ROMs is most frequently justified if they allow for higher computational efficiency with respect to state-of-the-art approaches, like full FE models or classical reduction techniques, like CB-CMS, commonly implemented in commercial software.

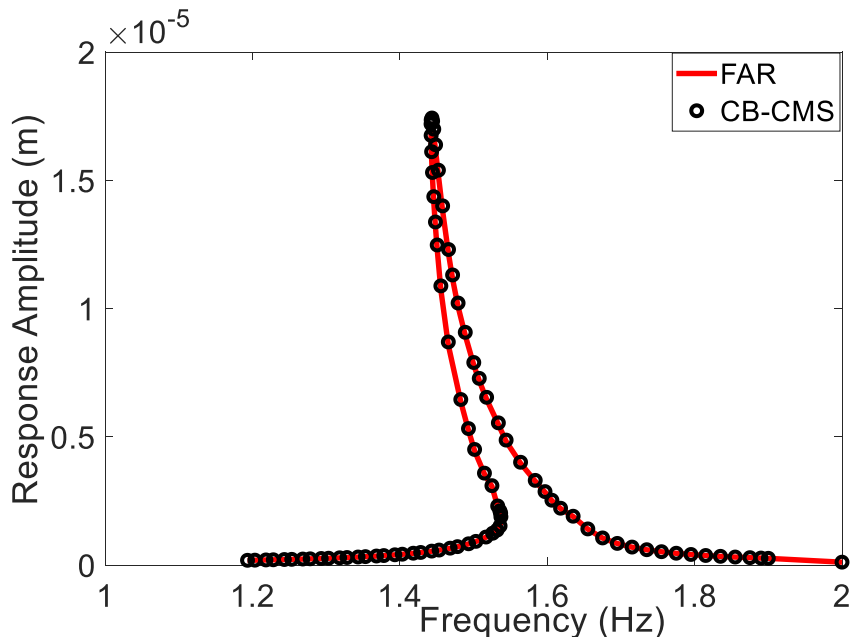
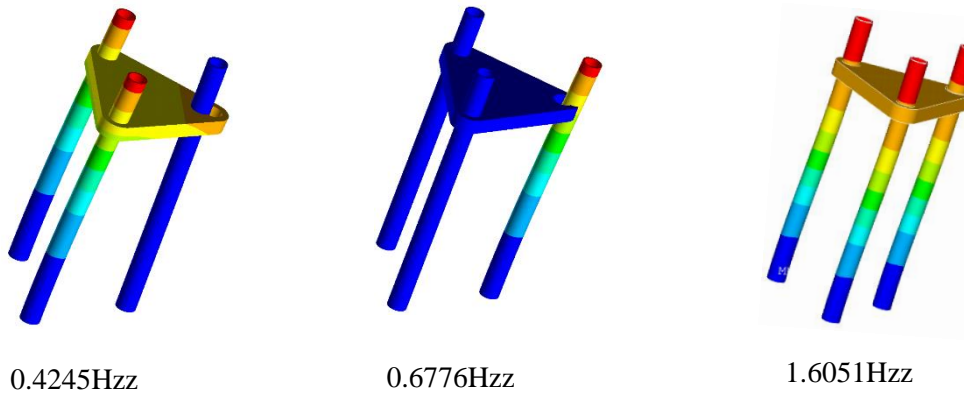


Figure 14. The top 3 images show two modes of the jackup platform with fully open contact (left and center), and one mode with fully sliding contact; the bottom plot shows the amplitude of the nonlinear response of the jackup platform at point C obtained using two computational methods (FAR and CB-CMS)

To examine the computational effectiveness of the proposed approach, the average calculation time per iteration for other approaches, namely the reference CB-CMS approach and the approach based on SVD reduction, are computed over the same frequency range (Table 2).

Table 2. A comparison of CPU times (seconds)

Pre-stressed Cases	CB-CMS (Reference)	SVD Conditioning	FAR
Rectangular Plate	15	1.8	0.5
Co-axial Cylinders	1221	184	56

Both the SVD conditioning and the FAR approach utilize the BLM reduction, and hence they are relatively fast. The FAR approach gains a significant time advantage over the SVD conditioning approach and even more so over the CB-CMS approach because the ROM applied in the reduction process is adapting depending on the changes in the contact conditions at every frequency. Therefore, the excess computational time consumed by the presence of less participating modes in the ROM is eliminated.

## 2.4. Conclusions

A reduced order modelling strategy was presented to analyze the dynamics of structures with intermittent contacts. In this approach, the state-of-the-art HBM was used to transform the governing equations of motion from the time to the frequency domain, and generalized bi-linear modes that correspond to normal modes of linear systems with special boundary conditions at the contact surfaces were applied to reduce the number of equations of motion. The proposed method is characterized by an adaptive strategy, namely frequency-adaptive reduction, used to determine adaptively the extent of the contact area during vibration. The modal participation factor and modal

selection criteria algorithms were developed to automatically update and select the optimal size of the ROM needed for the reduction strategy at every frequency step.

The proposed reduction method was applied to two systems exhibiting vibrations with and without pre-stress. The results demonstrate the accuracy of the resulting adaptive ROMs in predicting the nonlinear forced response of the system in broad frequency ranges. The use of the frequency-adaptive ROM rather than a constant ROM approach or the classical CB-CMS approach allows significant computational time savings without significant loss of accuracy. The proposed method is able to accurately predict both softening and hardening behaviors expected for contacts that are initially open or initially sliding. Even though the method was shown as applied to specific cases, it can also be extended to other complex geometric applications with localized intermittent contacts since the physics of the dynamics is expected to be similar.

## **CHAPTER III**

### **3. Nonlinear Substructuring for Multiple Intermittent Contacts: FAR**

#### **Approach**

##### **3.1. Introduction**

The design and analysis of various structural applications have continued to evolve over the years as the interest in predicting the behavior of recent and complicated systems grows. An example of such situation include understanding the dynamics of structures with multiple intermittent contact such as cracks, joints, or combination of both. Structural application of such systems include, but not limited to, turbine blades with multiple cracks, hull-legs interactions of a Jackup platform etc. Obtaining solutions of these highly nonlinear systems usually require fine model discretization especially around the neighborhood of the contact interfaces and also require efficient iteration techniques to handle the high volume of iteration associated with nonlinear mathematical models. The computational capacity needed to solve these problems is high and limited despite growing computing capacities in recent years. These limitations make model order reduction techniques an important research focus in the field of structural dynamics.

The conventional component mode synthesis (CMS) [50][51][52] has been adopted in the past to tackle some of these challenges through modal reduction and assembly of substructured components, which can lead to a very large finite element system. Several other improved

approaches of this technique has been suggested to accommodate special variabilities [53], however handling systems with multiple contact nonlinearities via substructuring techniques can be further explored. The present work is directed at contributing to the endeavors of the structural dynamic community in providing novel and efficient reduced-order modelling techniques well suited to the study of large systems with local intermittent contact nonlinearity. In this work, we introduce a method relying on a substructuring approach to benefit from the flexibility of standard CMS techniques. The main feature of this method combines the bilinear reduction of local contact nonlinearities using the frequency adaptive reduction (FAR) with a modified interface characteristic constraint reduction to handle systems with multiple local nonlinearities.

The steady-state response of the nonlinear system will be obtained using the harmonic balance method (HBM). The HBM has already shown its high analytical efficiency in obtaining the nonlinear forced response of structures with local contact nonlinearities [54]. The main challenge of HBM is that the size of the nonlinear equations is increased by a factor equal to the number of retained harmonic coefficients. In spite of this, the HBM is preferable to traditional time iteration methods used to solve nonlinear systems e.g. using Runge-Kutta, Newmark approach [55] because of their computational constraint for the dynamic analysis of large FE structures, since small time steps are always required for capturing high frequency dynamics on contact interfaces [56]. Therefore, a preferable approach to solve these nonlinearities in a large assembly using HBM is to reduce the model size by several orders of magnitudes via reduced order modeling (ROM) techniques [46]. It is however worthy of note that it is generally impossible to generate a closed form equation for the harmonic expression of nonlinear forcing functions that are included in the frequency domain HBM equations. The alternating frequency-time technique (AFT) [6][46] has been previously proposed to address this issue. This conventional practice [57-67] involve the

numerical computation of the nonlinear forces in the time domain as a function of displacements using Fourier transforms, augmentation of the result as may be necessary, and finally converting back into the frequency domain using inverse Fourier transform.

The component mode synthesis (CMS) techniques have been severally applied toward the modal reduction of large scaled linear and nonlinear structures. The type of the technique differs by the method of development and selection of the Ritz vectors used to perform the model reduction. Hurty and Craig-Bampton being early developers of this technique employed the fixed interface vibration modes [[52] [68] to reduce components of linear systems. Both methods are very efficient in the order reduction of large systems with localized nonlinearities. These CMS techniques reduces each linear subcomponent model with few selected fixed-interface modes and fully retained static constraint modes to account for internal and interface deformations respectively. The nonlinear subcomponent elements are then integrated through their retained nodes. For FEA models with many subcomponents and large interface DoFs, the size of the CMS model can be very large as it is directly proportional to the size of the static modes and the number of DoFs involved in nonlinearities [69]. If not addressed, solving such a reduced order model with too many DoFs would obviously impact the convergence speed.

Bilinear reduced order model is one of the early techniques used in the linearization of systems with nonlinear intermittent contacts. It is based on the ideas of using bilinear modes (BLMs) to represent the dynamics of local piecewise linear systems [42][9][19]. BLMs are the associated normal modes of linear systems with special boundary conditions (BCs) at the surface where the intermittent contact occurs. The concept of BLM through FAR [70] was used to accurately predict the nonlinear dynamics of a prestressed rectangular cracked plate with intermittent contact by adaptively selecting the generated modes at every solution frequency. Other

techniques developed via the idea of BLM include bilinear amplitude approximation (BAA) [71] and piecewise linear modes (PLMs) [47]. The former calculates amplitudes of the periodic nonlinear steady-state response at resonant frequencies using modes similar to BLMs and the latter is used to generate ROMs consisting of normal modes of the piecewise linear systems, which approximate the instantaneous structural dynamics of the nonlinear system. BLMs can also be used to capture the nonlinear response of a system by approximating the dominant POMs calculated from the nonlinear response. The contribution suggested in this paper is to apply this concept in manner that accommodates the analysis of newly formed local nonlinearities within the system without necessarily remodeling the entire system.

To address the CMS technique inefficiency associated with retaining full size DoFs at the boundary interfaces, various interface reduction techniques have been propose to condense these static impulse modes. In Ref [72], Becker and Gaul developed the common interface reduction method to obtain and efficiently select interface constraint modes when using the Craig-Bampton CMS (CB-CMS). In this approach, a secondary modal analysis of the coupled global matrix of the system containing reduced constraint modes from the initial sub-model modal analysis. Numerical convergence can sometime be an issue with this technique because it lacks enough local flexibility in the interface that allow for a better accurate description of the interface movement. In Ref [73], Hong et al. proposed another approach for reducing the local interface by performing secondary eigenanalysis on the sub-models of a CB-CMS ROM. This allows for the characteristic constraint modes to be determined without knowledge of the adjacent structure(s). Another approach to reduce the number of nonlinear DOFs was developed by generating joint interface modes (JIMs) [74]. As proposed by Witteveen, JIMs are generated by statically condensing the whole structure to the joint interface DOFs while maintaining Newton's third law on the interface. This produces



a reduced system that is used for a secondary modal analysis with the resulting modes referred to as JIMs. Trial vector derivatives (TVDs) approach [75][18] is another method of computing joint modes based on modal derivatives. Modes generated with TVD tend to span the solution subspace of the nonlinear system by improving the subspace generated by CMS. TVDs are obtained by the first-order Taylor expansion of the CMS generated subspace. Proper orthogonal decomposition (POD) is then used to obtain the most influencing TVD vectors. Other interface reduction ideas can be explored in [76][74].

The objective of this paper is to perform analyze the theory behind the synthesis of frequency adaptive bilinear reduced order created with fixed-interface and characteristic constraint modes. The methodologies to compute bilinear ROMs using FAR and the derivation of the characteristic constraint modes and how to use these in a substructuring framework to solve systems with multiple local contact nonlinearities. The proposed concept is applied to two cases namely; rectangular flat plate with double crack and an offshore platform with multiple hull-legs in intermittent contact.

### **3.2. Substructuring**

Consider a finite element model of a structure with multiple intermittent contacts divided into  $N_s$  non-overlapping substructures and such that no two substructures share similar intermittent contact. In other words no partitioning line crosses the intermittent contact surface areas. Figure 15 below illustrates such system with a rectangular plate connected to three cylinders such that each of the cylinders is centered at three of the plate's quadrants. The plate and the cylinders contact interfaces will experience intermittent contacts if externally excited. The equation of motion governing each subcomponent can be written as

$$\mathbf{M}^{(s_i)} \ddot{\mathbf{q}}^{(s_i)} + \mathbf{C}^{(s_i)} \dot{\mathbf{q}}^{(s_i)} + \mathbf{K}^{(s_i)} \mathbf{q}^{(s_i)} = \mathbf{F}_{ps}^{(s_i)} + \mathbf{F}_{ex}^{(s_i)} + \mathbf{F}_{nl}^{(s_i)}, \quad \text{for } i = 1, \dots, N \quad (22)$$

where  $(\dot{\quad})$  represents a time derivative and superscript  $(s_i)$  indicates the variable for subcomponent  $s_i$ . For substructures with intermittent contacts,  $\mathbf{M}^{(s_i)}$ ,  $\mathbf{C}^{(s_i)}$  and  $\mathbf{K}^{(s_i)}$  are the mass, viscous damping and stiffness matrices associated with fully open (no contact) contact node pairs on the contact interfaces.  $\mathbf{F}_{ps}^{(s_i)}$  is the vector of pre-stress forces,  $\mathbf{F}_{ex}^{(s_i)}$  is the excitation vector,  $\mathbf{F}_{nl}^{(s_i)}$  is the vector of nonlinear contact forces acting on the contact nodes of nonlinear substructures  $s_i$ , and  $\mathbf{q}^{(s_i)}$  is the vector of physical DoFs.

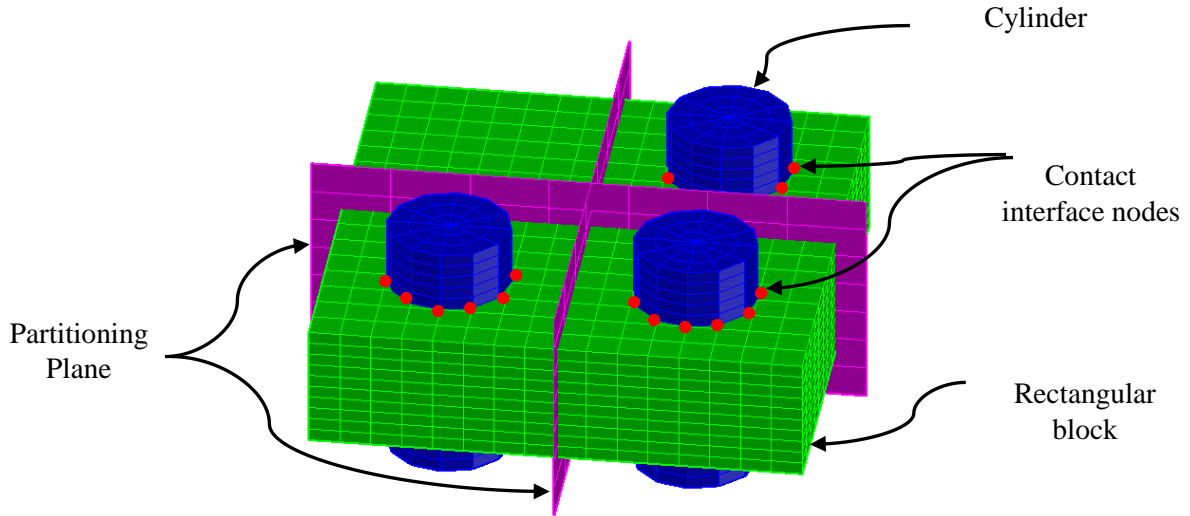


Figure 15. An illustration of a partitioned rectangular plate with linear and nonlinear substructures

### 3.3. Component Mode Synthesis

A knowledge of the stress concentrations in a structure is an important early design process computed from the static analysis of the finite element models of the structure. Such FE models often contain very large DoFs because of fine meshing required for computational accuracy. The computational cost associated with this analysis can still be handled using efficient solvers.

However, using the same refined model for dynamic problems, such as computing vibration modes, harmonic and transient responses, results in unacceptably long computation times making the time required for handling similar model with nonlinearities even ridiculously longer. In the same vein, stress fluctuations or stress increase in certain parts of a structure can lead to newly developed local nonlinearities which were initially not accounted for in the initial FE model. Remodeling the entire system at every occurrence of such new nonlinearity can be very demanding and redundant. Hence the need for a reduction method that reduces the size the dynamic problem without modifying the model's mesh and allows for handling existing and newly formed local nonlinearities only within the neighborhood of their existence.

Similar to modal superposition, the full set of physical DoFs,  $\mathbf{q}^{(s_i)}$  is approximated by a set of displacement shapes and corresponding amplitudes called the generalized DoFs as

$$\mathbf{q}^{(s_i)} = \tilde{\mathbf{T}}^{(s_i)} \tilde{\mathbf{p}}^{(s_i)} \quad (23)$$

where  $\tilde{\mathbf{T}}^{(s_i)} \in \mathbf{R}^{n \times m}$  is the reduction transformation matrix with  $m < n$ . Generally, CMS technique involves three major steps. First, the large model is partitioned into substructures as earlier explained. Then the substructures are discretized and reduced using Eq. (23) such that the resulting set of DoFs consists of a mixture between physical and generalized DoFs (only the internal DoFs are reduced). However, in the present work, we intend to construct the reduction matrix  $\mathbf{T}$  to transform all the physical DoFs (internal, contact and boundary DoFs) into fewer generalized DoFs. Finally, the global model is obtained by assembling the substructures. Usually, coupling of substructures using the generalized coordinates  $\mathbf{p}$  is a rather difficult task and is generally rarely done in CMS procedures because the DoFs on the substructure boundaries are not reduced. The reduction of the internal DoFs is derived similar to the CB-CMS constrain modes such that,

For linear substructure:

$$\mathbf{q}^{(s_i)} = \begin{Bmatrix} \mathbf{q}_i^{(s_i)} \\ \mathbf{q}_b^{(s_i)} \end{Bmatrix}, \tilde{\mathbf{p}}^{(s_i)} = \begin{Bmatrix} \mathbf{p}_i^{(s_i)} \\ \mathbf{q}_b^{(s_i)} \end{Bmatrix} \text{ and } \tilde{\mathbf{T}}^{(s_i)} = \begin{bmatrix} \boldsymbol{\Phi}^{(s_i)} & \boldsymbol{\Psi}^{(s_i)} \\ \mathbf{0} & \mathbf{I} \end{bmatrix} \quad (24)$$

and for substructure with contact,

$$\mathbf{q}^{(s_i)} = \begin{Bmatrix} \mathbf{q}_i^{(s_i)} \\ \mathbf{q}_{nl}^{(s_i)} \\ \mathbf{q}_b^{(s_i)} \end{Bmatrix}, \tilde{\mathbf{p}}^{(s_i)} = \begin{Bmatrix} \mathbf{p}_i^{(s_i)} \\ \mathbf{q}_{nl}^{(s_i)} \\ \mathbf{q}_b^{(s_i)} \end{Bmatrix} \text{ and } \tilde{\mathbf{T}}^{(s_i)} = \begin{bmatrix} \boldsymbol{\Phi}^{(s_i)} & \mathbf{0} & \boldsymbol{\Psi}^{(s_i)} \\ \mathbf{0} & \mathbf{I} & \mathbf{0} \\ \mathbf{0} & \mathbf{0} & \mathbf{I} \end{bmatrix} \quad (25)$$

where  $\mathbf{q}_i^{(s_i)}$ ,  $\mathbf{q}_b^{(s_i)}$ , and  $\mathbf{q}_{nl}^{(s_i)}$  are the physical internal DoFs, physical boundary DoFs and the physical contact interface DoFs of substructure  $s_i$ .  $\mathbf{p}_i^{(s_i)}$  is the generalized internal DoFs.  $\boldsymbol{\Phi}^{(s_i)}$ , and  $\boldsymbol{\Psi}^{(s_i)}$  are the fixed interface modes and constraint modes for the substructure  $s_i$ . Obtaining  $\boldsymbol{\Phi}^{(s_i)}$  for the linear structures has been developed in previous literatures [77][68], however the constraint modes of substructures with contact nonlinearity is explained next.

### 3.4. Model Reduction

The structure described in Figure 15 can be conveniently partitioned into four equal sectors; three sub-models with intermittent contacts and one without contact as depicted by the schematic representation in Figure 16. In order to reduce the EoMs of each subcomponents as shown in Eq. (22), the equations are projected onto the reduction transformation matrix  $\mathbf{T}^{(s_i)}$  containing a set of Ritz vectors needed to capture the kinematics of each substructure. The reduction transformation matrix applied to the EoM of structures without nonlinearities (linear structure) is very similar to CB-CMS reduction matrix with very slight changes that will be explained later. However constructing  $\mathbf{T}^{(s_i)}$  for a nonlinear substructure requires special attention and is detailed in subsequent sections. The EoMs of each subcomponent is transformed thus

$$\mathbf{M}^{(s_i)} \mathbf{T}^{(s_i)} \ddot{\mathbf{p}}^{(s_i)} + \mathbf{C}^{(s_i)} \mathbf{T}^{(s_i)} \dot{\mathbf{p}}^{(s_i)} + \mathbf{K}^{(s_i)} \mathbf{T}^{(s_i)} \mathbf{p}^{(s_i)} = \mathbf{F}_{ps}^{(s_i)} + \mathbf{F}_{ex}^{(s_i)} + \mathbf{F}_{nl}^{(s_i)}, \quad \text{for } i = 1, \dots, N \quad (26)$$

$$\mathbf{T}^{(s_i)T} \mathbf{M}^{(s_i)} \mathbf{T}^{(s_i)} \ddot{\mathbf{p}}^{(s_i)} + \mathbf{T}^{(s_i)T} \mathbf{C}^{(s_i)} \mathbf{T}^{(s_i)} \dot{\mathbf{p}}^{(s_i)} + \mathbf{T}^{(s_i)T} \mathbf{K}^{(s_i)} \mathbf{T}^{(s_i)} \mathbf{p}^{(s_i)} = \mathbf{T}^{(s_i)T} \mathbf{F}_{ps}^{(s_i)} + \mathbf{T}^{(s_i)T} \mathbf{F}_{ex}^{(s_i)} + \mathbf{T}^{(s_i)T} \mathbf{F}_{nl}^{(s_i)} \quad (27)$$

$$\bar{\mathbf{M}}^{(s_i)} \ddot{\mathbf{p}}^{(s_i)} + \bar{\mathbf{C}}^{(s_i)} \dot{\mathbf{p}}^{(s_i)} + \bar{\mathbf{K}}^{(s_i)} \mathbf{p}^{(s_i)} = \bar{\mathbf{F}}_{ps}^{(s_i)} + \bar{\mathbf{F}}_{ex}^{(s_i)} + \bar{\mathbf{F}}_{nl}^{(s_i)}, \quad \text{for } i = 1, \dots, N \quad (28)$$

where,

$$\bar{\mathbf{M}}^{(s_i)} = \mathbf{T}^{(s_i)T} \mathbf{M}^{(s_i)} \mathbf{T}^{(s_i)}, \quad \bar{\mathbf{C}}^{(s_i)} = \mathbf{T}^{(s_i)T} \mathbf{C}^{(s_i)} \mathbf{T}^{(s_i)}, \quad \bar{\mathbf{K}}^{(s_i)} = \mathbf{T}^{(s_i)T} \mathbf{K}^{(s_i)} \mathbf{T}^{(s_i)},$$

$$\bar{\mathbf{F}}_{ps}^{(s_i)} = \mathbf{T}^{(s_i)T} \mathbf{F}_{ps}^{(s_i)}, \quad \bar{\mathbf{F}}_{ex}^{(s_i)} = \mathbf{T}^{(s_i)T} \mathbf{F}_{ex}^{(s_i)}, \quad \text{and} \quad \bar{\mathbf{F}}_{nl}^{(s_i)} = \mathbf{T}^{(s_i)T} \mathbf{F}_{nl}^{(s_i)} \quad (29)$$

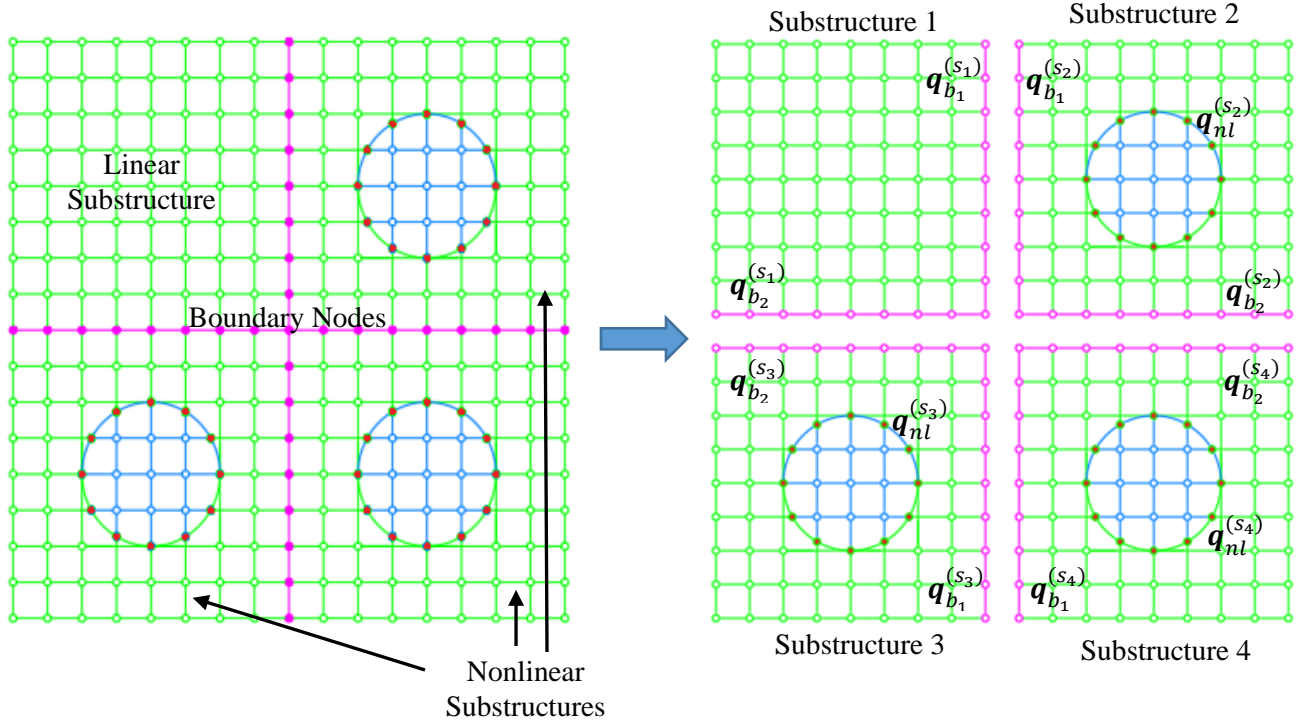


Figure 16. Schematic representation of the discretized model

In this work we use the fixed-interface modes developed in [25] as the internal modes for the linear components and fixed-interface bilinear modes as internal modes for substructures with nonlinearities. Note that for the linear subcomponent, while any linear substructuring (e.g. CB-CMS) modal bases could be used for its reduction, the reduction bases developed hereafter is preferable because of the nonlinear effect that neighboring substructures can have on the dynamics of common boundaries.

### 3.4.1. Fixed Interface Bilinear Reduction

Various previous works [39][40] have in the past employed bilinear reduction method in the approximate reduction of a nonlinear system with intermittent contact. The idea of bilinear reduction hinges on the concept that the nodes at the interface of a contact area will either be open, closed or switching (i.e. in intermittent contact) over given period of vibration. Therefore, the nonlinear behavior exhibited by nodes with intermittent contact can be modelled using its linear characteristics at open and closed conditions. Consider the fixed interface bilinear reduction of the fourth subcomponent in Figure 17, and assuming all the nodes at the contact interface are switching, then the first linear system is when a stick boundary condition is enforced on the contact node pairs and the subcomponent interfaces are fixed (Figure 17). The second linear system is derived by allowing an open condition between contact nodes pairs at the contact interface and imposing fixed boundary conditions at the subcomponent interfaces (Figure 17).

The corresponding eigenvalue problem for both cases are

$$\begin{aligned} \mathbf{K}_c^{(s_i)} \mathbf{U}_c^{(s_i)} - \lambda_c \mathbf{M}_c^{(s_i)} \mathbf{U}_c^{(s_i)} &= \mathbf{0} \\ \mathbf{K}_o^{(s_i)} \mathbf{U}_o^{(s_i)} - \lambda_o \mathbf{M}_o^{(s_i)} \mathbf{U}_o^{(s_i)} &= \mathbf{0} \end{aligned} \quad (30)$$

where  $\mathbf{M}_c^{(s_i)}$ ,  $\mathbf{M}_o^{(s_i)}$ ,  $\mathbf{K}_c^{(s_i)}$ ,  $\mathbf{K}_o^{(s_i)}$  are the respective mass matrices and stiffness matrices of the stuck and open linear systems of substructure  $s_i$  with local nonlinearities,  $\lambda_{c,c}$  and  $\lambda_{c,o}$  are the eigenvalues of the stuck and open linear systems respectively, and  $\mathbf{U}_c^{(s_i)}$  and  $\mathbf{U}_o^{(s_i)}$  are the fixed interface bilinear modes (FI-BLMs) of the substructure. Candidate FI-BLMs within the solution frequency range are selected and included in matrix  $\mathbf{B}^{(s_i)}$  as

$$\mathbf{B}^{(s_i)} = \left[ \mathbf{U}_{c_1}^{(s_i)}, \mathbf{U}_{c_2}^{(s_i)}, \dots, \mathbf{U}_{c_{m_{max}}}^{(s_i)}, \mathbf{U}_{o_1}^{(s_i)}, \mathbf{U}_{o_2}^{(s_i)}, \dots, \mathbf{U}_{o_{m_{max}}}^{(s_i)} \right] \quad (31)$$

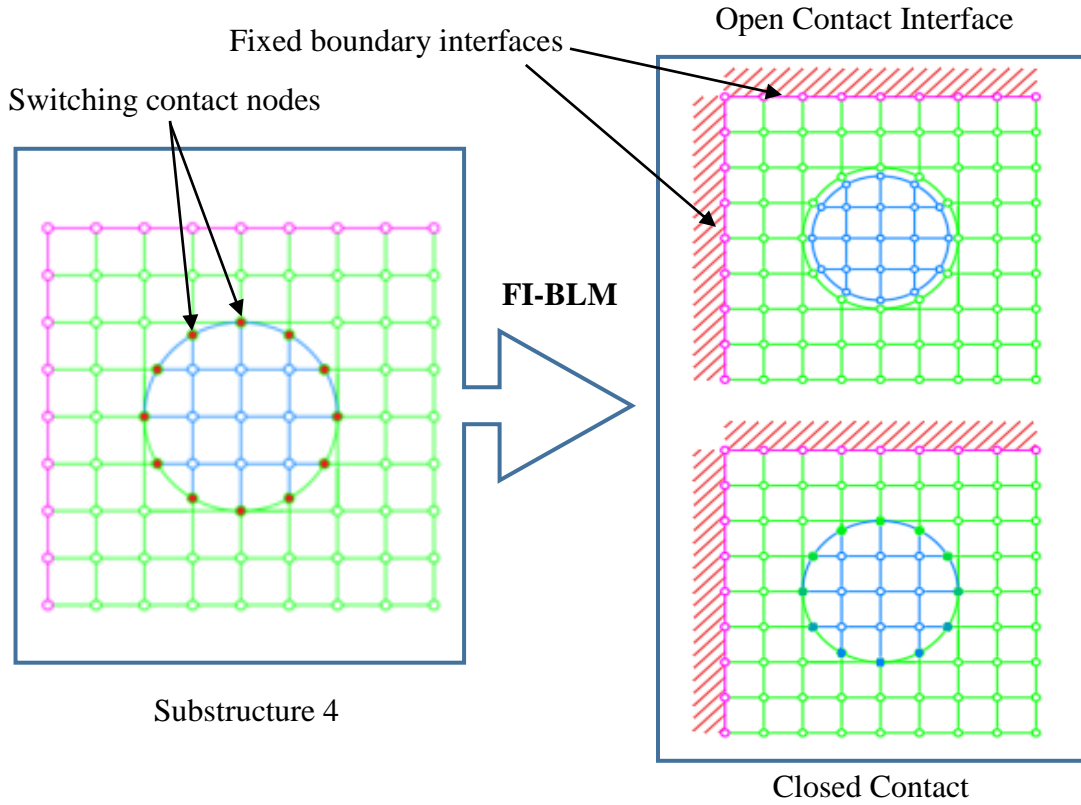


Figure 17. Bilinear expansion of substructure 4 using fixed interface bilinear modes (FI-BLM)

Note that the stuck condition can be obtained by augmenting and coupling the normal stiffness values corresponding to the contact pair nodes in the subcomponent stiffness matrix  $\mathbf{K}^{(s_i)}$ . Having obtained the FI-BLMs, we use the FAR modal selection technique described in [70] to

select the optimal set BLMs adequate to capture the dynamics of the subcomponent. The FAR method thrives on selection of new BLMs to update the reduction matrix at every frequency step and at the same time eliminating redundant BLMs from the matrix. This allows for faster convergence in that it corrects the assumption that all nodes at the contact interface are switching nodes and avoids considerably reduces the number of equations solved at every frequency. FAR is composed of two main proponents namely; modal selection criteria (MSC) and modal participation criteria (MPC). At the MSC stage, new BLMs are generated from the updated contact boundary condition of the component at the current frequency of solution and each of the new BLMs are tested for linear independence with the vectors in the current reduction matrix. If the BLM is linearly independent with the reduction matrix such that the residual is much lesser than one, then the BLM is added to reduction matrix otherwise the BLM is disregarded at that frequency. The MPC is necessary to continually reduce the size of the reduction matrix by eliminating vectors with relatively low modal amplitude at immediate solution frequency.

Below is the summary of FAR selection and elimination procedure required to compute the internal DoFs reduction matrix  $\Phi^{(s_i)}$  for substructures with contact nonlinearity:

- a. Initialize the internal DoFs reduction matrix  $\Phi^{(s_i)}$  to include modes generated with the initial state of the contact surface.
- b. Generate FI-BLMs and concatenate them in matrix  $\Phi^{(s_i)}$
- c. Check linear independence of vectors in  $\mathbf{B}^{(s_i)}$  and matrix  $\Phi^{(s_i)}$  such that

$$r_n^{(s_i)} = \frac{\|\mathbf{B}_n^{(s_i)} - \Phi^{(s_i)} \mathbf{k}_n^{(s_i)}\|}{\|\mathbf{B}_n^{(s_i)}\|}, \text{ where } \Phi^{(s_i)} \mathbf{k}_n^{(s_i)} = \mathbf{B}_n^{(s_i)} \text{ for } n = 1, 2, 3, \dots, m$$

- d. If  $r_n^{(s_i)} \ll 1$ , then  $\mathbf{B}_n^{(s_i)}$  is included in matrix  $\Phi^{(s_i)}$
- e. Apply reduction matrix  $\Phi^{(s_i)}$  to EoM and solve for modal amplitudes  $\mathbf{p}_{FAR}^{(s_i)}$
- f. Eliminate vectors with low modal amplitudes i.e.

$$\frac{|\mathbf{p}_{FAR,n}^{(s_i)}|}{\|\mathbf{p}_{FAR}^{(s_i)}\|_\infty} < \varepsilon_2, \text{ where } \varepsilon_2 \ll 1$$

- g. Repeat steps (b)-(f) at next frequency step.



### 3.4.2. Boundary Interface Reduction

Besides the fixed interface modes, constraint modes  $\Psi^{(s_i)}$  are included in the reduction matrix of substructures in order to account for deformations at the boundary, or interface DoFs. Without the interface reduction, one constraint mode is required to be computed for every interface nodes by computing the static deflection to a unit displacement at each boundary DoF while holding all the other boundary coordinates fixed. Since this is a static mode type, the derivation will start with the linear static equilibrium obtained when neglecting dynamic effects.

$$\mathbf{K}^{(s_i)} \mathbf{q}^{(s_i)} = \mathbf{F}_{ps}^{(s_i)} + \mathbf{F}_{ex}^{(s_i)} \quad (32)$$

Partitioning the system of equations by the distinguishing boundary DOFs

$$\begin{bmatrix} \mathbf{K}_{ii}^{(s_i)} & \mathbf{K}_{ib}^{(s_i)} \\ \mathbf{K}_{bi}^{(s_i)} & \mathbf{K}_{bb}^{(s_i)} \end{bmatrix} \begin{Bmatrix} \mathbf{q}_i^{(s_i)} \\ \mathbf{q}_b^{(s_i)} \end{Bmatrix} = \begin{Bmatrix} \mathbf{F}_{ps}^{(s_i)} \\ \mathbf{0} \end{Bmatrix} + \begin{Bmatrix} \mathbf{F}_{ex}^{(s_i)} \\ \mathbf{0} \end{Bmatrix} \quad (33)$$

In order to determine how the internal DoFs displace due to displacements of the boundary DoFs, one can statically condense the internal DoF set onto the boundary:

$$\mathbf{q}_i^{(s_i)} = -\mathbf{K}_{ii}^{(s_i)-1} \mathbf{K}_{ib}^{(s_i)} \mathbf{q}_b^{(s_i)} \quad (34)$$

$$\Psi^{(s_i)} = -\mathbf{K}_{ii}^{(s_i)-1} \mathbf{K}_{ib}^{(s_i)} \quad (35)$$

where  $-\mathbf{K}_{ii}^{(s_i)-1}$  is the inverse of  $-\mathbf{K}_{ii}^{(s_i)}$  and may be interpreted as the flexibility (inverse stiffness)

of the internal DoFs. Similarly for substructure with contact,

$$\mathbf{K}^{(s_i)} \mathbf{q}^{(s_i)} = \mathbf{F}_{ps}^{(s_i)} + \mathbf{F}_{ex}^{(s_i)} + \mathbf{F}_{nl}^{(s_i)} \quad (36)$$

$$\begin{bmatrix} \mathbf{K}_{ii}^{(s_i)} & \mathbf{K}_{inl}^{(s_i)} & \mathbf{K}_{ib}^{(s_i)} \\ \mathbf{K}_{nli}^{(s_i)} & \mathbf{K}_{nlnl}^{(s_i)} & \mathbf{K}_{nlb}^{(s_i)} \\ \mathbf{K}_{bi}^{(s_i)} & \mathbf{K}_{bnl}^{(s_i)} & \mathbf{K}_{bb}^{(s_i)} \end{bmatrix} \begin{Bmatrix} \mathbf{q}_i^{(s_i)} \\ \mathbf{q}_{nl}^{(s_i)} \\ \mathbf{q}_b^{(s_i)} \end{Bmatrix} = \begin{Bmatrix} \mathbf{F}_{ps}^{(s_i)} \\ \mathbf{0} \\ \mathbf{0} \end{Bmatrix} + \begin{Bmatrix} \mathbf{F}_{ex}^{(s_i)} \\ \mathbf{0} \\ \mathbf{0} \end{Bmatrix} + \begin{Bmatrix} \mathbf{0} \\ \mathbf{f}_{nl} \\ \mathbf{0} \end{Bmatrix} \quad (37)$$

$$\mathbf{q}_i^{(s_i)} = -\mathbf{K}_{ii}^{(s_i)-1} (\mathbf{K}_{ib}^{(s_i)} \mathbf{q}_b^{(s_i)} + \mathbf{K}_{inl}^{(s_i)} \mathbf{q}_{nl}^{(s_i)}) \quad (38)$$

Since the dynamic effect of the contact nonlinearities on the internal DoFs has been captured by the FI-BLMs, and only the effect of the boundary is being considered, then

$$\boldsymbol{\Psi}^{(s_i)} = -\mathbf{K}_{ii}^{(s_i)-1} \mathbf{K}_{ib}^{(s_i)} \quad (39)$$

The above results show that the static constraint modes is the same irrespective of the type of the substructure.

In many applications like the case being considered, the DoFs at the boundary interface can be very large i.e. size of  $\boldsymbol{\Psi}^{(s_i)}$  is large compared to the number of vectors in  $\boldsymbol{\Phi}^{(s_i)}$  therefore impacting the overall reduction process. The boundary interface reduction proposed here is similar to that suggested by Castanier et. al. [25], where characteristic constraint modes were used in the boundary interface reduction. This idea involves the calculation of a secondary eigenvalue analysis on the assembled linear mass and stiffness matrices corresponding to the boundary interface DoFs. While this technique is similar to what we propose, the difference is that our idea includes nonlinear contact effect at the substructure. This is accomplished by imposing the bilinear boundary conditions at the contact surfaces before performing the secondary eigenanalysis of paired assemblies. A reduction of these boundary interface DoFs can be achieved through system-level characteristic constraint modes (slightly) different approaches involving a secondary modal analysis. This approach is initiated by first assembling the substructures in pairs using the primal formulation [68][78].

As an example, and without any loss of generality, coupling subcomponents  $s_i$  and  $s_j$  from our model produces the following undamped, free equations of motion

$$\mathbf{M}^{(s_i, s_j)} \ddot{\mathbf{q}}^{(s_i, s_j)} + \mathbf{K}^{(s_i, s_j)} \mathbf{q}^{(s_i, s_j)} = \mathbf{0} \quad (40)$$

where,

$$\mathbf{M}^{(s_i, s_j)} = \begin{bmatrix} \mathbf{M}_{ii}^{(s_i)} & \mathbf{0} & \mathbf{M}_{inl}^{(s_i)} & \mathbf{0} & \mathbf{M}_{ib}^{(s_i)} \\ \mathbf{0} & \mathbf{M}_{ii}^{(s_j)} & \mathbf{0} & \mathbf{M}_{inl}^{(s_j)} & \mathbf{M}_{ib}^{(s_j)} \\ \mathbf{M}_{nli}^{(s_i)} & \mathbf{0} & \mathbf{M}_{nlnl}^{(s_i)} & \mathbf{0} & \mathbf{M}_{nlb}^{(s_i)} \\ \mathbf{0} & \mathbf{M}_{nli}^{(s_j)} & \mathbf{0} & \mathbf{M}_{nlnl}^{(s_j)} & \mathbf{M}_{nlb}^{(s_j)} \\ \mathbf{M}_{bi}^{(s_i)} & \mathbf{M}_{bi}^{(4)} & \mathbf{M}_{bnl}^{(s_i)} & \mathbf{M}_{bnl}^{(4)} & \mathbf{M}_{bb} \end{bmatrix}, \quad (41)$$

$$\mathbf{K}^{(s_i, s_j)} = \begin{bmatrix} \mathbf{K}_{ii}^{(s_i)} & \mathbf{0} & \mathbf{K}_{inl}^{(s_i)} & \mathbf{0} & \mathbf{K}_{ib}^{(s_i)} \\ \mathbf{0} & \mathbf{K}_{ii}^{(s_j)} & \mathbf{0} & \mathbf{K}_{inl}^{(s_j)} & \mathbf{K}_{ib}^{(s_j)} \\ \mathbf{K}_{nli}^{(s_i)} & \mathbf{0} & \mathbf{K}_{nlnl}^{(s_i)} & \mathbf{0} & \mathbf{K}_{nlb}^{(s_i)} \\ \mathbf{0} & \mathbf{K}_{nli}^{(s_j)} & \mathbf{0} & \mathbf{K}_{nlnl}^{(s_j)} & \mathbf{K}_{nlb}^{(s_j)} \\ \mathbf{K}_{bi}^{(s_i)} & \mathbf{K}_{bi}^{(s_j)} & \mathbf{K}_{bnl}^{(s_i)} & \mathbf{K}_{bnl}^{(s_j)} & \mathbf{K}_{bb} \end{bmatrix}, \text{ and } \mathbf{q}^{(s_i, s_j)} = \begin{Bmatrix} \mathbf{q}_i^{(s_i)} \\ \mathbf{q}_i^{(s_j)} \\ \mathbf{q}_{nl}^{(s_i)} \\ \mathbf{q}_{nl}^{(s_j)} \\ \mathbf{q}_b \end{Bmatrix}$$

A second modal analysis is performed on the assembled mass and stiffness matrices corresponding to the contact and boundary DoFs highlighted by the boxes in Eq. (41). As stated earlier, bilinearity is used to resolve the nonlinear contact effect in the assembly. For example, if we consider the subassembly between two substructure with nonlinearity (e.g. subassembly between substructure 3 and 4 as shown in Figure 18), four combinations of eigenanalysis is performed

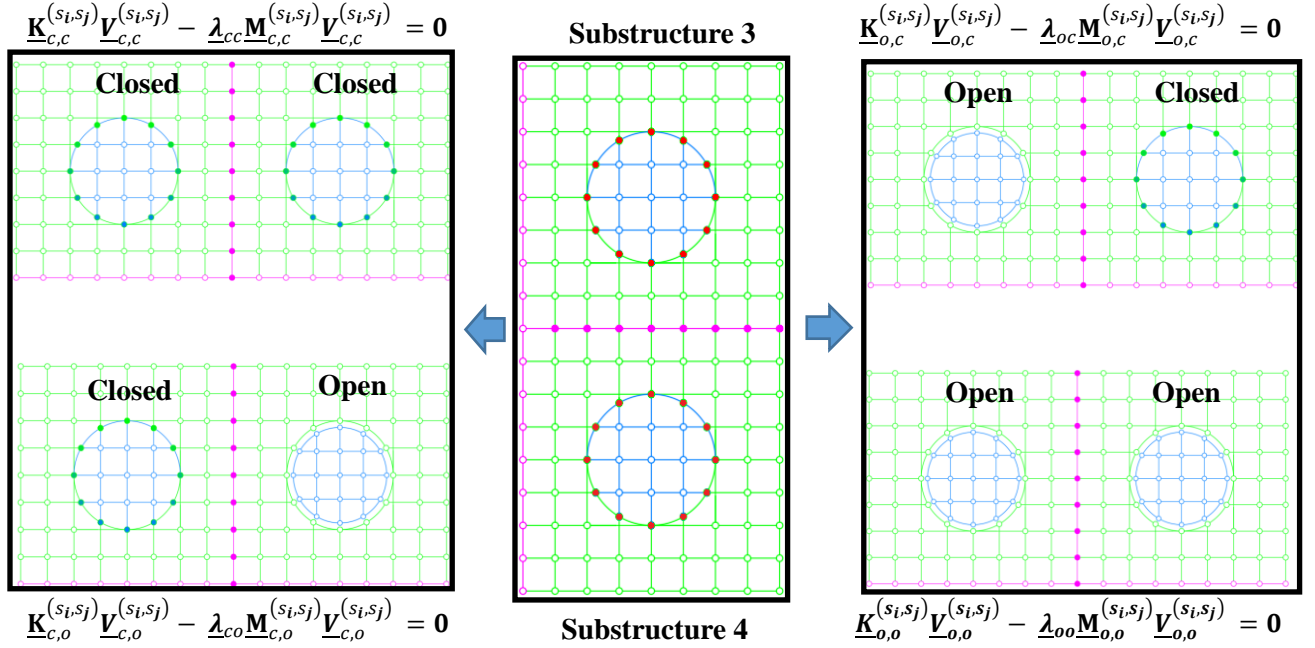


Figure 18. Subassembly between substructures 3 & 4 with the bilinear combinations.

$$\begin{aligned} \mathbf{K}_{o,o}^{(s_i, s_j)} \mathbf{V}_{o,o}^{(s_i, s_j)} - \lambda_{oo} \mathbf{M}_{o,o}^{(s_i, s_j)} \mathbf{V}_{o,o}^{(s_i, s_j)} &= \mathbf{0} \\ \mathbf{K}_{o,c}^{(s_i, s_j)} \mathbf{V}_{o,c}^{(s_i, s_j)} - \lambda_{oc} \mathbf{M}_{o,c}^{(s_i, s_j)} \mathbf{V}_{o,c}^{(s_i, s_j)} &= \mathbf{0} \\ \mathbf{K}_{c,o}^{(s_i, s_j)} \mathbf{V}_{c,o}^{(s_i, s_j)} - \lambda_{co} \mathbf{M}_{c,o}^{(s_i, s_j)} \mathbf{V}_{c,o}^{(s_i, s_j)} &= \mathbf{0} \\ \mathbf{K}_{c,c}^{(s_i, s_j)} \mathbf{V}_{c,c}^{(s_i, s_j)} - \lambda_{cc} \mathbf{M}_{c,c}^{(s_i, s_j)} \mathbf{V}_{c,c}^{(s_i, s_j)} &= \mathbf{0} \end{aligned} \quad (42)$$

where the underbar, ‘\_’, represent quantities of the contact and boundary interfaces between subassemblies. Subscripts ‘o’ and ‘c’ represent open and closed (stuck) contact conditions and are separated by comma in the order corresponding to the identities of paired substructures in the subassembly. E.g.  $\underline{\mathbf{K}}_{o,o}^{(s_i,s_j)}$  represent the contact-boundary stiffness matrix of subassembly  $s_i, s_j$  (which includes substructures  $s_i$  and  $s_j$ ) when switching contact nodes of substructure  $s_i$  is open and switching contact nodes for substructure  $s_j$  is closed.  $\underline{\mathbf{V}}_{o,o}^{(s_i,s_j)}$ ,  $\underline{\mathbf{V}}_{o,c}^{(s_i,s_j)}$ ,  $\underline{\mathbf{V}}_{c,o}^{(s_i,s_j)}$ , and  $\underline{\mathbf{V}}_{c,c}^{(s_i,s_j)}$  are generally referred to as the bilinear boundary constraint modes. Note that in the case of subassemblies with only one nonlinear substructure, only two eigenanalysis will be performed (i.e. similar to the FL-BLM eigenanalysis in Eq.(42) but with the appropriate subassembly mass and stiffness matrices).

All the bilinear boundary constrain modes whose frequencies are within the solution frequency range are included as candidates in the boundary reduction matrix.

$$\hat{\Psi}^{(s_i,s_j)} = \left[ \underline{\mathbf{V}}_{o,o}^{(s_i,s_j)}, \underline{\mathbf{V}}_{o,c}^{(s_i,s_j)}, \underline{\mathbf{V}}_{c,o}^{(s_i,s_j)}, \underline{\mathbf{V}}_{c,c}^{(s_i,s_j)} \right] \quad (43)$$

where  $\underline{\mathbf{V}}$  is the matrix containing frequency based selection of the bilinear boundary constraint modes. A second selection process is conducted on the candidate vectors in  $\hat{\Psi}^{(s_i,s_j)}$  to ensure proper conditioning of the reduction matrix. To do this, we again employ the FAR selection technique [70] as summarized earlier. The outcome of this selection yields the boundary reduction matrix  $\hat{\Psi}_b^{(s_i,s_j)}$  for the interface between substructure  $s_i$  and  $s_j$ . Note that  $\hat{\Psi}_b^{(s_i,s_j)}$  only contains the DoFs associated with only the nodes at the boundary. The number of vectors in  $\hat{\Psi}_b^{(s_i,s_j)}$  is lesser than the physical DoFs in the boundary interface and can therefore applied to reduce the boundary DoFs shared by subassemblies  $s_i$  and  $s_j$  during their respective substructure reduction. In order

words, after computing all the boundary reduction matrices from all subassembly combinations, all the boundary reduction matrices associated with each substructure  $s_i$  are arranged in a block diagonal matrix to form boundary reduction matrix  $\hat{\Psi}_b^{(s_i, s_j)}$  for that substructure. The number of blocks is equal to the number of substructures that are connected to the substructure being considered. For our model, each substructure is connected to two other substructures hence the boundary reduction matrix of substructure  $s_i$  is of the form

$$\hat{\Psi}_b^{(s_i)} = \begin{bmatrix} \hat{\Psi}_b^{(s_i, s_j)} & \mathbf{0} \\ \mathbf{0} & \hat{\Psi}_b^{(s_i, s_k)} \end{bmatrix} \quad (44)$$

where  $j = 1, 2 \dots 4$ ,  $j$  and  $k$  are the numerical representation of the substructures sharing boundaries with substructure  $s_i$ . Figure 19 below shows the construction of the boundary reduction matrices for our model.

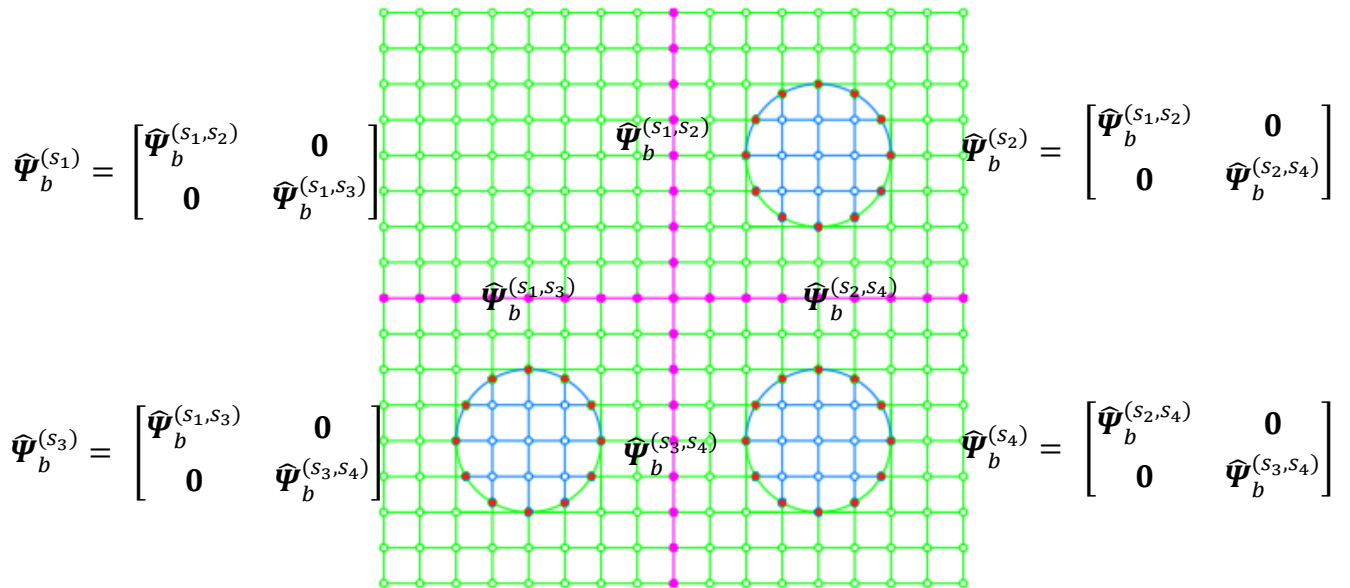


Figure 19. A simple schematic to demonstrate the construction of boundary reduction matrices

Now we apply  $\Phi^{(s_i)}$ ,  $\Psi^{(s_i)}$  and  $\widehat{\Psi}_b^{(s_i)}$  to develop a robust reduction transformation  $\mathbf{T}^{(s_i)}$  needed to reduce all physical DoFs  $\mathbf{q}_b^{(s_i)}$  to the generalized coordinates  $\mathbf{p}_b^{(s_i)}$  (as in Eq.(23)) as

$$\mathbf{q}^{(s_i)} = \mathbf{T}^{(s_i)} \mathbf{p}^{(s_i)} \quad (45)$$

where,

$$\mathbf{T}^{(s_i)} = \begin{bmatrix} \Phi_{ii}^{(s_i)} & \Phi_{inl}^{(s_i)} & \Psi^{(s_i)} \\ \Phi_{nli}^{(s_i)} & \Phi_{nlnl}^{(s_i)} & \mathbf{0} \\ \mathbf{0} & \mathbf{0} & \mathbf{I} \end{bmatrix} \begin{bmatrix} \mathbf{I} & \mathbf{0} & \mathbf{0} \\ \mathbf{0} & \mathbf{I} & \mathbf{0} \\ \mathbf{0} & \mathbf{0} & \widehat{\Psi}_b^{(s_i)} \end{bmatrix} \quad (46)$$

$$\mathbf{T}^{(s_i)} = \begin{bmatrix} \Phi_{ii}^{(s_i)} & \Phi_{inl}^{(s_i)} & \Psi^{(s_i)} \widehat{\Psi}_b^{(s_i)} \\ \Phi_{nli}^{(s_i)} & \Phi_{nlnl}^{(s_i)} & \mathbf{0} \\ \mathbf{0} & \mathbf{0} & \widehat{\Psi}_b^{(s_i)} \end{bmatrix} \quad (47)$$

$$\mathbf{q}^{(s_i)} = \begin{Bmatrix} \mathbf{q}_i^{(s_i)} \\ \mathbf{q}_{nl}^{(s_i)} \\ \mathbf{q}_b^{(s_i)} \end{Bmatrix}, \mathbf{p}^{(s_i)} = \begin{Bmatrix} \mathbf{p}_i^{(s_i)} \\ \mathbf{p}_{nl}^{(s_i)} \\ \mathbf{p}_b^{(s_i)} \end{Bmatrix} \quad (48)$$

### 3.5. Global Assembly

To predict the overall dynamics of a substructured system, the mass and stiffness matrices as obtained in Eq. (29) for each substructure have to be assembled. This final process has to be done such that neighboring substructures interact with each other after assembly. To achieve this, the compatibility and equilibrium conditions needs to be satisfied at the boundaries. Compatibility ensures that the boundary displacement fields  $\mathbf{p}_b^{(s_i)}$  of connecting substructure boundaries must be identical. In other words,  $\mathbf{p}_b^{(s_1)} - \mathbf{p}_b^{(s_2)} = \mathbf{0}$  must be satisfied at all connecting boundary nodes. Equilibrium condition enforces that the connection forces between neighboring substructures must be equal in magnitude and opposite in direction. Assembling the substructured EoMs using standard finite element techniques automatically causes the unknown reaction forces at the

boundary to cancel (i.e. satisfying the equilibrium condition), and the resulting EoM for the assembled system becomes,

where,

$$\mathbf{M}\ddot{\mathbf{p}} + \mathbf{C}\dot{\mathbf{p}} + \mathbf{K}\mathbf{p} = \mathbf{F}_{ps} + \mathbf{F}_{ex} + \mathbf{F}_{nl} \quad (49)$$

$$\mathbf{M} = \begin{bmatrix} \bar{\mathbf{M}}^{(s_1)} & \mathbf{0} & \mathbf{0} & \mathbf{0} \\ \mathbf{0} & \bar{\mathbf{M}}^{(s_2)} & \mathbf{0} & \mathbf{0} \\ \vdots & \vdots & \ddots & \vdots \\ \mathbf{0} & \mathbf{0} & \mathbf{0} & \bar{\mathbf{M}}^{(s_N)} \end{bmatrix}, \mathbf{C} = \begin{bmatrix} \bar{\mathbf{C}}^{(s_1)} & \mathbf{0} & \mathbf{0} & \mathbf{0} \\ \mathbf{0} & \bar{\mathbf{C}}^{(s_2)} & \mathbf{0} & \mathbf{0} \\ \vdots & \vdots & \ddots & \vdots \\ \mathbf{0} & \mathbf{0} & \mathbf{0} & \bar{\mathbf{C}}^{(s_N)} \end{bmatrix}, \mathbf{p} = \begin{Bmatrix} \mathbf{p}^{(s_1)} \\ \mathbf{p}^{(s_2)} \\ \vdots \\ \mathbf{p}^{(s_N)} \end{Bmatrix}$$

$$\mathbf{K} = \begin{bmatrix} \bar{\mathbf{K}}^{(s_1)} & \mathbf{0} & \mathbf{0} & \mathbf{0} \\ \mathbf{0} & \bar{\mathbf{K}}^{(s_2)} & \mathbf{0} & \mathbf{0} \\ \vdots & \vdots & \ddots & \vdots \\ \mathbf{0} & \mathbf{0} & \mathbf{0} & \bar{\mathbf{K}}^{(s_N)} \end{bmatrix}, \mathbf{F}_{ps} = \begin{Bmatrix} \bar{\mathbf{F}}_{ps}^{(s_1)} \\ \bar{\mathbf{F}}_{ps}^{(s_2)} \\ \vdots \\ \bar{\mathbf{F}}_{ps}^{(s_N)} \end{Bmatrix}, \mathbf{F}_{nl} = \begin{Bmatrix} \bar{\mathbf{F}}_{nl}^{(s_1)} \\ \bar{\mathbf{F}}_{nl}^{(s_2)} \\ \vdots \\ \bar{\mathbf{F}}_{nl}^{(s_N)} \end{Bmatrix}, \mathbf{F}_{ex} = \begin{Bmatrix} \bar{\mathbf{F}}_{ex}^{(s_1)} \\ \bar{\mathbf{F}}_{ex}^{(s_2)} \\ \vdots \\ \bar{\mathbf{F}}_{ex}^{(s_N)} \end{Bmatrix} \quad (50)$$

Next we need to couple the substructure with a Boolean operator that satisfies both the compatibility condition stated above. Such coupling can be done in two ways; primal and dual assembly. The first results in a set of unique boundary DoFs, whereas the latter retains the full set of global DoFs. In this research primal assembly is considered because compatibility can be easily enforced since the boundary modes are computed via subassemblies. This global assembly method is intuitive in application, but has the limitation that assembled interfaces must have conforming meshes. Boundary DoFs of one substructure will be eliminated such that any adjacent components share the same set of interface DoFs. The unique set of degrees of freedom that is retained after primal assembly will be denoted by  $\hat{\mathbf{p}}$ . Primal assembly only works for matching interface meshes and therefore it does not matter which displacement field is retained and which is eliminated. For the model we are considering, the Boolean matrix is selected such that

$$\mathbf{p} = \begin{Bmatrix} \mathbf{p}^{(s_1)} \\ \mathbf{p}^{(s_2)} \\ \mathbf{p}^{(s_3)} \\ \mathbf{p}^{(s_4)} \end{Bmatrix} = \begin{Bmatrix} \mathbf{p}_i^{(s_1)} \\ \mathbf{p}_b^{(s_1,s_2)} \\ \mathbf{p}_b^{(s_1,s_3)} \\ \mathbf{p}_{FAR}^{(s_2)} \\ \mathbf{p}_b^{(s_2,s_1)} \\ \mathbf{p}_b^{(s_2,s_4)} \\ \mathbf{p}_{FAR}^{(s_3)} \\ \mathbf{p}_b^{(s_3,s_1)} \\ \mathbf{p}_b^{(s_3,s_4)} \\ \mathbf{p}_{FAR}^{(s_4)} \\ \mathbf{p}_b^{(s_4,s_2)} \\ \mathbf{p}_b^{(s_4,s_3)} \end{Bmatrix} = \mathbf{B} \begin{Bmatrix} \mathbf{p}_i^{(s_1)} \\ \mathbf{p}_b^{(s_1,s_2)} \\ \mathbf{p}_b^{(s_1,s_3)} \\ \mathbf{p}_{FAR}^{(s_2)} \\ \mathbf{p}_b^{(s_2,s_4)} \\ \mathbf{p}_{FAR}^{(s_3)} \\ \mathbf{p}_b^{(s_3,s_4)} \\ \mathbf{p}_{FAR}^{(s_4)} \end{Bmatrix} = \mathbf{B}\hat{\mathbf{p}} \quad (51)$$

In the above, only the unique boundary DoFs of substructure  $s_1$ ,  $s_2$ , and  $s_3$  were retained in the assembled system. Applying the transformation in Eq. (51) above to the combined equation of motion in Eq. (49) we have

$$\mathbf{MB}\ddot{\hat{\mathbf{p}}} + \mathbf{CB}\dot{\hat{\mathbf{p}}} + \mathbf{KB}\hat{\mathbf{p}} = \mathbf{F}_{ps,R} + \mathbf{F}_{ex,R} + \mathbf{F}_{nl,R} \quad (52)$$

premultiplying the above equation by  $\mathbf{B}^T$

$$\mathbf{B}^T(\mathbf{MB}\ddot{\hat{\mathbf{p}}} + \mathbf{CB}\dot{\hat{\mathbf{p}}} + \mathbf{KB}\hat{\mathbf{p}}) = \mathbf{B}^T(\mathbf{F}_{ps} + \mathbf{F}_{ex} + \mathbf{F}_{nl}) \quad (53)$$

$$\hat{\mathbf{M}}\ddot{\hat{\mathbf{p}}} + \hat{\mathbf{C}}\dot{\hat{\mathbf{p}}} + \hat{\mathbf{K}}\hat{\mathbf{p}} = \hat{\mathbf{F}}_{ps} + \hat{\mathbf{F}}_{ex} + \hat{\mathbf{F}}_{nl} \quad (54)$$

where

$$\begin{aligned} \hat{\mathbf{M}} &= \mathbf{B}^T\mathbf{MB}, & \hat{\mathbf{C}} &= \mathbf{B}^T\mathbf{CB}, & \hat{\mathbf{K}} &= \mathbf{B}^T\mathbf{KB}, \\ \bar{\mathbf{F}}_{ps} &= \mathbf{B}^T\mathbf{F}_{ps}, & \bar{\mathbf{F}}_{ex} &= \mathbf{B}^T\mathbf{F}_{ex}, & \bar{\mathbf{F}}_{nl} &= \mathbf{B}^T\mathbf{F}_{nl} \end{aligned} \quad (55)$$

Finally, Figure 20 below shows the brief summary of reduction process. It includes all the strategic reduction process in developing a ROM for structures with multiple nonlinearities using substructuring techniques and the FAR.



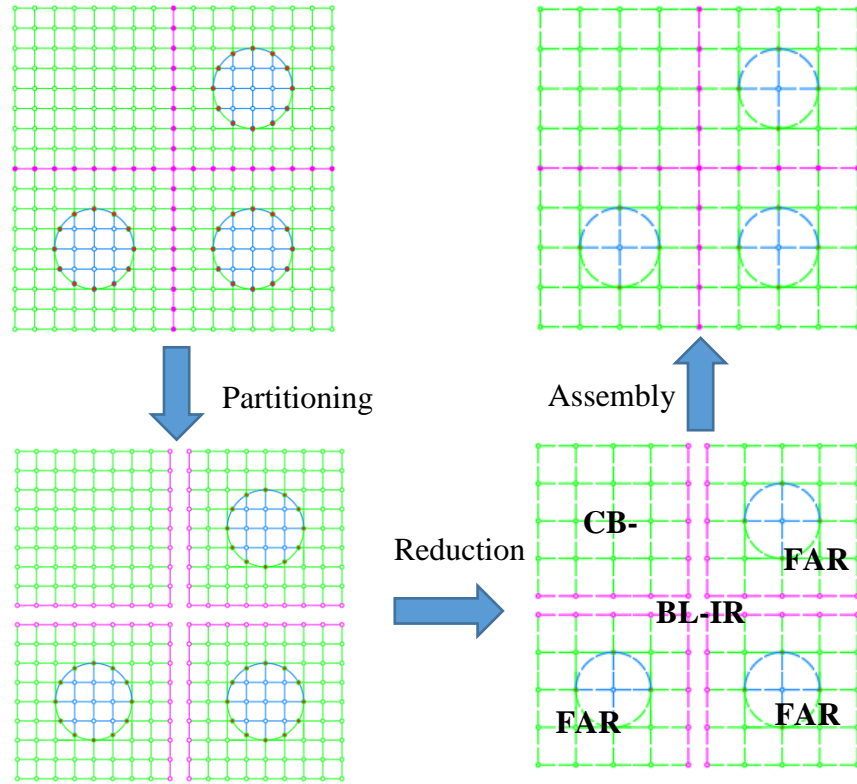


Figure 20. Conceptual diagram showing the reduced order model process.

### 3.6. Results

#### 3.6.1. Test Case 1

In this section, a test case study of the dynamic analysis presented thus far is applied to a rectangular plate with double lateral crack as shown by the thick red lines in Figure 21. The figure also shows the geometric configuration of the plate, the plan view of the contact pair nodes of the structure as well as the partitioning plane highlighted by thick dashed lines. The material properties of the plate include the Young's modulus  $E = 2.0 \times 10^5$  MPa, Poisson's coefficient  $\nu = 0.3$ , and density  $\rho = 7,800$  kg/m<sup>3</sup>. Similar to the application in the previous chapter, the plate is modelled in ANSYS using linear solid elements with  $\sim 18,400$  DoFs. The boundaries for both the top and bottom partitions are modelled with 150 nodes and each of the cracks have 50 contact node pairs. For this analysis, only the in-plane bending mode of the system is focused on with negligible

slip between contact node pairs. Results obtained through the nonlinear substructuring approach are validated by the application of the FAR on the CB-CMS model without substructuring.

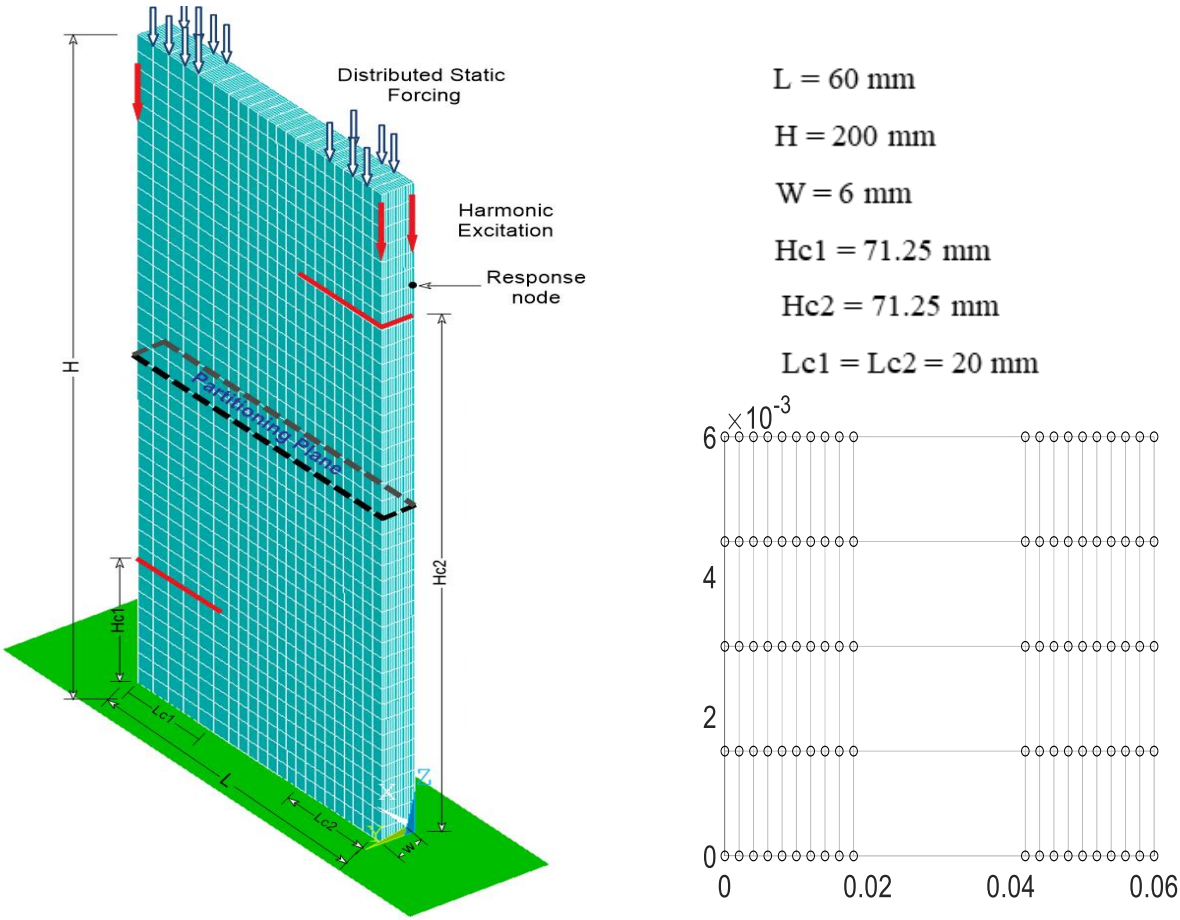


Figure 21. Geometry and pre-stressed contact condition of a Rectangular plate with double cracks.

The first result shown on the left side of Figure 22 is the frequency response of the plate with a harmonic excitation amplitude of 0.01N at both ends of the top substructure. The behavior of the system as measured from the response node shows a linear behavior. This is because both top and bottom cracks remain sliding over the interested frequency range. The substructuring solution is also observed to match the validation approach perfectly. In addition, the size of the combined ROM was 4 and remained constant during the entire frequency sweep.

Increasing the excitation amplitude by a factor of 10 on both ends of the top plate generated the result presented on the right side of Figure 22 .During this analysis, the contact pairs of the cracks were sliding at frequencies far away from the resonant frequency. As the solution approaches the resonance frequency, the contact node pairs at the lower substructure's crack interface begins to open gradually. The phenomenon is indicated as the beginning of softening behavior on the response curve. At resonant frequency and frequency in its neighborhood, all contact node pairs for both the lower and upper subcomponents had opened, making the softening more pronounced at these frequencies. The solution from the substructuring technique also matches closely with the results used for validation. As shown in Figure 22, the size of the combined ROM varied significantly along the response curve as a result of the application of FAR in the analysis. The model is further challenged by limiting the application of the excitation force to one end of the structure. Figure 23 shows the result obtained from exciting the system with 0.1N from the right corner of the top plate. Compared to results from Figure 15 there is more pronounced softening in the current analysis due to quicker switching time between the fully opened contact node pairs and fully closed contact node pairs.

Figure 24 shows the result from the parametric analysis done by varying the excitation parameters. It shows how the plate transitions the linear low response curve to the nonlinear high response solution.

### **3.6.2. Test Case 2**

Figure 25 shows a more challenging application of this novel ROM method to a Jackup platform with multiple intermittent contact areas on two of the three supporting legs of the platform. This is to simulate a case where the rack and pinion gears connecting hull and legs of a platform has

significant clearances and backlashes in two of the legs, causing a hull-leg intermittent contact situation resulting from environmental loads on the structure.

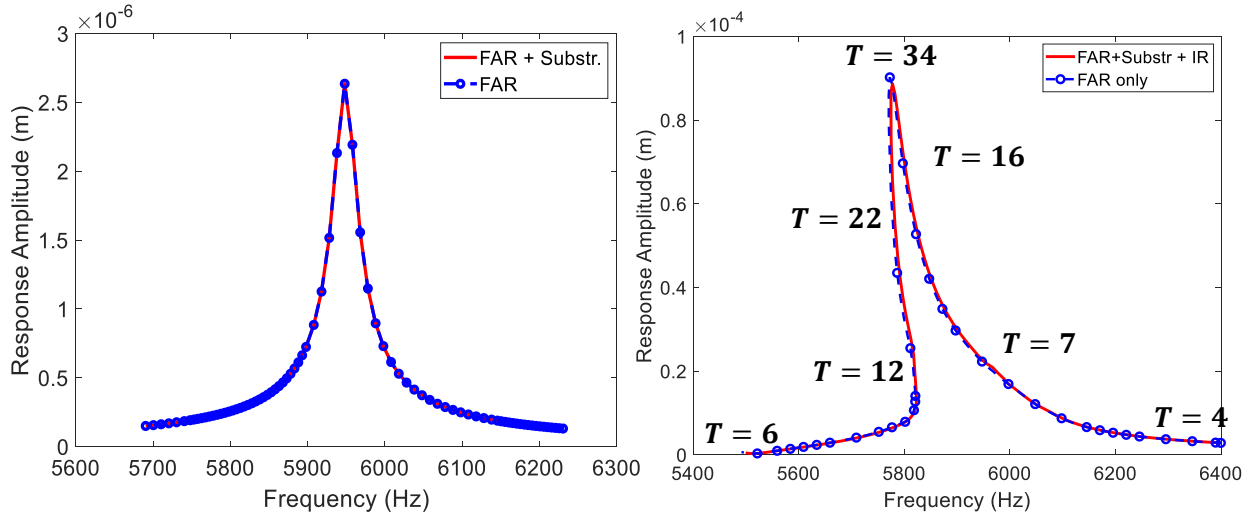


Figure 22. First in-plane bending response of double cracked plate excited at both ends with  $F_{ex} = 0.01\text{N}$  (Left), and  $F_{ex} = 0.1\text{N}$  (Right).

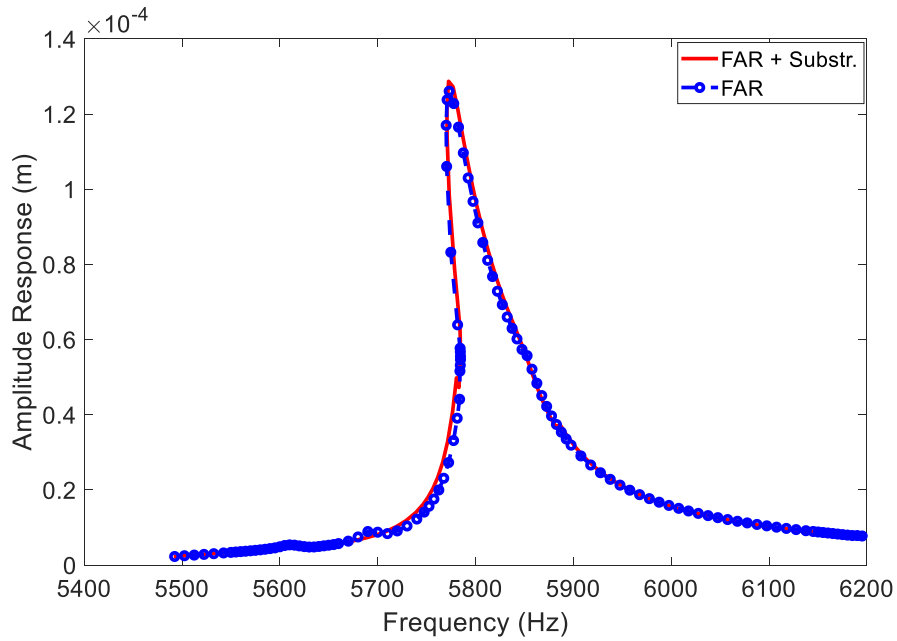


Figure 23. First in-plane bending response of double cracked plate excited at one end with  $F_{ex} = 0.1\text{N}$ .

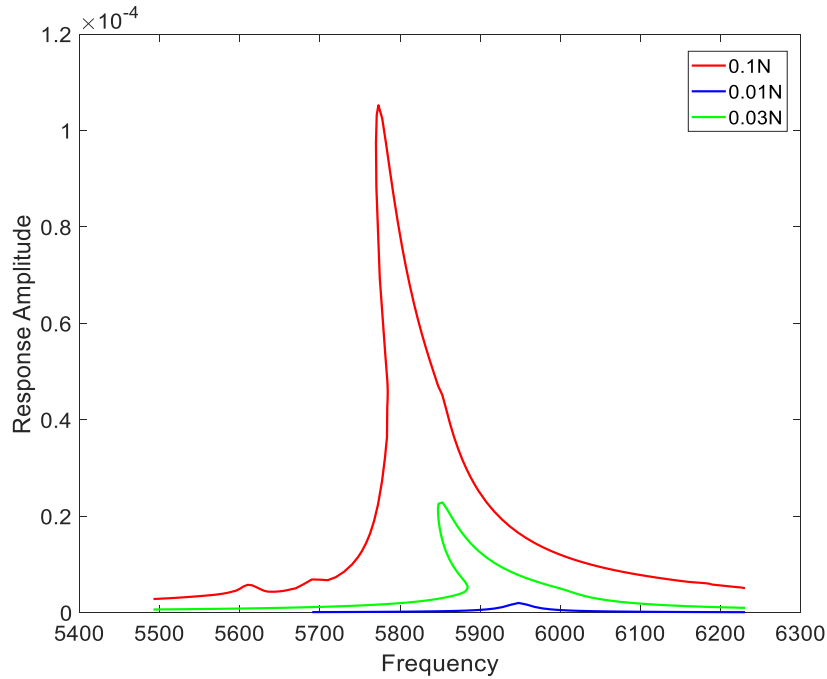


Figure 24. Variation of the response amplitude curve with variation in excitation amplitude.

Like in the rectangular plate test case, the platform is modelled in ANSYS using linear solid elements with  $\sim 170,000$  DoFs. The structure is tripartitely partitioned along the hull, as shown by the red thick lines in Figure 26, such that each substructure has a leg and a component hull with two interface connecting to adjacent substructures. Considering the relatively small amount of the contact nodes at the local contact interfaces compared to the total nodes of the system, and the predicted contact pattern from the first in-plane bending mode excitation, the legs with the contact interfaces are modelled stiffer than the rest of the platform in order to increase the difference in frequency between the fully opened and fully closed contact interface conditions. Also note that the normal contact stiffness  $k_n$  at the contact interfaces is  $5.68 \times 10^7$  N/m with negligible friction and slip between contact node pairs.

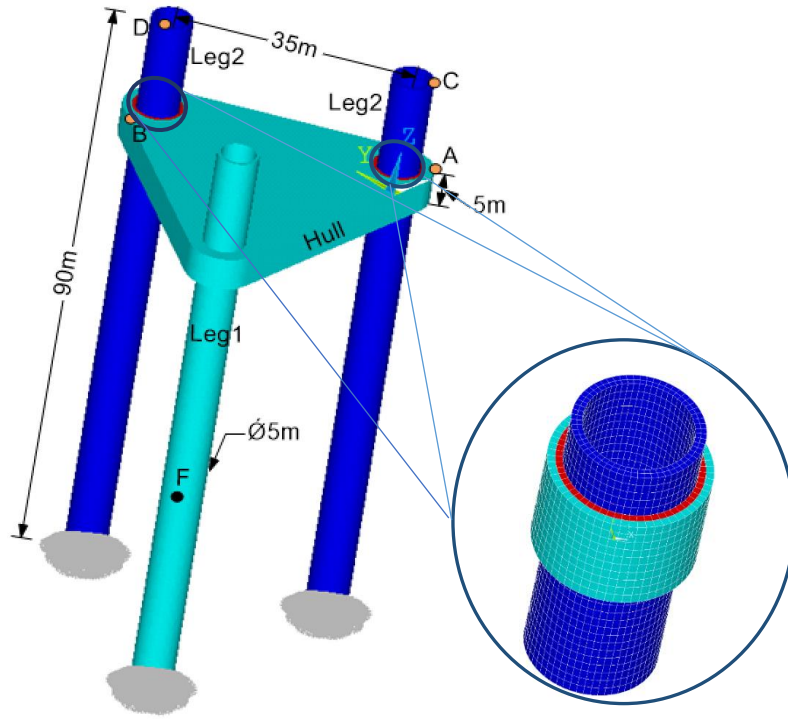


Figure 25. Jackup platform model with two local intermittent contacts at then interface between the hull (triangular shape), leg 2 and leg 3.

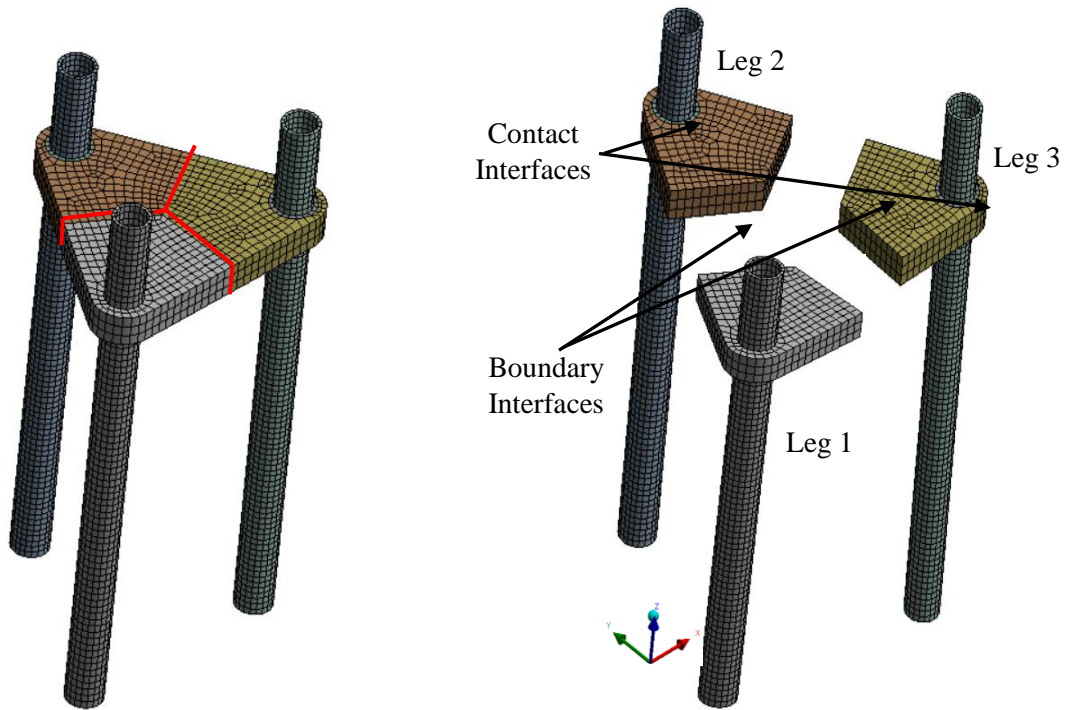


Figure 26. FE model of the partitioned and exploded view of a Jackup platform with double intermittent contacts.

The platform is modelled with 0.2m gap between the contact pair nodes at the contact interfaces to mimic backlash clearance from the rack and pinion present in an actual Jackup platform. Therefore the contact node pairs is expected to be opened during static conditions and at low excitation frequency of the platform. Figure 27 shows the modes of the global linearized fully closed and fully opened contact interface conditions which provides insight into the bases selection for the nonlinear contact problem. As expected the modal frequencies of the fully closed BC is higher than the fully opened BC and therefore more opened BC modes are likely to be selected in approximating the dynamics of the platform within a specified frequency range of solution than the closed BC modes.

The normal modes and frequencies of paired subassemblies of the subcomponents with fully closed and fully opened contact BCs are also shown in Appendix A. This highlights the predicted dynamic behavior at connecting boundary interfaces of the paired components to enable mode selection for the boundary interface DOFs reduction. The bilinear constrain modes are generated from these type of subassemblies. Only few of these subassemblies is shown because the logic of symmetry can be used to determine the outcome of other possible combinations.

The nonlinear frequency response of the Platform at different location of the platform is shown in Figure 28. The platform is excited laterally at point F on leg 1, which is rigidly connected to the hull, as shown in Figure 25. The response displacement is measured at points A, B, C and D of the platform. The hardening behavior of the platform is common in the response at all the locations, although the motion trajectory are different.

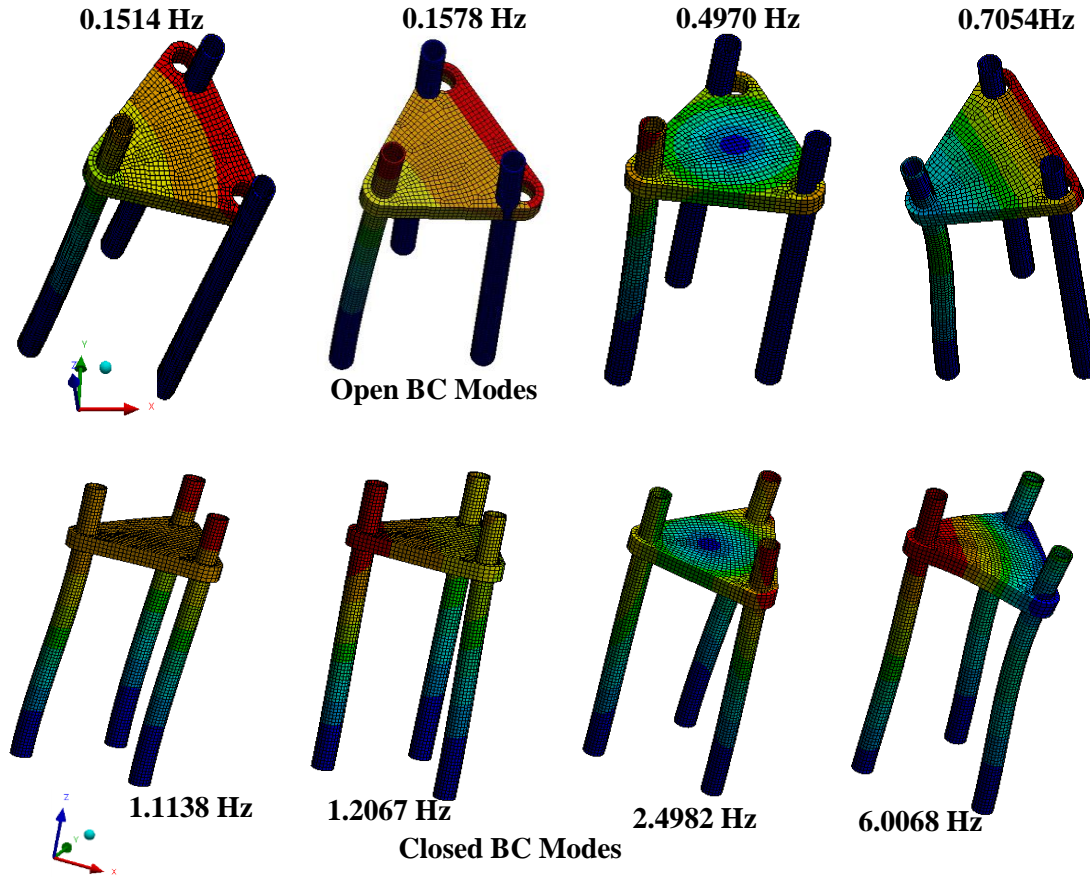


Figure 27. Mode shapes of the linearized fully open and fully closed contact BC of the jackup platform.

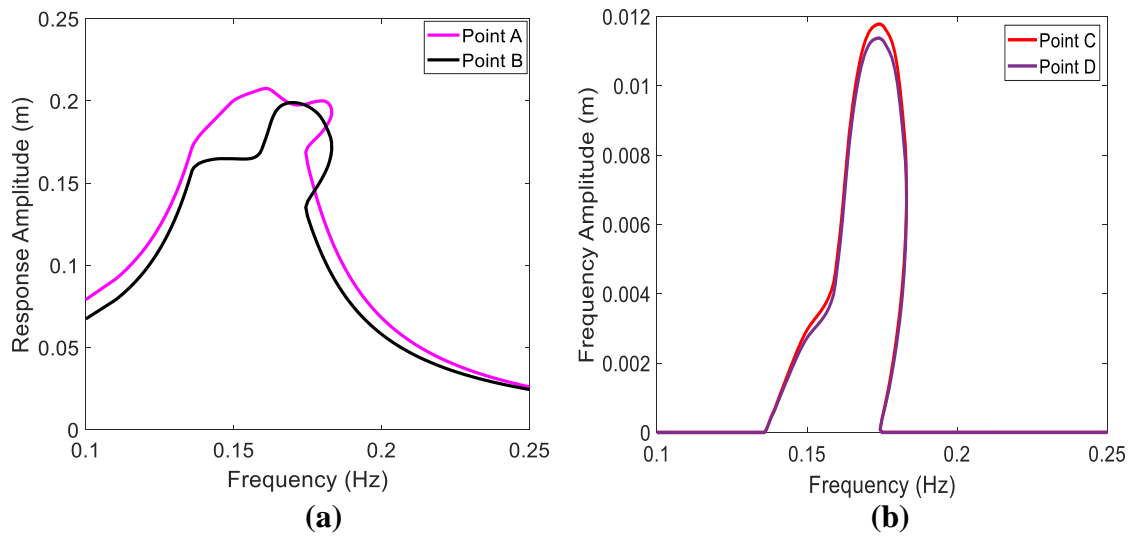


Figure 28. (a) Frequency response curve of platform measured at point A and B. (b) Frequency response curve of platform measured at point C and D.



As expected, the response curves of Legs 1 and 2 (Figure 28b) are similar and experience a relatively moderate hardening because at any instant in time, with the system operating in the neighborhood of the resonant frequency, almost the same number of contact pairs nodes are switching but at opposite halves of the legs. However, the motion trajectory measured from the platform close to the contact interface appears to me more complicated as seen in Figure 28a. This is due to the effect from the fluctuation in the number of switching nodes at the platform's contact interface.

The result obtained from the implementation of substructuring with boundary reduction combined with the FAR technique is validated in Figure 29. The new concept (indicated as 'FAR+SUB+IR') is compared with the application of FAR on the full structure (indicated as 'FAR') and using FAR with subtracting but without boundary interface reduction (indicated as 'FAR+SUB'). The performance of the new approach is very competitive to the other proven approaches. The 'FAR+SUB+IR' outperforms the 'FAR+SUB' in that the large amount of equations associated with boundary interface DoFs (~150 per interface) in the later, is considerably reduced (maximum total of 8). While novel method suffers an increase in the size of the ROM compared to the FAR only method, the advantages it provides through substructuring is very significant especially in large systems susceptible to local structural changes.

Figure 30 shows the variation in the ROM size of the assembled system over the solution frequency range. The FAR inherent advantage of optimal variation in ROM size is clearly visible and the MPC value  $\epsilon_2$ , with the minimum number of the maximum ROM size at an acceptable error is used in this analysis ( $\epsilon_2 = 2 \times 10^{-3}$ ). Figure 31 shows the frequency response of the platform at different values of the MPC value  $\epsilon_2$ .

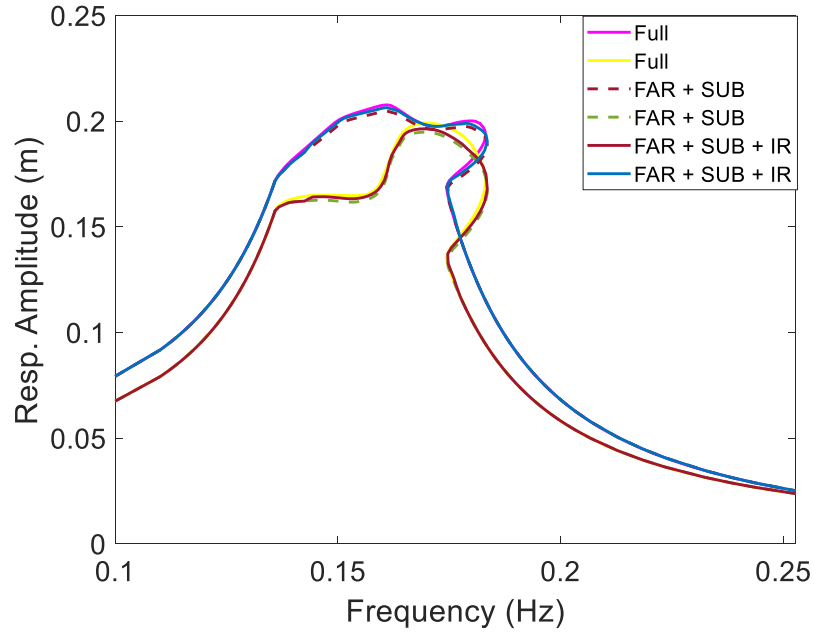


Figure 29. Comparison of frequency response of platform from new approach to other standard methods.

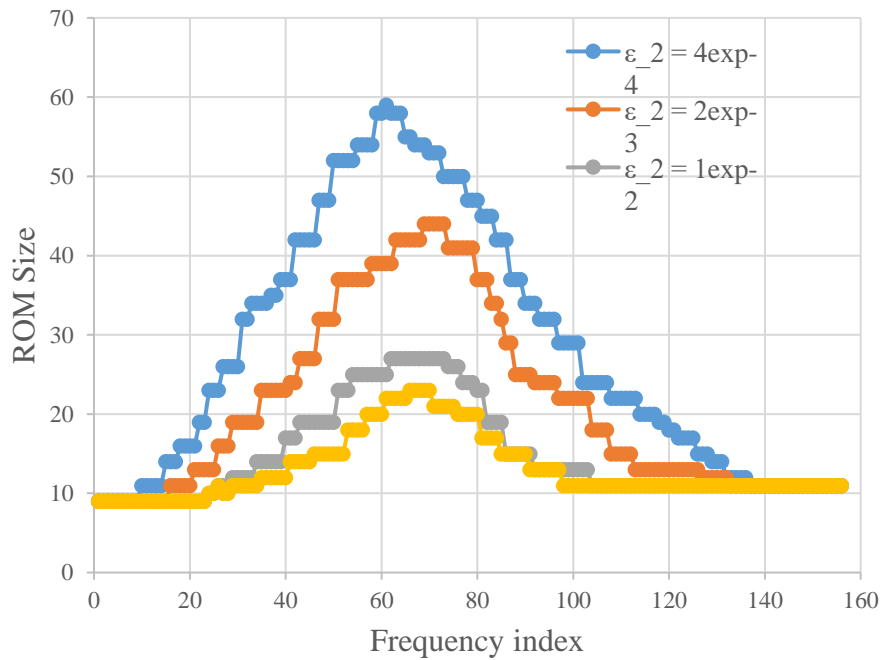


Figure 30. ROM Size variation with variation in MPC cutoff parameter  $\epsilon_2$ .

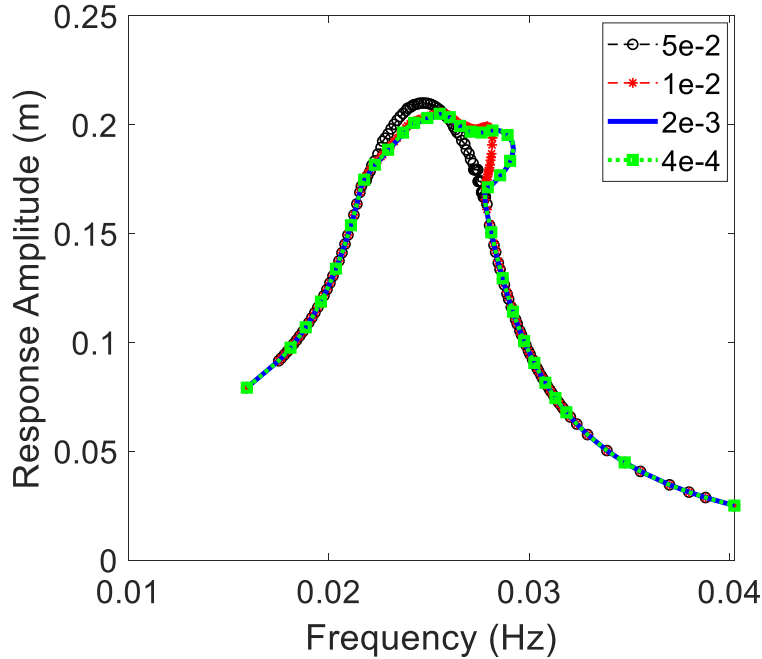


Figure 31. Parametrization effect of MPC cutoff value  $\varepsilon_2$  on the frequency response curve.

### 3.7. Conclusion

A nonlinear substructuring strategy is developed for solving systems with multiple intermittent contacts and tested with the FAR approach. The method is based on the conventional CB-CMS technique, which have shown to be effective methods for linear problems. By the inclusion of bilinear modes in the reduction basis, the reduced systems are able to capture the nonlinearities from intermittent contacts. Bi-linearity is applied in the form of FI-BLMs which are similar to the regular fixed interface modes but adding the contact effect. In order to select the optimal set of FI-BLMs and therefore minimize the size of the global reduction matrix, the FAR was applied. Besides the nonlinear reduction, the DoFs at the boundary interfaces connecting the substructures is also reduced. The interface reduction is done at the substructure level by pairing adjacent substructures and using the bilinear constraint mode idea to obtain the interface modes. Combination of few selected modes of all the interfaces associated with a substructure is the

applied along with the regular CB-CMS static constrain modes to transform the boundary DoFs. The method was first applied to a rectangular plate with double intermittent contact to test the strength of the approach. Results from different loading conditions show a good agreement with the benchmark. A second test case of a Jackup platform with intermittent contact surfaces at two of the three hull-legs interfaces was also considered. Solutions obtained from the novel method showed very good prospects and advantages compared to other proven methods used applied in comparison. Therefore based on the nonlinear solutions presented in this two test cases, the accuracy and usability of the developed method can be concluded to be effective in tracking the behavior of system with multiple intermittent contacts.

## CHAPTER IV

### **4. Bi-linear modelling of legged micro-robot locomotion based on contact dynamics and vibration in multiple modes**

#### **4.1. Introduction**

In recent years, the desire to design high fidelity dynamic models to capture both structural motions and contact behavior of microscale robots have continue to gain significant attention due to increased potential area of applicability of this systems. Some of the potential area of applicability include biomedical and bioengineering (minimally invasive surgeries, drug administration, therapeutics and tissue engineering), military (disaster response, rescue and tactical operations) and system monitoring [79]. Effective application of this microrobots require constant research and improvement in developing new actuation mechanisms, power source, control systems and dynamic modelling concepts to achieve higher precision and accuracy during their operations. This work introduces the concept of bilinear reduced order modelling in predicting the dynamics of a legged, piezoelectric driven microrobot.

Several Dynamic concepts to model the locomotion of small scaled mobile systems has been studied in the past. Some of this idea include modelling and testing of centimeter scaled robots with locomotion principle similar to that obtained in biological organisms [80][81]. These works details the dynamic interaction between different parts (foot–terrain and foot–body interaction) of a silicon micromachined robot in predicting the global motion of the robot.

Characterization of the nonlinear interaction between the foot and terrain is done with consideration of the nonlinear air damping and adhesion in estimating microrobotic dynamics. The leg-body interaction on the other hand is influenced by the elastic structural resonances of the legs and body of the microrobot. This has tendencies to be very complicated considering modal coupling interaction between each leg and the body or among the legs. Lumped parameter models used in simplification of the legs and body as implemented in these works will not capture such modal interactions especially in relation to the foot-terrain interactions. This research proposes the FE modelling of microrobot with bilinear contact modelling of the foot-ground interaction.

The research proposes a mathematical model to investigate the motion of a legged, piezoelectric driven microrobot working with stick-slip principle. An earlier attempt in Ref. [82] developed a theoretical analysis of a single legged microrobot with the assumption that the relative mass of the leg compared to the body of the robot is negligible. This assumption, which can result in considerable error in design, fabrication parameters and control of the system, was eliminated in a later research. The recent work [83] considered a multiple legged robot with continuous mass and elastic distribution. The forced response of the microrobot under the effect of a driving voltage excitation was determined from the formulated equation of motion using the assumed-mode method. The physical characteristics of the robot coupled with the friction force distribution was used to determine the direction of motion of the microrobot. Also, the effect of the mass distribution between the robot's body and its legs on the average velocity is examined and some predictions for appropriate operating conditions of the microrobot was provided. One major drawback of this model is that only the fundamental mode is included in the analysis and separation of the leg from the ground was analyzed.

Other techniques have improved on adding important design considerations to improve on the previous model. A recent research, developed a validation model to analyze the dynamic impact behavior on the locomotion of a millimeter-scale multi-legged microrobot under the influence of relatively small-scaled excitation. In the attempt to address the modal interaction challenge, multiple vibration modes were included in the modelling of all the legs. The dynamics of adhesion and rest between the feet and ground was distinguished for a better understanding of the adhesion influence on microrobot dynamics. The model was proposed to predict the robot forward motion and individual leg motion after obtaining cogent design parameters and prefabrication analysis.

## **4.2. Robot Locomotion**

The motion of a hexapod-legged microrobot can be very complex considering that their locomotion is a concept mostly inspired by multipod invertebrates like insects. Therefore it is important to understand and simplify nature and process of motion to be studied. Figure 32 shows the architecture of the FEM model of to be studied. The general design is motivated by a type of millimeter-scale, piezoelectric and polymer thin-film robot fabricated with micro-machining with a rigid body and multiple pairs of legs on both sides of the body as shown in Figure 33a [ 84]. Figure 33b shows the experimental model that motivated this study. The centimeter-scale 6-legged prototype was made with 3D-printed polylactic acid (PLA) frame bonded with piezoelectric ceramic strips as actuators. Similar to the understudied prototype, the FEM robot is made up of six arms, leg, feet and one main body rigidly connected to one another as illustrated in the diagram. The robot is actuated by a combination of six PZTs with each connected to the arm linkages connecting the main body and the legs of the robot. The PZT is actuated such that it generates a bending moment to rotate the robot foot out of plane.

Conceptually, the locomotion of this robot is based on alternating excitation of the PZTs in a manner that alternatively excites the extreme legs on one side and the mid leg on the other side of the robot simultaneously. Note that the PZT is deliberately connected to the arm to extend beyond the leg width to create asymmetry along the lateral axis of the arms. This asymmetry allows the arm, during the upward stroke of the leg, to experience a residual moment along the lateral axis therefore creating an angle between the longitudinal axis of the leg and the vertical (normal to the ground) during the downward stroke. This angular contact of the leg-foot assembly with the ground will propel it forward. The overall motion and position of the robot at the end of each step cycle (a complete upward and downward stroke of the leg) will depend on the magnitude of the resultant lateral moment generated by all the legs. In order to minimize the power needed to excite the robot, the PZTs are operated at frequency near the resonance of the robot.

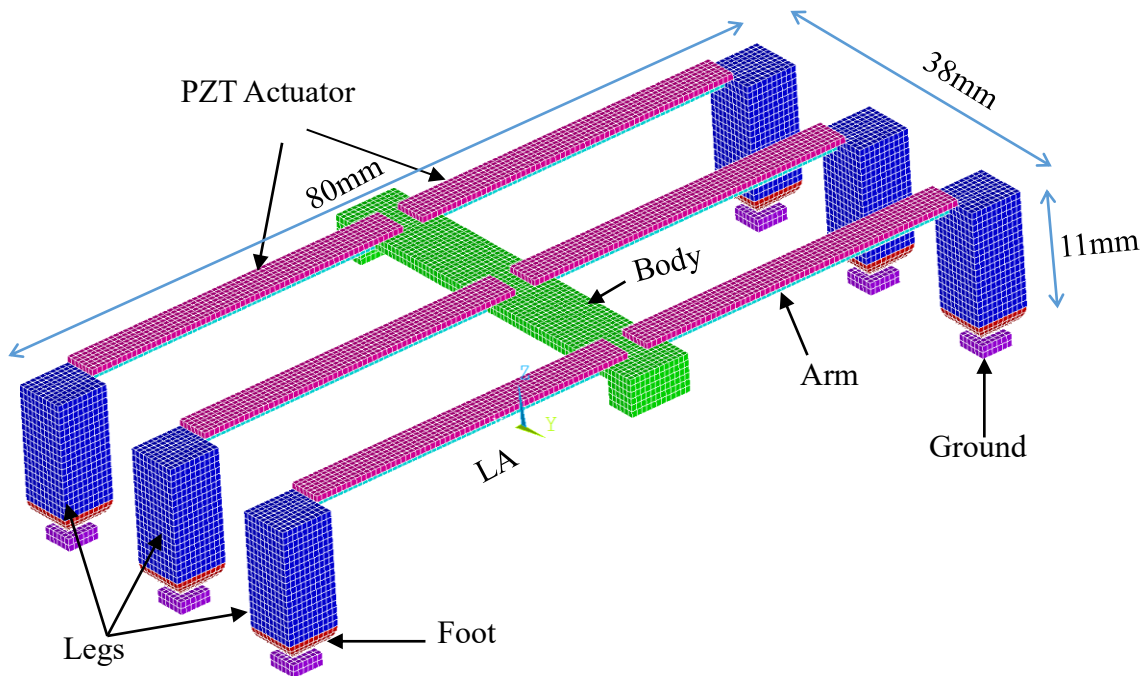


Figure 32. FEM model of PZT actuated, centimeter scale hexapod microrobot



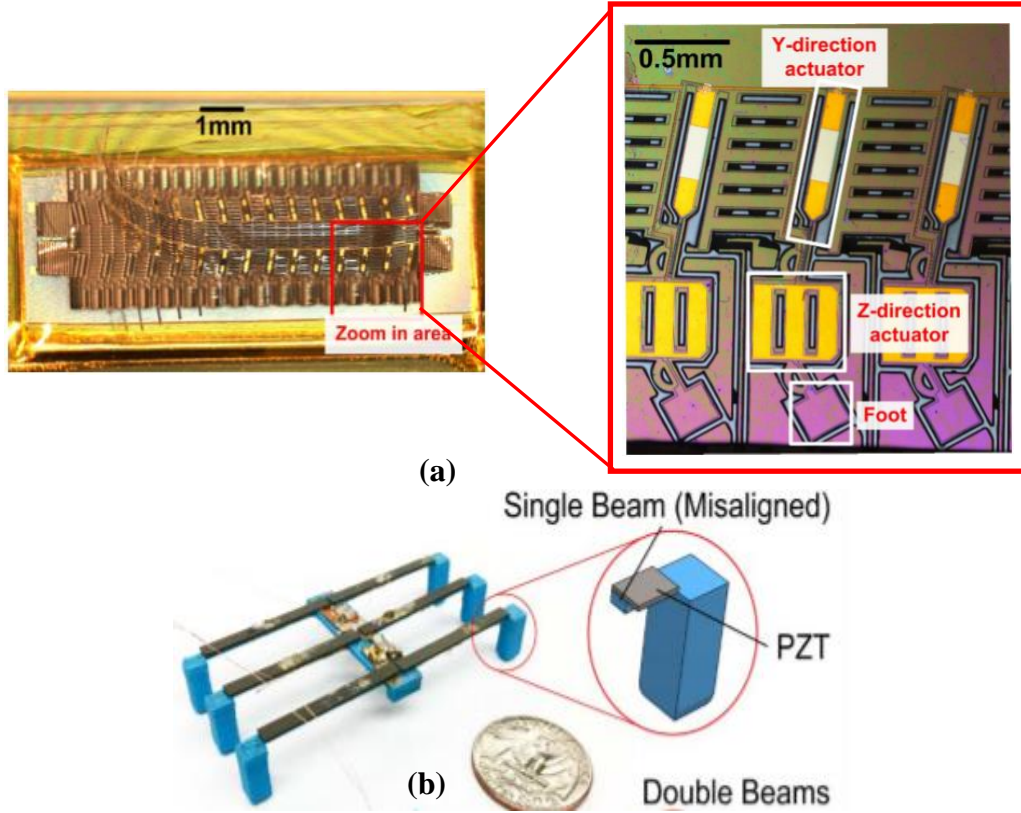


Figure 33. (a) Picture of a silicon micromachined millimeter-scale microwalking robot [84]. (b) Photo of a centimeter-scale walking robot prototype with the leg schematic [85].

### 4.3. Robot Structural Modeling

Modelling of the centimeter scaled, hexapod micro robot shown in Figure 32 is generated by the FEA of its dynamic and rigid body vibration. The robot body and the leg-foot assembly are modelled to be relatively rigid compared to the compliant arm linkages connecting the body and leg-foot assembly of the robot. The locomotion of the robot is highly dependent on both modal vibration of the arm linkages and the nature of the nonlinear interaction between the foot and the ground. The governing equation of motion computed in terms of the physical displacement  $\mathbf{q}$  is written as

$$\mathbf{M}\ddot{\mathbf{q}} + \mathbf{C}\dot{\mathbf{q}} + \mathbf{K}\mathbf{q} = \mathbf{F}_{ps} + \mathbf{F}_{ex} + \mathbf{F}_{nl}, \quad (56)$$

where  $(\dot{\phantom{x}})$  is the time derivative.  $\mathbf{M}$ ,  $\mathbf{C}$  and  $\mathbf{K}$  are the mass, viscous damping and stiffness matrices of the entire robot.  $\mathbf{F}_{ps}$  is the vector of pre-stress forces applied to the body and is used to model gravity in the system,  $\mathbf{F}_{ex}$  is the excitation vector generated from the Piezoelectric actuation,  $\mathbf{F}_{nl}$  is the vector of nonlinear contact forces acting at the foot-ground contact pairs.

In order to resolve the complexity associated with the nonlinear contact force which could make Eq. (56) difficult to solve, the HBM is used to obtain the steady state solution of the model. In order to use HBM, we assume that the steady state displacements and nonlinear forces are periodic. Hence, they are expressed as a sum of harmonic terms. As the harmonic functions are linearly independent, equating their coefficients yields a set of algebraic balance equations in the frequency domain for harmonic-indices  $h = 0$  to  $h = nH$  at a frequency  $\omega$  as follows:

$$\begin{aligned} \mathbf{K}\mathbf{q}^0 &= \mathbf{F}_{ps} + \mathbf{F}_{ex}^0 + \mathbf{F}_{nl}^0, & h = 0, \\ [- (h\omega)^2\mathbf{M} + jh\omega\mathbf{C} + \mathbf{K}]\mathbf{q}^h &= \mathbf{F}_{ex}^h + \mathbf{F}_{nl}^h, & h = 1, \dots, nH, \end{aligned} \quad (57)$$

$\mathbf{q}^h$  can then be solved using iterative method that tries to minimize the residual of the equations. Calculating the frequency equivalent of the nonlinear contact force requires the AFT procedure [6][42] and the contact model described later. To perform AFT, the Fourier coefficients of the relative tangential and normal displacements are extracted at all the foot-ground contact node pairs in  $\mathbf{q}^h$ . The inverse Fourier transform of these coefficients generates the periodic functions in the time domain. The equivalent contact forces are then calculated using the contact model and then converted back to the frequency domain via another Fourier transformation. The nonlinear forcing  $\mathbf{F}_{nl}^h$  is obtained by calculating the local nonlinear forces on all the nodes at every foot and then assembled accordingly.

Considering that the behavior of the untethered microrobot is a combined motion of the dynamic and rigid body vibration of the system, the nonlinear force is not only a function of contact node pair DoFs, normal to the ground, in  $\mathbf{q}^h$  but also a function of the rigid body mode DoFs as shown in Eq (58).

$$\bar{\mathbf{F}}_{nl}^h(\mathbf{q}_{m(z)}^h, \mathbf{q}^{r_3}, \dot{\mathbf{q}}^{r_1}t, \dot{\mathbf{q}}^{r_2}t) \quad (58)$$

where  $\mathbf{q}_{m(z)}^h$  is the contact node pair DoFs normal to the ground and  $\mathbf{q}^{r_1}$ ,  $\mathbf{q}^{r_2}$  and  $\mathbf{q}^{r_3}$  are the rigid body DoFs associated with the x, y and z directions as shown in Figure 34.

For the rigid body, the combined rigid body mode transformation matrix can be written as

$$\mathbf{\Phi}^r = [\mathbf{\Phi}^{r_1} \quad \mathbf{\Phi}^{r_2} \quad \mathbf{\Phi}^{r_3}] \quad (59)$$

where  $\mathbf{\Phi}^{r_1}$ ,  $\mathbf{\Phi}^{r_2}$  and  $\mathbf{\Phi}^{r_3}$  are the rigid body modes in the lateral (x and y) and normal (z) directions.

The rigid body coordinates  $\mathbf{q}^r$  is defines as

$$\mathbf{q} = \mathbf{\Phi}^r \mathbf{q}^r \quad (60)$$

Sustituting Eq. (60) into the EoM in Eq. (56) and premultiplying by  $\mathbf{\Phi}^{rT}$  yields

$$\mathbf{M}^r \ddot{\mathbf{q}}^r + \mathbf{C}^r \dot{\mathbf{q}}^r + \mathbf{K}^r \mathbf{q}^r = \mathbf{F}_{ps}^r + \mathbf{F}_{ex}^r + \mathbf{F}_{nl}^r \quad (61)$$

where

$$\begin{aligned} \mathbf{M}^r &= \mathbf{\Phi}^{rT} \mathbf{M} \mathbf{\Phi}^r, \mathbf{C}^r = \mathbf{\Phi}^{rT} \mathbf{C} \mathbf{\Phi}^r, \mathbf{K}^r = \mathbf{\Phi}^{rT} \mathbf{K} \mathbf{\Phi}^r, \mathbf{F}_{ps}^r = \mathbf{\Phi}^{rT} \mathbf{F}_{ps}, \\ \mathbf{F}_{nl}^r &= \mathbf{\Phi}^{rT} \mathbf{F}_{nl}^h, \text{ and } \mathbf{F}_{ex}^r = \mathbf{\Phi}^{rT} \mathbf{F}_{ex}^h. \end{aligned} \quad (62)$$

For rigid body motion  $r_1$  and  $r_2$ , taking the following into account; steady state ( $\ddot{\mathbf{q}}^r = \mathbf{0}$ ), zero eigenvalues ( $\mathbf{K}^r = \mathbf{0}$ ) and zero prestress gives

$$\begin{aligned} \mathbf{C}^r \dot{\mathbf{q}}^r &= \mathbf{F}_{ex}^r + \mathbf{F}_{nl}^r \quad \text{for } r = r_1 \text{ and } r_2 \\ \mathbf{q}^{r_1} &= \dot{\mathbf{q}}^{r_1} * t \text{ and } \mathbf{q}^{r_2} = \dot{\mathbf{q}}^{r_2} * t \end{aligned} \quad (63)$$

where  $t$  is the total sticking and sliding time during a period of vibration. Invoking zero eigenvalues and zero external forcing on rigid body  $r_3$  gives

$$\mathbf{M}^r \ddot{\mathbf{q}}^r + \mathbf{C}^r \dot{\mathbf{q}}^r = \mathbf{F}_{ps}^r + \mathbf{F}_{nl}^r, \quad \text{for } r = r_3 \quad (64)$$

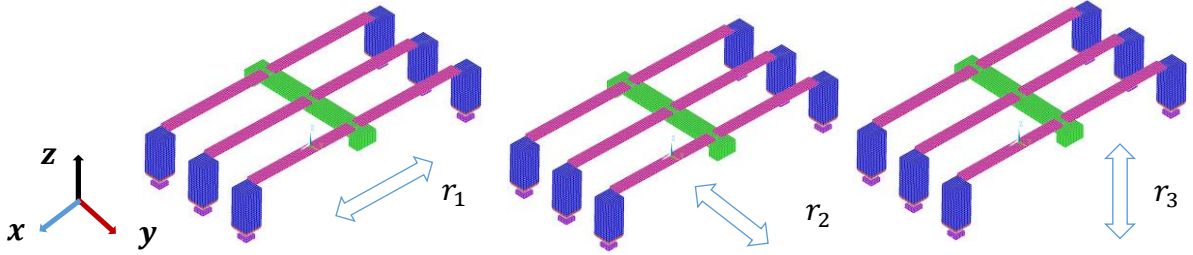


Figure 34. Rigid body motion considered in analysis of the microrobot

The damping term  $\mathbf{C}^r$  in the rigid body motions  $r_1$  and  $r_2$  from Eq. (63), is modelled with proportional damping such that

$$\mathbf{C}^r = \alpha \mathbf{M} \quad (65)$$

where  $\alpha$  is the mass proportion coefficient and will be referred to as the rigid body constant hereafter. The dynamic harmonic EoM in Eq. (57) and the rigid body equations in Eq. (63) and Eq. (64) are solved simultaneously using the ALC

#### 4.4. Nonlinear friction force

The nonlinear force  $F_{nl}$  in Eq. (56) is associated with friction which accounts for the local elastic restoring forces during the stick phase and dissipative forces during the slide phase of the microrobot. Given that the aim of this study is to obtain the steady-state response of the microrobot under a periodic forcing, the dissipative energy at the contact during a period of the motion is calculated by a quasi-static analysis. This analysis can be achieved by Colomb's law. Consider the leg-ground contact setup shown in Figure 35.

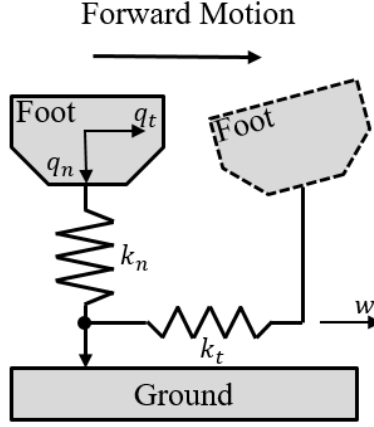


Figure 35. Schematic view of the contact model between the robot's foot and ground

The contact node pair at any point between the foot and the ground has a contact stiffness represented by springs. Piezoelectric excitation effect on the leg causes relative displacement in the normal direction  $n$  resulting in either a stick or separation depending on the conditions in the equation below,

$$\bar{\mathbf{F}}_{nl}^n = \begin{cases} k_n \bar{q}_n & \text{if } \bar{q}_n > 0 \\ 0 & \text{if } \bar{q}_n \leq 0 \end{cases} \quad (66)$$

Separation occurs at the lower branch when relative displacement is negative and therefore the normal nonlinear force  $\bar{\mathbf{F}}_{nl}^n = 0$ , and  $\bar{\mathbf{F}}_{nl}^n = k_n \bar{q}_n$  when the contact condition is stuck. Similarly, the tangential friction force is dependent on the tangential relative displacement and its magnitude and direction determined according to the following equation,

for  $\bar{\mathbf{F}}_{nl}^n = 0$ ,

$$\bar{\mathbf{F}}_{nl}^t = 0 \quad (67)$$

otherwise

$$\bar{\mathbf{F}}_{nl}^t = \begin{cases} k_t(q_t - w) & \text{if } k_t|q_t - w| < \mu N \\ -\mu \bar{\mathbf{F}}_{nl}^n & \text{if } k_t(q_t - w) \geq \mu N \\ \mu \bar{\mathbf{F}}_{nl}^n & \text{if } -k_t(q_t - w) \geq \mu N \end{cases} \quad (68)$$

If separated i.e.  $\bar{F}_{nl}^n = 0$  then the tangential frictional force is zero. The contact pair are in stick condition at the top branch of the equation. This is equivalent to when  $w$  remains constant i.e. velocity  $\dot{w} = 0$ . The last two branches of the equation represent positive and negative slip or sliding conditions of the contact pairs. It's important to note that while it is not possible to pre-determine the contact condition at each instant of time, we can assume the stick condition at the initial time which would eventually converge to the right condition over a period.

#### 4.5. Reduced order modeling

The FEM solution of the multi-legged microrobot considered in this research require a large DoF due to the fine discretization of the model, especially near the foot-ground assembly, necessary for accurate and reliable dynamic solution. However the cost of modelling such high fidelity system come at a heavy and expensive computational cost. Also, considering the complex nature of the nonlinear forces likely to be generated from the incessant interaction of the robot foot with the ground, the full order analysis of the system will result into a set of highly nonlinear, coupled EoM. The CB-CMS and FAR bilinear reduction techniques explained in chapter two are employed to address these challenges. The internal linear DoF of the robot is considerably reduced via CB-CMS by projecting the equation of motion on a set of linearly independent fixed interface modes,  $\Phi_{CB}$  augmented with certain interface constrain modes  $\Psi$ . The contact dynamics is also approximated as the linear combination of sets of bilinear modes with special boundary conditions. FAR is applied to select the optimal set bilinear vectors included in the reduction matrix at every solution frequency being considered.

#### 4.6. Numerical Results

A centimeter-scale 6-legged robot model is designed to validate the locomotion model developed in previous section. The simulated robot motion at different frequencies was thus compared with

experimental measurement. Some of the experimental results, obtained from [85], are shown in Appendix B.

#### 4.6.1. Parameter Identification

Due to the high level of uncertainty in the material properties of the experimental robot’s material and the variation in the contact model parameters, certain parameters must be identified before validating the accuracy of the proposed model. To do this, we first investigate the effect of these parameters on the locomotion of the robot to identify the sensitivity of these parameters. By tuning each parameter over their estimated limits, it is possible to understand the magnitude of their effect on the robot dynamics. During the sensitivity analysis of any certain parameter, all the other parameters are held constant at their nominal value. The results in Figure 36 shows the summary of the sensitivity analysis of the model, where the velocity of the robot was measured as each parameter is perturbed. The result shows a nonlinear effect of the parameters with the robot’s speed and the order of parameter sensitivity as: normal stiffness  $k_n$ , tangential stiffness  $k_t$ , friction coefficient  $\mu$ , elasticity  $E$ , rigid body constant  $\alpha$  and density  $\rho$ .

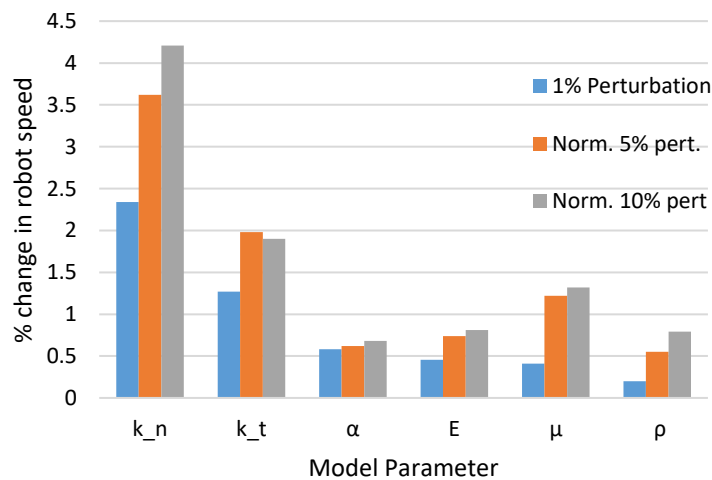


Figure 36. Sensitivity analysis of model parameters from 1% to 10% perturbation

Appropriate values of these sensitive parameters, for analysis, can be selected either by trial and error or by solving a nonlinear optimization problem using selected few experimental data obtained from the robot motion at discrete number of frequency points. To optimize the parameters, aggregate sum of squares of the residuals of the objective function,  $\varphi$ , over the frequency range of interest is minimized as

$$\min \varphi = \sum_{i=1}^n \|\mathbf{S}^*_{\omega_i} - \mathbf{S}_{\omega_i}\|^2 \quad (69)$$

$$\mathbf{S}_{\omega_i}(E, \rho, k_n, k_t, \mu, \alpha)$$

such that

$$E_{min} \leq E \leq E_{max}, \rho_{min} \leq \rho \leq \rho_{max}, k_{nmin} \leq k_n \leq k_{nmax}, k_{tmin} \leq k_t \leq k_{tmax}, \mu_{min} \leq \mu \leq \mu_{max} \text{ and } \alpha \geq 0 \quad (70)$$

where vectors  $\mathbf{S}^*$  and  $\mathbf{S}$  are the measured and computed speed of robot. The parameter limits used in the optimization function are from the estimated material properties of PLA [85]. Table 3 shows the optimal parameters used in validation analysis

Table 3. Robot model parameters obtained from optimization.

Parameter	Value
Elasticity $E$	2.55 GPa
density $\rho$	$1.23 * 10^3 \text{ Kg/m}^3$
normal stiffness $k_n$	$1.02 * 10^6 \text{ N/m}$
tangential stiffness $k_t$	$6.24 * 10^4 \text{ N/m}$
friction coefficient $\mu$	0.32
rigid body constant $\alpha$	2.4



Figure 37 shows the forward and vertical motion of two different legs (frontal and middle legs) of the robot. The robot shows very little motion in the vertical direction at low frequencies, but the middle leg shows some motion in the forward direction. This can only be attributed to the middle leg undergoing some periodic dynamic deformation but not necessarily causing the motion of the entire robot. This is confirmed in Figure 38 which shows the magnitude of the robot's forward velocity versus frequency. At first resonance, approximately 140Hz, there is significant motion in both the upward and forward direction. This further confirms the intended locomotion process described earlier, that the robot will move in the horizontal direction as a consequence of the robot leg making angular connection with the ground during the downward stroke of its vertical motion. The impulsive reversal of the robot's motion around the fundamental frequency is also observed in some experimental results and might require further analysis to understand this behavior, perhaps it could be a modal interaction phenomenon. The microrobot continues to go through a couple of forward and backward motion or combination of both depending on the excitation frequency until at around 152Hz when it reaches second resonance.

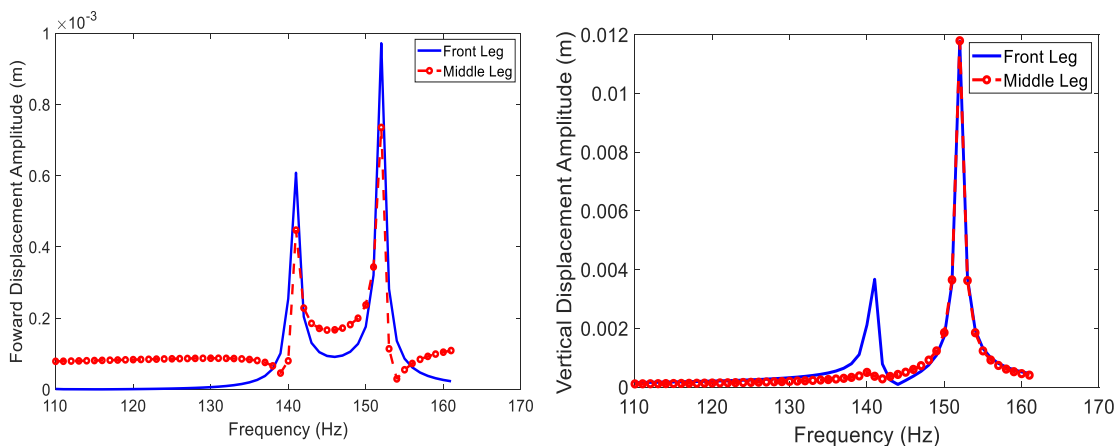


Figure 37. Frequency response of the forward and vertical displacement amplitude measured at the front and middle leg of the microrobot

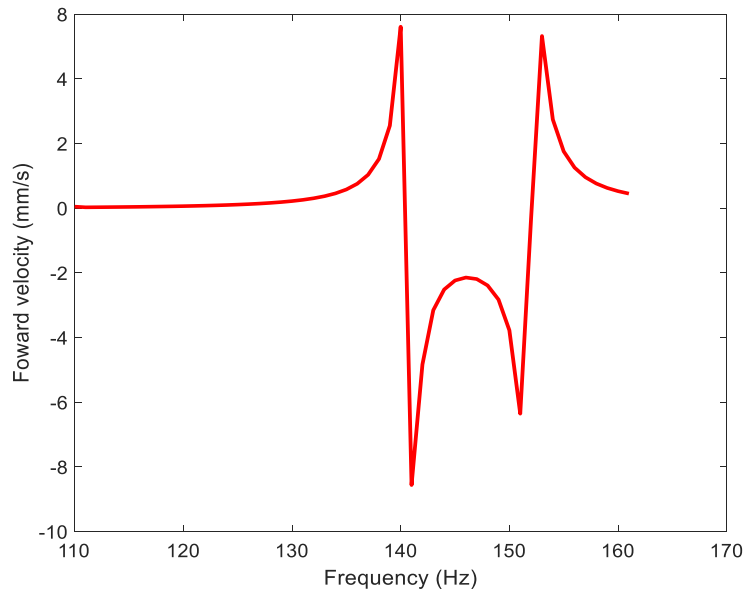


Figure 38. Frequency response of the robot's forward velocity

#### 4.6.2. Model vs Experimental Results

The characteristic time domain response of the microrobot over a period of vibration is shown in Figure 39. This measurement is taken at the fundamental frequency and at lower forcing amplitude. The combined motion of the dynamic and rigid body dynamics indicated by the solid sinusoidal line shows that the robot is horizontally displaced over a period. Therefore, confirming that the feet has an impact with the ground at least once during a vibration cycle as is the case in the experiments. The dashed line in the figure indicates the robot dynamic motion without including rigid body modes. In this case the robot has no displacement at the end of the cycle.

Comparison between the FEM solution and the experimental results shows that the direction of robot motion is generally the similar in both cases. As earlier stated the experimental results reported in this work can be found in Appendix B.

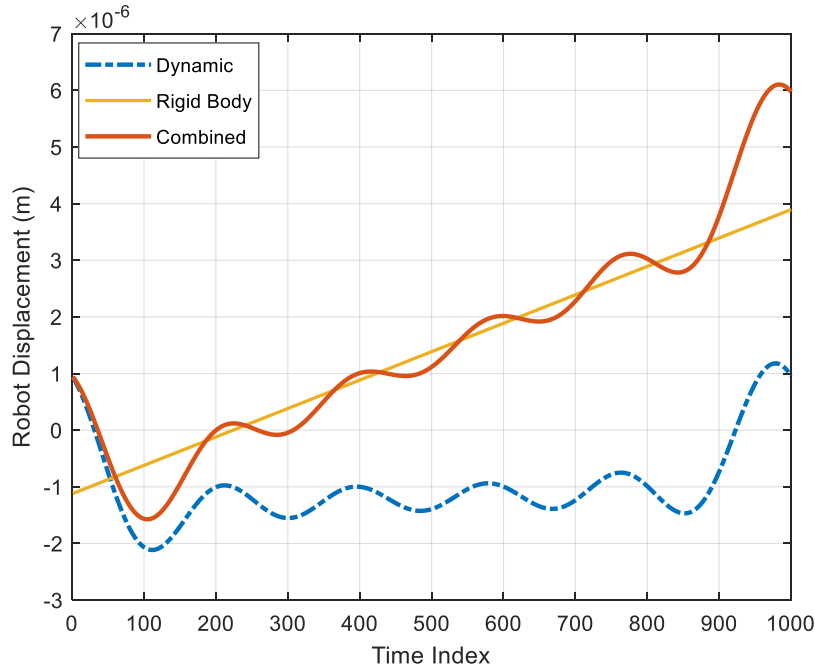
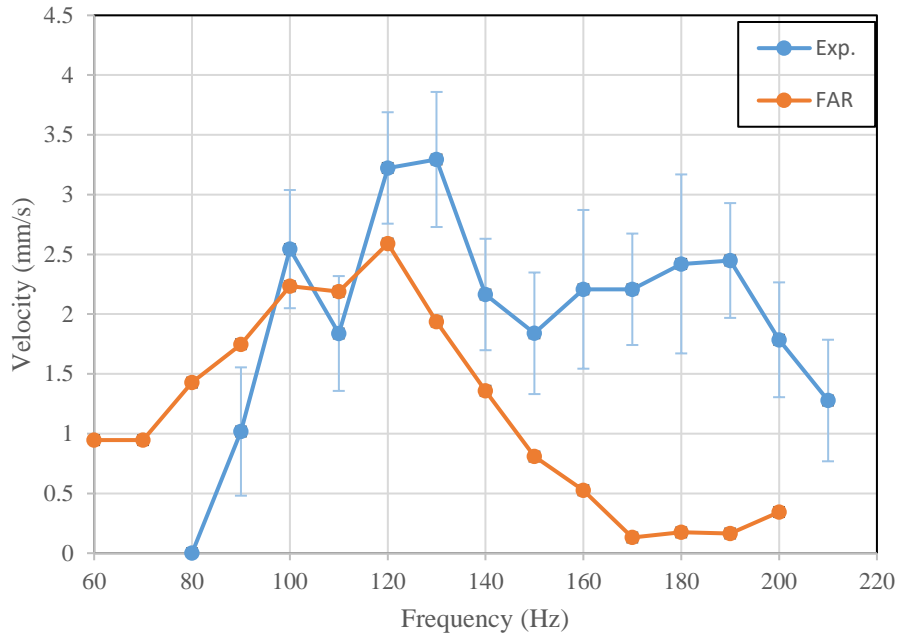
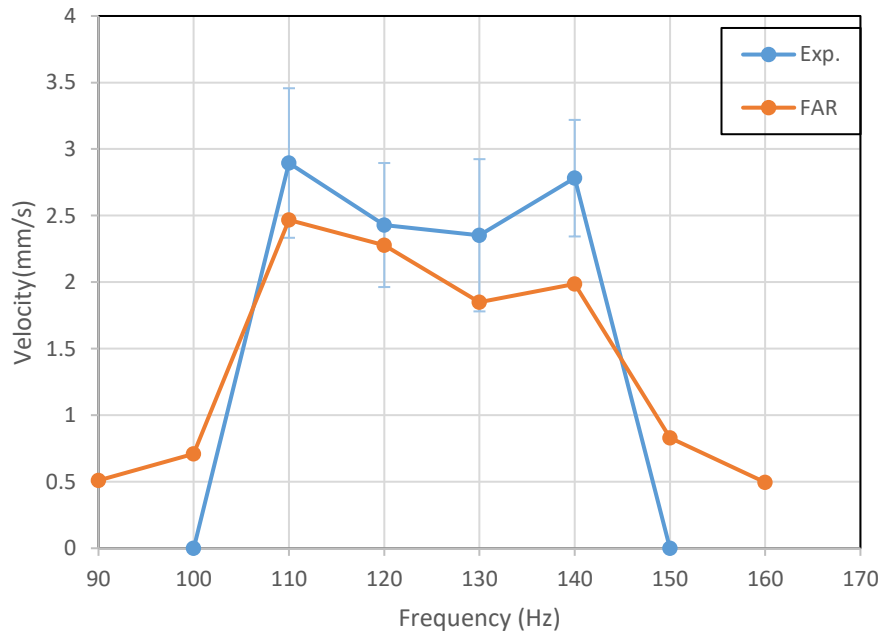


Figure 39. Periodic motion of the dynamic, rigid body and combined motions of the microrobot.

Figure 40a and Figure 40b shows the observed and FEM velocities versus frequency with actuation voltage of 30V on wooden and steel grounds respectively. Within certain frequency range, the predicted velocity modelled the experimental velocity well especially at lower to mid-range frequencies but begins to deviate at frequencies above the fundamental frequency. This could likely mean that a different set of system parameters need to be generated to predict dynamics at higher frequencies or the mathematical model adjusted to handle some of the unanticipated dynamics at these higher frequencies. Given that the optimization parameters used are identified at 30V and 110-130Hz, a more robust optimization to capture better universal system parameters might be necessary.



(a)



(b)

Figure 40. Relationship between the average velocity frequency response of the experimental and simulation results of the microrobot with (a) wooden ground (b) steel ground.

In Figures 41 and Figure 42, the dynamics of the robot around the first resonance (110Hz-140Hz) was studied under different excitation voltages to observe the validity range of the model. While it is generally observed that the model solution drift from the observed velocity at higher excitation amplitudes, the error is minimal at frequencies closer to the resonant frequency. The increasing error at higher frequencies could likely be as a result of the microrobot bouncing a lot such that some of its legs remains in the air for too long before making contact with the ground.

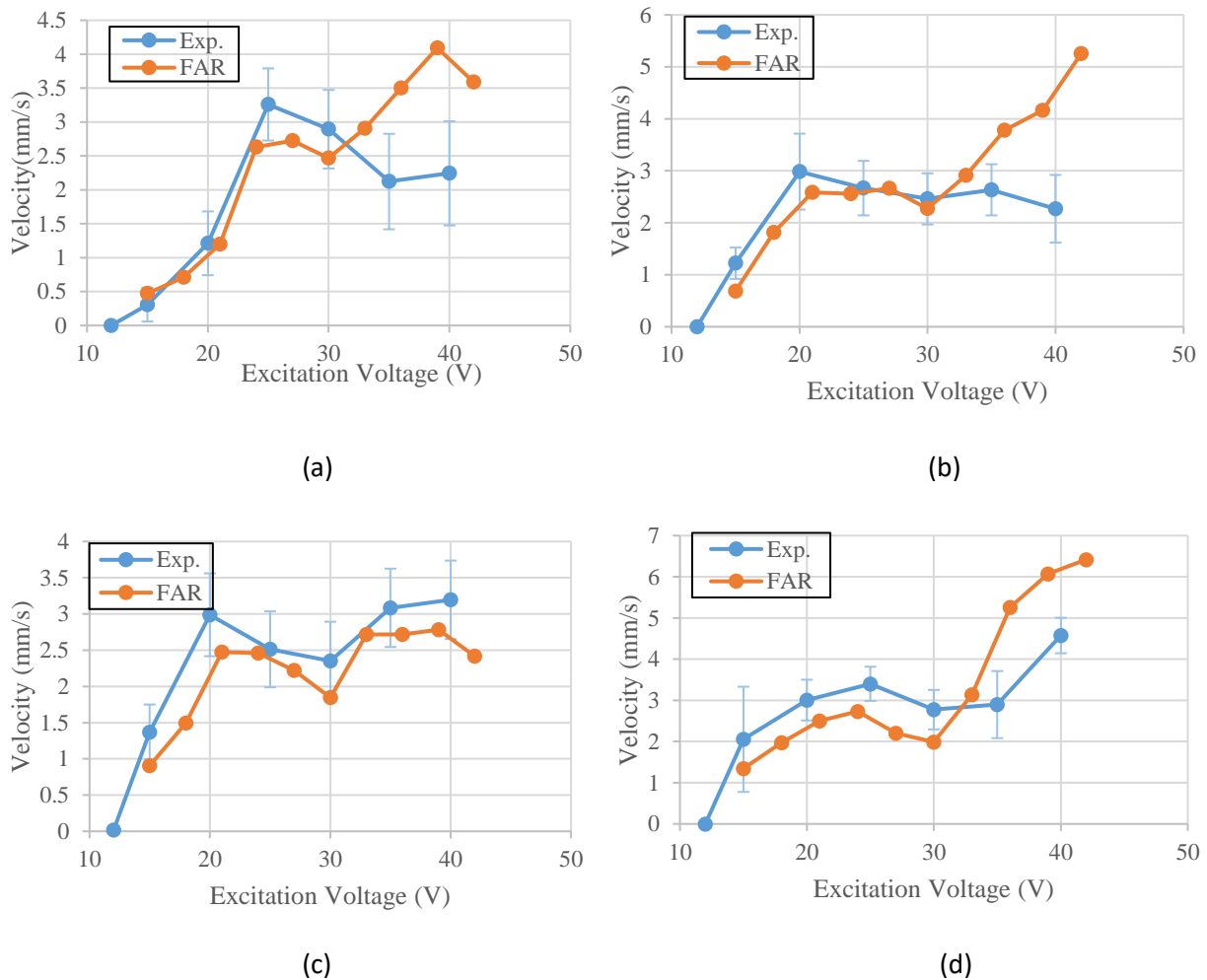
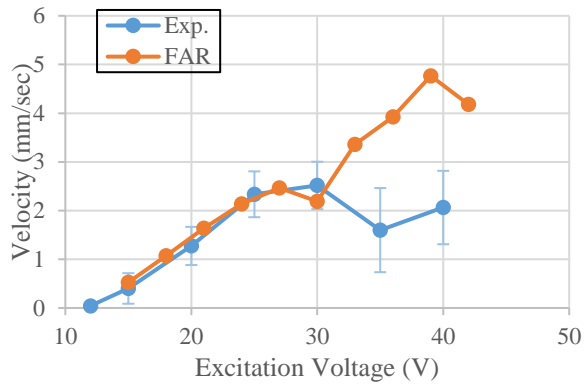
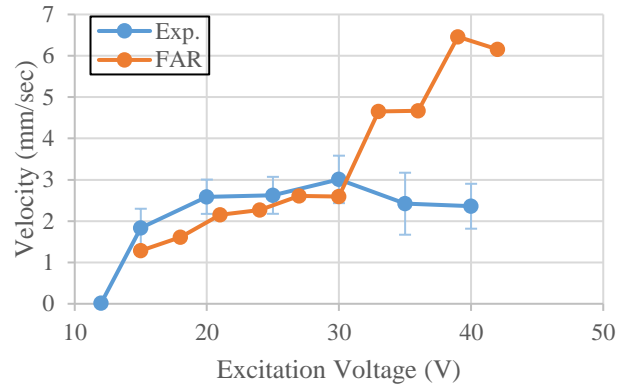


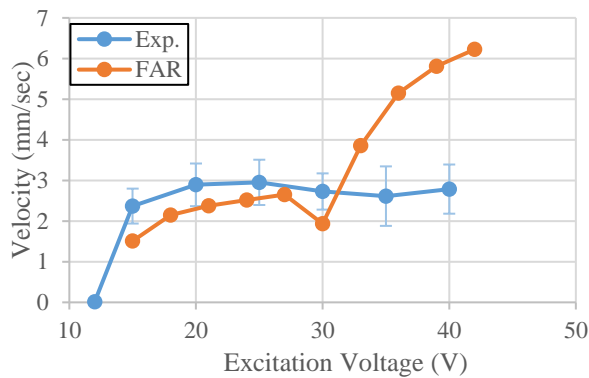
Figure 41. Relationship between the excitation voltage and the average robot velocity of the experimental and simulation results with steel ground at (a) 110Hz (b) 120Hz (c) 130Hz (d) 140Hz.



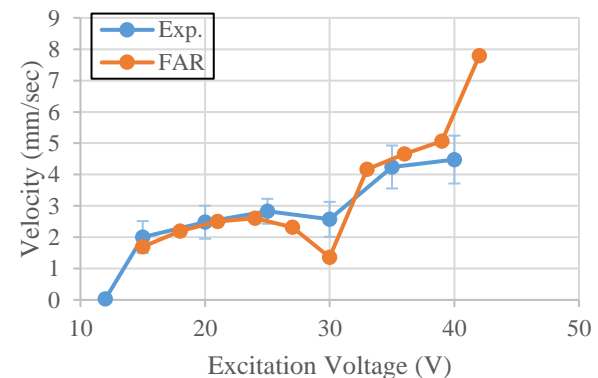
(a)



(b)



(c)



(d)

Figure 42. Relationship between the excitation voltage and the average robot velocity of the experimental and simulation results with wooden ground at (a) 110Hz (b) 120Hz (c) 130Hz (d) 140Hz.

#### 4.7. Conclusion

A FEM model is presented to predict the dynamics of centimeter scale hexapod microrobot. The robot was harmonically excited at its legs in manner similar to excitation from a piezoelectric ceramic bonded to the legs (as done in the prototype). The model includes integration of the dynamic and rigid body motion of the robot to formulate a coupled EoM describing the motion of the systems in three DoFs. The interaction between the robot feet and the ground is modelled using the stick, slip and separation contact model along with the Coulomb's friction. The bilinear ROM

is used to simplify the nonlinear motion of the foot-ground interaction and FAR mode selection technique is used in selecting optimal modes for the reduction process.

To validate the model, results were obtained from a previously fabricated prototype with similar dimensions and properties as the FEM model. The prototype is actuated by piezoelectric ceramic strips bonded to a 3D printed body, and are experimentally characterized in terms of leg and body dynamics as well as walking speed. The experimental results obtained from the prototype include velocities of the robot under varying actuation voltages and frequencies around the resonant frequency. The model was able to predict the resonant frequency of the prototype after the model parameters was identified from solving a nonlinear optimization problem. The optimization is used to extract values of the model parameter that minimizes the residual between experimental and simulated velocities at low excitation amplitude.

Compared with the experimental data, the model was able to capture the locomotion gait of the microrobot and the vertical leg trajectory of the robot within some excitation frequencies. The horizontal velocity of the robot was also captured at frequencies lower and close to the resonant frequency and at lower excitation amplitudes. Some limitation of this model is its inability to predict the robot behavior at high frequencies and high excitation amplitude.

## Chapter V

### 5. Conclusions, Contributions and Future work

In this dissertation, novel methods for computing the dynamic behavior of structures with local intermittent contacts were developed. There is high interest in developing fast and reliable methods for predicting the behavioral characteristics of systems with intermittent contacts. Past methods developed for this type of systems suffer from a high number of DoFs caused by complex motions at the contact interface. While previous approaches may be employed in most cases, an equally reliable but faster and more versatile is often needed in design and analysis. The understanding of the nonlinear dynamics of systems with intermittent contacts, especially cracks can be very useful in making timely and important reliability decisions on operability of the overall system. Three types of ROMs were developed to predict the behavior the effect of intermittent contacts on different systems with a broad range of attributes.

In chapter two, a first ROM was developed using the BLM concept combined with a special two step selection algorithm referred to as the FAR algorithm. The main goal of this ROM is to develop an optimal transformation matrix which spans the solution space of a system at a given frequency using the bilinear modes of the system at neighboring frequencies. The two steps of the FAR algorithm are the MSC and MPC. The MSC selects bilinear modes with frequencies within the frequency range of interest and based on their linear independence into the transformation matrix. The MPC deselects bilinear modes with relatively low modal amplitude from the



transformation matrix. The addition and removal of vectors into and out of the transformation matrix significantly saves computational cost and makes this approach unique. The technique was demonstrated for a cracked rectangular plate, a set of overlapping coaxial cylinders, and a simplified jackup platform (with intermittent contact between the hull and one of its three legs). Results were validated with solution from the full nonlinear DOF model (only CB-CMS reduced model). The FAR-based model was shown to be reliable, accurate and fast with minimal ROM size at every frequency solution.

Nonlinear intermittent contacts are usually local, i.e. the number of DoFs at the contact interface is much less compared to the entire system's DoF. The second ROM developed in chapter three helps to narrow the number of nonlinear models to only within the region of the contact interface. This ROM uses a conventional substructuring method (CB-CMS) combined with FAR and with boundary interface reduction techniques. This approach accommodates systems with multiple nonlinearities either preexisting or newly formed. In the case of newly formed intermittent contacts, this approach alleviates remodeling of the entire system but rather only the affected subcomponents. After partitioning of the system into subcomponents, the original CB-CMS is used to reduce subcomponents with only linear DoFs, a modified CB-CMS is used to reduce subcomponents with nonlinear DoFs and a set of boundary interface modes of component subassemblies are used to reduce the interface DoFs. The modified CB-CMS contains fixed interface bilinear modes (FI-BLMs) instead of the regular fixed interface modes. FAR is employed in the selection process of FI-BLMs. The new ROM was demonstrated for a rectangular plate with two cracks at opposite sides and also for a jackup platform with hull-leg contact interfaces at two of its three legs. The ROMs predicted the response of these structures accurately and efficiently.

The bilinear FAR concept was further challenged in chapter four to predict the behavior of a centimeter scaled hexapod microrobot. To accurately model the robot, the previously developed model was modified to include rigid body dynamics and friction. The robot is made of a pseudo rigid body connected to six flexible arms which are connected to the legs and feet of the robot. The robot is excited at the arms in a manner similar to the excitation direction of a PZT actuator. The foot-ground interaction was modelled with FAR selected bilinear modes to reduce the order of the model for the robot. For validation, the performance of simulation results were compared with experimental measurements from the literature.

The major research contributions made during this research work include:

- Developed a novel frequency adaptive reduction (FAR) method using bi-linear reduced order modelling to predict the behavior of structures with intermittent contacts.
  - ❑ ROMs predicted the steady-state response with significantly reduced computation time compared to other analysis methods.
  - ❑ Developed approach was able to effectively predict significant softening and hardening behaviors characterized by contacts with separation.
  - ❑ Optimal of ROM selection reduced computational storage required during very wide range of frequency sweeps.
- A novel nonlinear ROM approach was developed, using the combination of conventional substructuring, FAR and boundary interface reduction techniques for forced harmonic response analysis of structures with multiple intermittent contacts.
  - ❑ Bilinear constraint modes significantly reduced the interface DoFs.
  - ❑ Efficient ROMs of full assembly were capable of capturing effects of local nonlinearities accurately.

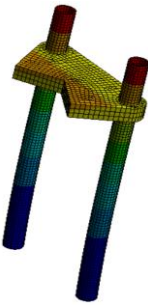
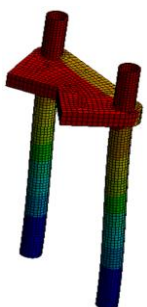
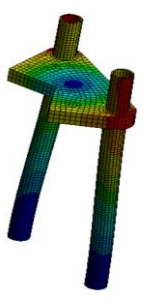
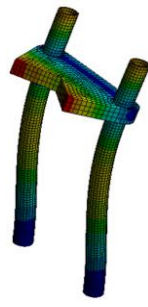
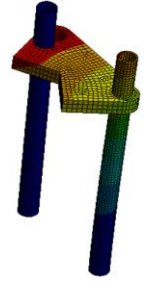
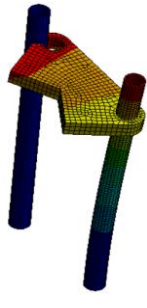
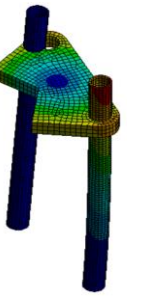
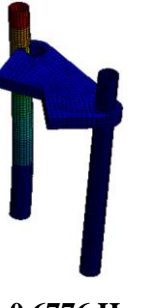
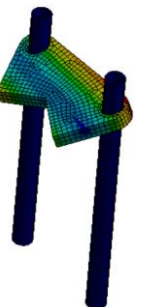
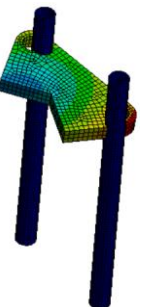
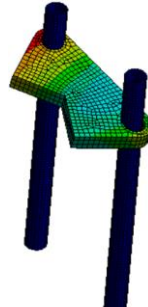
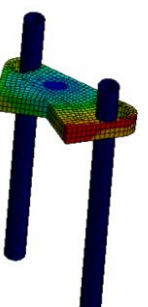
- A bilinear based ROM was developed to predict the locomotion of a hexapod microrobot.
  - ❑ Model result confirmed the predicted pattern of robot locomotion.
  - ❑ Model predicted the locomotion of robot around the first resonance.

Based on the work reported in this dissertation, some ideas for future research include:

- Prediction of the dynamic response of an offshore platform with fully modelled 3-D contact dynamics at all the hull leg interfaces
- Robust optimization for identifying microrobot's modelling parameters with experimental validation of the parameters

## Appendix A

### Subassemblies of Jackup Platform

<b>Boundary Conditions</b>	<i>First Mode</i>	<i>Second Mode</i>	<i>Third Mode</i>	<i>Fourth Mode</i>
<b>Legs 2 and 3 subassembly</b> Fully closed leg 2 and fully closed leg 3	 0.2798 Hz	 0.5340 Hz	 1.0359 Hz	 2.7366 Hz
<b>Legs 2 and 3 subassembly</b> Fully open leg 2 and fully closed leg 3	 0.1890 Hz	 0.1927 Hz	 0.6497 Hz	 0.6776 Hz
<b>Legs 2 and 3 subassembly</b> Fully open leg 2 and fully open leg 3	 3.01e-6 Hz	 5.36e-6 Hz	 7.77e-6 Hz	 9.11e-6 Hz

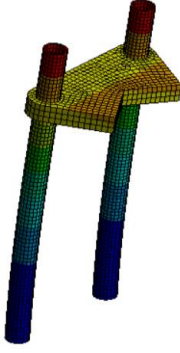
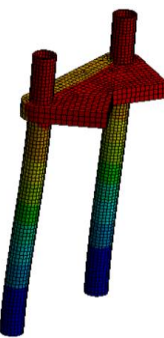
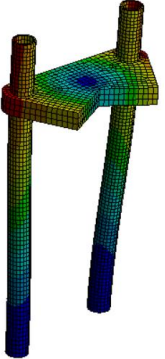

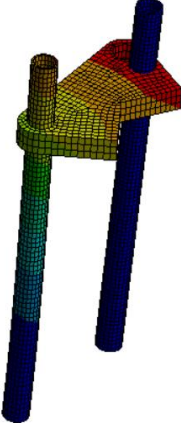
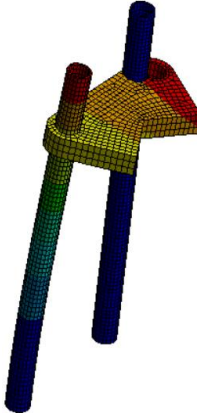
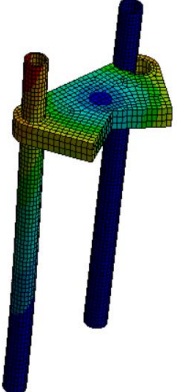
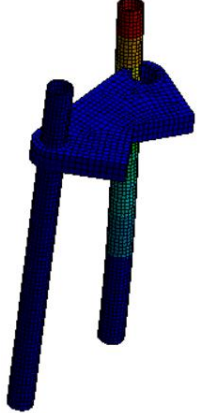
<p><b>Legs 1 and 2 subassembly</b></p> <p>Fixed leg 1 and Fully closed leg 2</p>	 <p><b>0.2798 Hz</b></p>	 <p><b>0.5347 Hz</b></p>	 <p><b>1.0365 Hz</b></p>	 <p><b>2.7392 Hz</b></p>
<p><b>Legs 1 and 2 Subassembly</b></p> <p>Fixed leg 1 and Fully closed leg 2</p>	 <p><b>0.18904</b></p>	 <p><b>0.1927 Hz</b></p>	 <p><b>0.6500 Hz</b></p>	 <p><b>0.6776 Hz</b></p>

Table A. 1. Subassemblies of different combinations of substructures of the Jackup platform with bilinear BCs.

## Appendix B

### Experimental Results of Microrobot

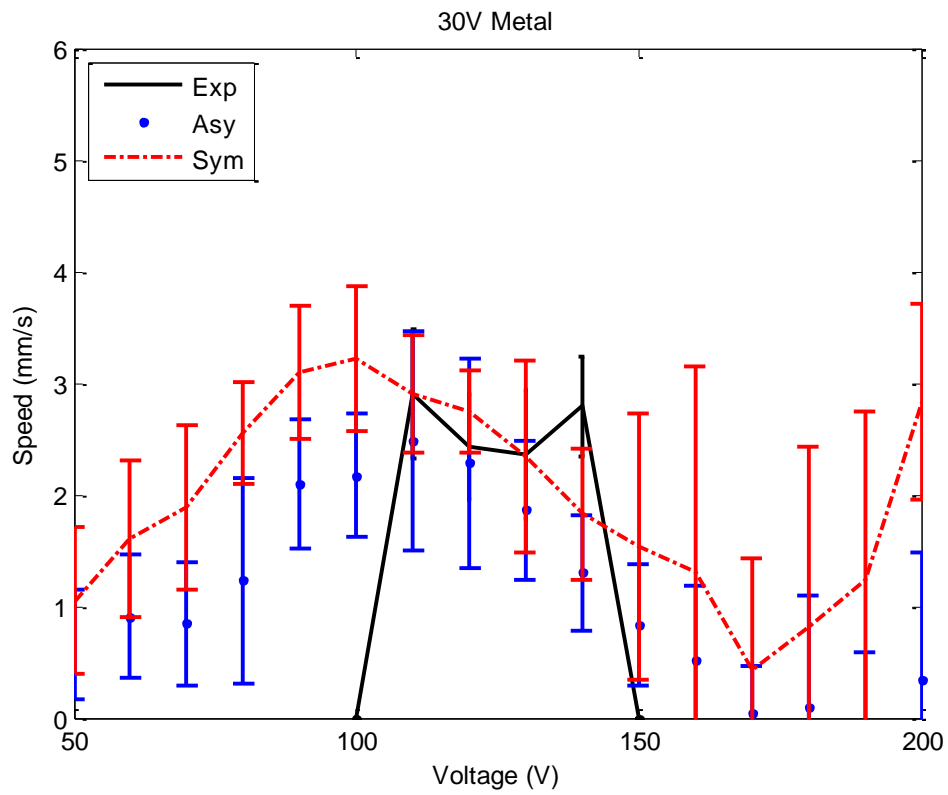


Figure B. 1. Excitation frequency vs robot speed at 30V with metal ground

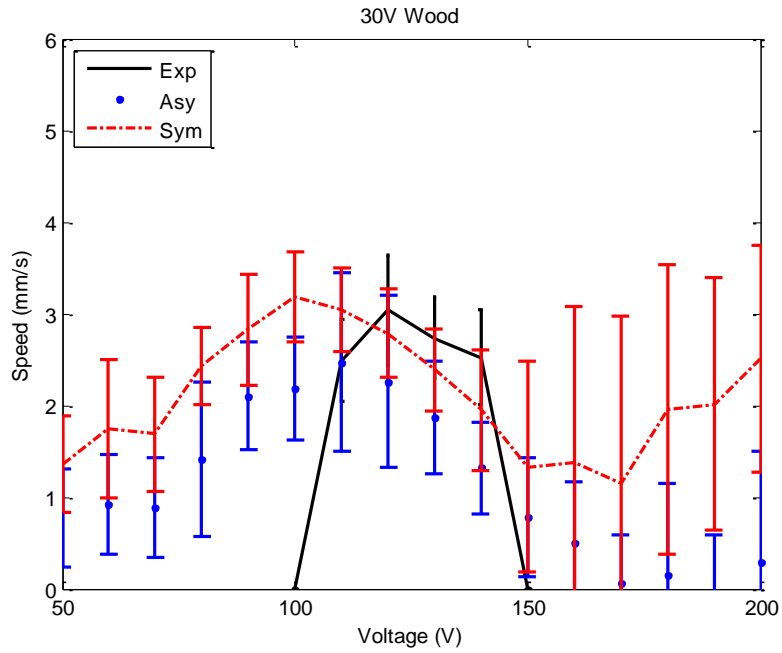


Figure B. 2. Excitation frequency vs robot speed at 30V with wooden ground

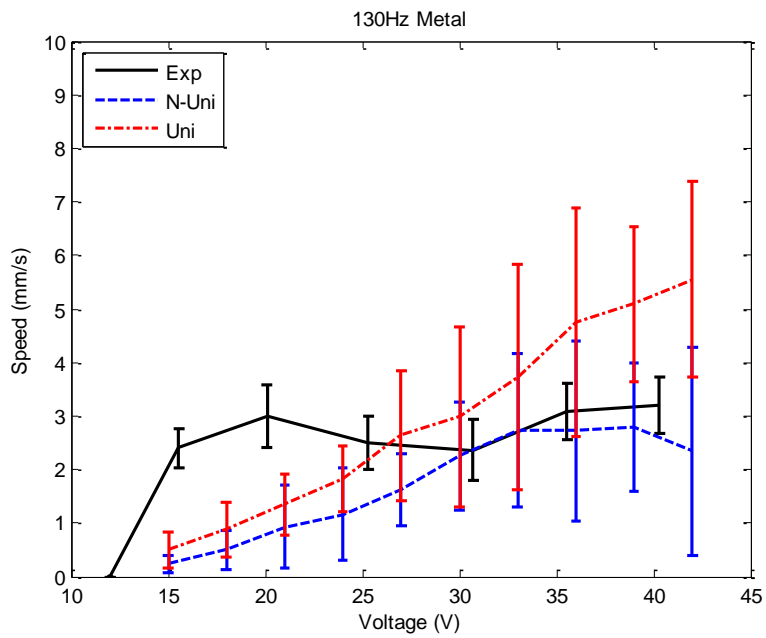


Figure B. 3. Excitation voltage vs robot speed at 130Hz with metal ground

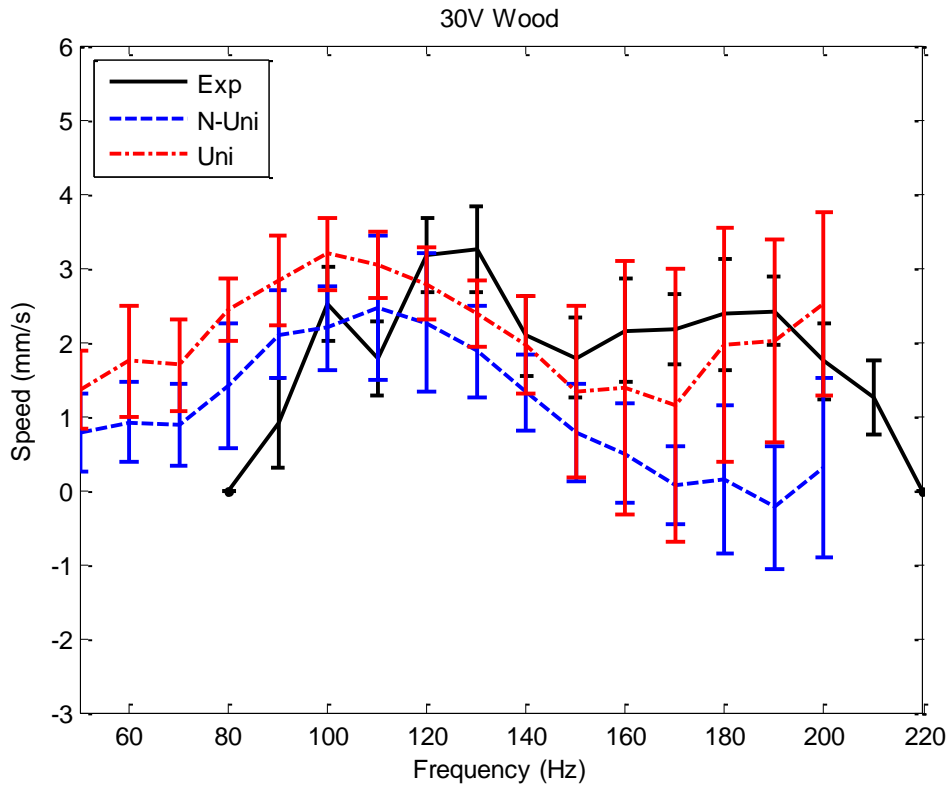


Figure B. 4. Excitation voltage vs robot speed at 130Hz with wooden ground



## References

- [1] O'Callahan, J., Avitabile, P., Riemer, R.: System equivalent reduction expansion process (SEREP). Proceedings of the 7<sup>th</sup> International Modal Analysis Conference, Las Vegas, NV, 29-37 (1989).
- [2] Irons, B.: Structural eigenvalue problem: elimination of unwanted variables. *AIAA Journal*, 3(5) 961-962 (1965).
- [3] Guyan, R.J.: Reduction of stiffness and mass matrices. *AIAA Journal*, 3(2), 380 (1965).
- [4] Butcher, E., Lu, R.: Order reduction of structural dynamic system with static piecewise linear nonlinearities. *Nonlinear Dynamics*, 49(3), 375-399 (2007).
- [5] Craig Jr, R.R., Chang, C.J.: Free interface methods of structure coupling for dynamic analysis. *AIAA Journal*, 14(11), 1633-1635 (1976).
- [6] Poudou, o., Pierre, C.: Hybrid Frequency-time domain methods for the analysis of complex structural system with dry friction damping, proceedings of the 44<sup>th</sup> AIAA/ASME/ASCE/AHS/ASC Structures, Structures, Structural Dynamics and Materials Conference Norfolk, VA, AIAA 2003-1411, (2003).
- [7] Poudou, O.: A new hybrid frequency-time domain method for the forced vibration of elastic structures with friction and intermittent contact, proceedings of the 10<sup>th</sup> International Symposium on Transport Phenomena and Dynamics of Rotating Machinery, Honolulu, Hawaii ISROMAC10-2004-068, (2004).
- [8] Shaw, S.W., Holmes, P.J.: A periodically forced piecewise linear oscillator. *Journal of Sound and Vibration*, 90(1), 129-155 (1983).
- [9] Chati, M., Rand, R., Mukherjee, S.: Modal analysis of a cracked beam. *Journal of Sound and Vibration*, 207, 249-270 (1997).
- [10] Saito, A., Castanier, M.P., Pierre, C.: Estimation and veering analysis of nonlinear resonant frequencies of cracked plates. *Journal of Sound and Vibration*, 326, 725-739 (2009).

- [11] Henshell, R. D., Ong, J. H.: Automatic Masters for Eigenvalue Economization, *Earthquake Engineering and Structural Dynamics*. 3(4), 375–383 (1975).
- [12] Shah, V.N., Raymund, M.: Analytical Selection of Masters for the Reduced Eigenvalue Problem. *International Journal for Numerical Methods in Engineering*, 18(1), 89–98 (1982).
- [13] Matta, K. W.: Selection of Degrees of Freedom for Dynamic Analysis, *Transactions of the ASME, Series J. Journal of Pressure Vessel Technology*, 109(1), 65–69 (1987).
- [14] Grinenko, N. I., Mokeev, V. V.: Problems of Studying Vibrations of Structures by the Finite-Element Method. *International Applied Mechanics*, 21(3), 231–235 (1985).
- [15] Bouhaddi, N., Fillod, R.: A Method for Selecting Master DOF in Dynamic Substructuring Using the Guyan Condensation Method, *Computers and Structures*, 45(5–6), 941–946 (1992).
- [16] Kim, K.O., Choi, Y.J.: Energy Method for Selection of Degrees of Freedom in Condensation. *AIAA Journal*, 38(7), 1253–1259 (2000).
- [17] Kim, H., Cho, M.: Two-level Scheme for Selection of Primary Degrees of Freedom and Semi-Analytic Sensitivity Based on the Reduced System, *Computer Methods in Applied Mechanics and Engineering*. 195(33–36), 4244–4268 (2006).
- [18] Segalman, D.J.: Model reduction of systems with localized nonlinearities. *ASME Journal of Computational and Nonlinear Dynamics* 2(3), 249–266. (2007).
- [19] Saito, A., Epureanu B.I.: Bilinear modal representations for reduced-order modeling of localized piece wise linear oscillators. *Journal of Sound and Vibration* 330(14), 3442–3457 (2011).
- [20] Zucca, S., Epureanu B.I.: Bi-linear reduced-order models of structures with friction intermittent contacts. *Nonlinear Dynamics* 77(3), 1055–1067 (2014).
- [21] Zucca, S., Epureanu, B.I.: Reduced order models for nonlinear dynamic analysis of structures with intermittent contacts. *Journal of Vibration and Control* 24(12), 2591–2604 (2018).
- [22] Wenneker, F., Tiso, P.: A Substructuring Method for Geometrically Nonlinear Structures. In *32nd International Modal Analysis Conference (IMAC XXXII)*, Orlando, Florida, 157-165 (2014).

- [23] Perez, R. A.: Multiscale Reduced Order Models for the Geometrically Nonlinear Response of Complex Structures, Ph.D Dissertation, Arizona State University, (2012).
- [24] Brahmi, K., Bouhaddi, N., Fillod, R.: Reduction of Junction Degrees of Freedom before Assembly in Dynamic Substructuring. Proceedings of the ASME Design Engineering Technical Conference (3), 699–708 (1995).
- [25] Castanier, M. P., Tan, Y. C., Pierre, C.: Characteristic Constraint Modes for Component Mode Synthesis. AIAA Journal 39(6), 1182–1187 (2001).
- [26] Balmés, E.: Use of Generalized Interface Degrees of Freedom in Component Mode Synthesis, Proceedings of International Modal Analysis Conference, Society for Experimental Mechanics, Bethel, CT, 204–210 (1996).
- [27] Erdem, E. Y., Chen, Y. M., Mohebbi, M., Suh, J. W., Kovacs, G. T., Darling, R. B., Bohringer, K. F.: Thermally Actuated Omnidirectional Walking Microrobot, J. Microelectromech. Syst., 19(3), 433–442 (2010).
- [28] Pierre, R. S., Vogtmann, D., Bergbreiter, S.: Model-Based Insights on the Design of a Hexapod Magnetic Walker, Experimental Robotics, Springer International Publishing, Cham, Switzerland, pp. 715–727 (2016).
- [29] Adams, G. G.: Imperfectly constrained planar impacts—a coefficient-of-restitution model Int. J. Impact Eng. 19693–701 (1997).
- [30] Lankarani, H. M., Nikravesh P. E.: Continuous contact force models for impact analysis in multibody systems Nonlinear Dyn. 5193–207 (1994).
- [31] Hurmuzlu, Y., Marghitu, D. B.: Rigid body collisions of planar kinematic chain with multiple contact points Int. J. Robot. Res. 1382–92 (1999).
- [32] Hurty, W.C.: Dynamic analysis of structural systems using component modes. AIAA Journal, 3(4), 678-685 (1965).
- [33] Craig, R.R., Bampton, M.C.: Coupling of substructures for dynamic analyses. AIAA Journal, 6(7), 1313-1319 (1968).
- [34] Saito, A., Castanier, M.P., Pierre, C., Poudou, O.: Efficient nonlinear vibration analysis of the forced response of rotating cracked blades. Journal of Computational and Nonlinear Dynamics, 4(1), 011005 (2009).

- [35] Nacivet, S., Pierre, C., Thouverez, F., and Jezequel, L.: A dynamic lagrangian frequency time method for the vibration of dry-friction-damped systems. *Journal of Sound and Vibration*, 265(1), 201 – 219 (2003).
- [36] Marinescu, O., Epureanu, B.I., Banu, M.: Reduced order models of mistuned cracked bladed disks. *Journal of Vibration and Acoustics*, 133, 051014 (2011).
- [37] Saito, A., Epureanu, B.I., Castanier, M.P., Pierre, C.: Node sampling for nonlinear vibration analysis of structures with intermittent contact. *AIAA Journal*, 48, 1903–1915 (2010).
- [38] Kerschen, G., Golinval, J., Vakakis A.F., et al.: The method of proper orthogonal decomposition for dynamical characterization and order reduction of mechanical systems: an overview. *Nonlinear Dynamics*, 41(1), 147–169 (2005).
- [39] Al-Shudeifat, M.A., Butcher, E.A.: Order reduction of forced nonlinear systems using updated LELSM modes with new Ritz vectors. *Nonlinear Dynamics*, 62(4), 821–840 (2010).
- [40] Kerschen, G., Peeters, M., Golinval, J. C., Vakakis, A. F.: Nonlinear normal modes, part 1: a useful framework for the structural dynamicist. *Mechanical Systems and Signal Processing*, 23(1), 170-194 (2009).
- [41] Zuo, L., Curnier, A.: Non-Linear Real And Complex Modes Of Conewise Linear Systems. *Journal of Sound and Vibration*, 174 (3), 289-313 (1994).
- [42] Zucca, S., Epureanu, B.I.: Bi-linear reduced-order models of structures with friction intermittent contacts. *Nonlinear Dynamics*, 77(3), 1055-1067 (2014).
- [43] Cardona, A., Lerusse, A., Geradin, M.: Fast fourier nonlinear vibration analysis. *Computational Mechanics*, 22(2), 128-142 (1998).
- [44] Firrone, C.M., Zucca, S.: Modelling friction contacts in structural dynamics and its application to turbine bladed disks. *Numerical Analysis - Theory and Application*, 14, 301-334 (2011).
- [45] Chan, T.F.C., Keller, H.B.: Arc-Length Continuation and multi-grid techniques for nonlinear elliptic eigenvalue problems. *SIAM Journal of Scientific and Statistical Computing*, 3(2), 173-194 (1982).

- [46] Cameron T.M., Griffin, J.H.: An alternating frequency/time domain method for calculating the steady-state response of nonlinear dynamic systems. *Journal of Applied Mechanics*, 56(1), 149-154 (1989).
- [47] Zucca, S., Epureanu, B.I.: Reduced order models for nonlinear dynamic analysis of structures with intermittent contacts. *Nonlinear Dynamics*, under review. *Journal of Vibration and Control*, 24(12), 2591-2604 (2017).
- [48] Lu, Y.J., Chen, Y.N., Tan, P.L., Bai, Y.: Prediction of most probable extreme values for jackup dynamic analysis, *Marine Structures*, 15(1), 15-34 (2002).
- [49] Wu, H.L., Chen, X.J., Huang, Y.X., Wang, B.: Influence of the legs underwater on the hydrodynamic response of the multi-leg floating structure, *Ships and Offshore Structures*, 9(6), 578-595 (2014).
- [50] Craig Jr, R.R.: *Structural dynamics*. New York, J. Wiley, (1981).
- [51] Bathe, K.J.: *Finite element procedures*. Prentice Hall, (1996).
- [52] Hurty, W.C.: Dynamic analysis of structural systems using component modes. *AIAA J*, 3 4), 678–85 (1965).
- [53] Klerk, D.D., Rixen D.J., Voormeeren S.N.: General framework for dynamic substructuring: history, review and classification of techniques. *AIAA J*; 46(5), 1169-81 (2008)
- [54] Petrov, E. P.: A High-Accuracy Model Reduction for Analysis of Nonlinear Vibrations in Structures with Contact Interfaces. *ASME J. Eng. Gas Turbines Power*, 133(10), 102503 (2011).
- [55] Huang, S.: *Dynamic Analysis of Assembled Structures with Nonlinearity*, Department of Mechanical Engineering, Ph. D. thesis, Imperial College London, UK. (2008).
- [56] Brake, M. R. W., Grob, J., Lacayo, R. M., Salles, L., Schwingshackl, C. W., Reuß, P., Armand, J.: *Reduced Order Modeling of Nonlinear Structures With Frictional Interfaces*, *The Mechanics of Jointed Structures: Recent Research and Open Challenges for Developing Predictive Models for Structural Dynamics*, M.R.W., Brake, ed., Springer International Publishing, Cham, 427–450 (2018).
- [57] Siewert, C., Panning, L., Wallaschek, J., Richter, C.: Multiharmonic Forced Response Analysis of a Turbine Blading Coupled by Nonlinear Contact Forces. *ASME J. Eng. Gas Turbines Power* 132(8), 82501 (2010).

- [58] Zucca, S., Firrone, C. M.: Nonlinear Dynamics of Mechanical Systems with Friction Contacts: Coupled Static and Dynamic Multi-Harmonic Balance Method and Multiple Solutions. *J. Sound Vib.*, 333(3), 916–926 (2014).
- [59] Petrov, E. P., Ewins, D. J.: Method for Analysis of Nonlinear Multiharmonic Vibrations of Mistuned Bladed Disks with Scatter of Contact Interface Characteristics. *ASME J. Turbomach.*, 127(1), 128–136 (2005).
- [60] Petrov, E. P.: A Method for Use of Cyclic Symmetry Properties on Analysis of Nonlinear Multiharmonic Vibrations of Bladed Disks. *ASME J. Turbomach.*, 126(1), 175–183 (2004).
- [61] Frey, C., Ashcroft, G., Kersken, H. P., Voigt, C.: A Harmonic Balance Technique for Multistage Turbomachinery Applications. *ASME Paper No. GT2014-25230* (2014).
- [62] Forster, A., Krack, M.: An Efficient Method for Approximating Resonance Curves of Weakly-Damped Nonlinear Mechanical Systems. *Comput. Struct.* 169, 81–90 (2016).
- [63] Cigeroglu, E., An, N., Menq, C. H.: Wedge Damper Modeling and Forced Response Prediction of Frictionally Constrained Blades. *ASME Paper No. GT2007-27963* (2007).
- [64] Cigeroglu, E., An, N., Menq, C. H.: Forced Response Prediction of Constrained and Unconstrained Structures Coupled Through Frictional Contacts, *ASME J. Eng. Gas Turbines Power*, 131(2), 022505 (2009).
- [65] Cigeroglu, E., Ozguven, H. N.: Nonlinear Vibration Analysis of Bladed Disks with Dry Friction Dampers. *J. Sound Vib.*, 295(3–5), 1028–1043 (2006).
- [66] Grolet, A., Thouverez, F.: On a New Harmonic Selection Technique for Harmonic Balance Method. *Mech. Syst. Signal Process.*, 30, 43–60 (2012).
- [67] Grolet, A., Thouverez, F.: Computing Multiple Periodic Solutions of Nonlinear Vibration Problems Using the Harmonic Balance Method and Groebner Bases. *Mech. Syst. Signal Process.* 52–53, 529–547 (2015).
- [68] Craig, R. R. J., Bampton, M. C. C.: Coupling of Substructures for Dynamic Analysis. *AIAA Journal*, 6(7), 1313-1319 (1968).
- [69] Krack, M., Salles, L., Thouverez, F.: Vibration Prediction of Bladed Disks Coupled by Friction Joints. *Arch. Comput. Methods Eng.*, 24(3), 589–636 (2017).

- [70] Odofin, A., Epureanu, B.: Frequency-adaptive bilinear reduced-order model for structures with intermittent contacts. *Nonlinear Dynamics*, 10.1007/s11071-019-05000-x (2019).
- [71] Jung, C., D’Souza, K., Epureanu, B.: Bilinear Amplitude Approximation for Piecewise-Linear Oscillators. *AIAA 2012-1793* (2012).
- [72] Becker, J., Gaul, L.: CMS Methods for Efficient Damping Prediction for Structures with Friction, *IMAC-XXVI*, Orlando, FL, Feb. 4–7 (2008).
- [73] Hong, S.-K., Epureanu, B. I.: Castanier, M. P.: Next-generation parametric reduced order models. *Mechanical Systems and Signal Processing*, 37(1–2), 403-421 (2013).
- [74] Witteveen, W., Irschik, H.: Efficient Mode-Based Computational Approach for Jointed Structures. *Joint Interface Modes*, *AIAA J.*, 47(1), 252 (2009).\*\*\*\*\*9
- [75] Witteveen, W., Pichler, F.: Efficient Model Order Reduction for the Dynamics of Nonlinear Multilayer Sheet Structures with Trial Vector Derivatives. *Shock Vib.*, 913136 (2014).
- [76] Tran, D. M.: Component mode synthesis methods using interface modes. Application to structures with cyclic symmetry, *Computers & Structures*. 79(2), 209-222 (2001).
- [77] Donders, S., Pluymers, B., Ragnarsson, P., Hadjit, R., Desmet, W.: The wave-based substructuring approach for the efficient description of interface dynamics in substructuring. *Journal of Sound and Vibration*, 329(8), 1062-1080 (2010).
- [78] Craig, R. R. J., Kurdila, A. J.: *Fundamentals of Structural Dynamics*, 2nd ed., Wiley, New York, 2006.
- [79] Driesen, W.: *Concept, Modeling and Experimental Characterization of the Modulated Friction Inertial Drive (MFID) Locomotion Principle: Application to Mobile Microrobots*. Ph.D. Thesis, Lausanne: EPFL (2008).
- [80] Full, R. J., Tu, M. S.: Mechanics of a Rapid Running Insect: Two-, Four- and Six-Legged Locomotion, *J. Exp. Biol.*, 156(1), 215–231 (1991)
- [81] Li, C., Pullin, A. O., Haldane, D. W., Lam, H. K., Fearing, R. S., and Full, R. J., Terradynamically Streamlined Shapes in Animals and Robots Enhance Traversability Through Densely Cluttered Terrain, *Bioinspiration Biomimetics*. 10(4), 046003 (2015).
- [82] Felso, G.: Theory of motion principle of a piezoelectric driven microrobot, *Periodica Polytechnica, Electrical Engineering*, BUTE, 227239 (2000).

- [83] Eigoli, A. K. Vossoughi, G.: Dynamic Modeling of Stick-Slip Motion in a Legged, Piezoelectric Driven Microrobot', International Journal of Advanced Robotic Systems. doi: 10.5772/9704 (2010).
- [84] Shin, M., Choi, J., Rudy, R. Q., Kao, C., Pulskamp, J. S., Polcawich, R. G., and Oldham, K. R.: Micro-Robotic Actuation Units Based on Thin-Film Piezoelectric and High-Aspect Ratio Polymer Structures. ASME Paper No. DETC2014-35145 (2014).
- [85] Qu, J., Teeple, C. B., Oldham, K. R.: Modeling Legged Microrobot Locomotion Based on Contact Dynamics and Vibration in Multiple Modes and Axes. ASME. J. Vib. Acoust, 139(3), 031013 (2017).